NASA TECHNICAL NOTE

AERODYNAMIC INTERFERENCE EFFECTS CAUSED BY PARALLEL-STAGED SIMPLE AERODYNAMIC CONFIGURATIONS AT MACH NUMBERS OF 3 AND 6

by John P. Decker

Langley Research Center
Langley Station, Hampton, Va.

1. Report No. NASA TN D-5379	2. Government Accession No.	3. Recipient's Catalog No.
4. Title and Subtitle AERODYNAMIC INTERFERENCE EFFECTS CAUSED BY PARALLEL-STAGED SIMPLE AERODYNAMIC CONFIGURATIONS AT MACH NUMBERS OF 3 AND 6		5. Report Date August 1969
		6. Performing Organization Code
7. Author(s) John P. Decker		8. Performing Organization Report No. L-5295
9. Performing Organization Name and Address NASA Langley Research Center Hampton, Va. 23365		10. Work Unit No. 124-07-05-02-23
		11. Contract or Grant No.
		13. Type of Report and Period Covered Technical Note
12. Sponsoring Agency Name and Address National Aeronautics and Space Administration Washington, D.C. 20546		
		14. Sponsoring Agency Code

15. Supplementary Notes

16. Abstract

A wind-tunnel investigation has been conducted to examine the aerodynamic interference effects associated with simple aerodynamic configurations placed parallel and in close proximity to each other. The configurations were 10^0 half-cone bodies that varied in length and were tested with and without simple delta wings. The flat surfaces of the configurations were adjacent to each other during testing. The effects of vertical spacing and relative incidence angle between the configurations were measured, and the resulting data were used to determine the influence of relative body size, nose bluntness, and lifting surfaces on the longitudinal aerodynamic characteristics of the lower configuration at Mach numbers of 3 and 6.

17. Key Words Suggested by Author(s) Parallel-stage separation Reusable launch vehicles	18. Distribution Statement Unclassified – Unlimited		
19. Security Classif. (of this report) Unclassified	20. Security Classif. (of this page) Unclassified	21. No. of Pages 85	22. Price* $3.00

*For sale by the Clearinghouse for Federal Scientific and Technical Information
Springfield, Virginia 22151

Page Intentionally Left Blank

AERODYNAMIC INTERFERENCE EFFECTS CAUSED BY
PARALLEL-STAGED SIMPLE AERODYNAMIC CONFIGURATIONS
AT MACH NUMBERS OF 3 AND 6

By John P. Decker
Langley Research Center

SUMMARY

A wind-tunnel investigation has been conducted to examine the aerodynamic inter-
ference effects associated with simple three-dimensional aerodynamic configurations
placed parallel and in close proximity to each other. The configurations were 10° half-
cone bodies that varied in length and were tested with and without simple delta wings.
The flat surfaces of the configurations were adjacent to each other during testing. The
effects of vertical spacing and relative incidence angle between the configurations were
measured, and the resulting data were used to determine the influence of relative body
size, nose bluntness, and lifting surfaces on the longitudinal aerodynamic characteristics
of the lower configuration at Mach numbers of 3 and 6.

Increasing the size of the upper configuration generally caused a progressive
decrease in the normal-force-curve slope and a progressive decrease in the static longi-
tudinal stability of the lower configuration. For the upper configuration larger than the
lower configuration, the data suggest some form of progressive blanketing since the
normal-force-curve slope decreases to zero and even negative values at some of the ver-
tical spacings investigated. Increasing the incidence angle of the upper configuration gen-
erally caused nose-up increments in the pitching-moment coefficient and negative incre-
ments in the normal-force coefficient of the lower configuration.

Blunting the nose of the upper and lower configuration or adding delta wings, with a
root chord equal to the body length, to either configuration or both the upper and lower
configuration had little effect on the longitudinal aerodynamic characteristics of the lower
configuration when compared with the data for the pointed-nose configurations or the
wingless configurations. However, these effects, which probably depend upon configura-
tion, amount of bluntness, and the wing planform shape and position, have not been
thoroughly investigated in this paper.

INTRODUCTION

Recent wind-tunnel test results on a parallel-staged reusable-launch-vehicle configuration, references 1 and 2, showed that large aerodynamic interferences could be expected during staging maneuvers in the sensible atmosphere. These interferences produced large changes in both the forces and moments on each of the two stages compared with the forces and moments at free-stream or interference-free conditions. The analytical results of references 1 and 2 on the relative behavior of the two stages showed that a potentially hazardous situation could be expected during staging at supersonic and hypersonic speeds.

The configuration employed in references 1 and 2 was relatively complex in shape and represented a reasonably realistic launch vehicle. Because of the resulting complex three-dimensional flow fields about this vehicle, the present investigation of simple configuration shapes was undertaken to establish some of the fundamental phenomena involved. The configurations employed were half-cone bodies to which could be attached flat-plate-type delta wings with a root chord equal to the body length. The bodies had a half-cone angle of 10° and the wings had a leading-edge sweep of 70°. The effects of vertical spacing and relative incidence angle between the configurations were measured, and the resulting data were used to determine the influence of relative body size, nose bluntness, and wings on the longitudinal aerodynamic characteristics of the lower configuration.

The tests were conducted in the 2-foot hypersonic facility at the Langley Research Center at nominal Mach numbers of 3 and 6. The upper and lower configurations were individually mounted in order to measure their individual forces and moments, and the tests were conducted so that the flat surfaces of the configurations were adjacent. The vertical spacing between the two configurations was varied, and the incidence angle between the upper and lower configuration was 0° (parallel), 2^O, or 5° for an angle-of-attack range of -9° to 12°.

SYMBOLS

The longitudinal aerodynamic characteristics for all configurations have been referred to the body axes. The aerodynamic coefficients were based on the geometry of the planform of the unblunted configurations, and the moment reference center was located at the centroid of the planform.

C_A axial-force coefficient, $\dfrac{\text{Axial force}}{qS}$

C_m pitching-moment coefficient, $\dfrac{\text{Pitching moment}}{qSL}$

C_{m_α} pitching-moment-curve slope, $\dfrac{\partial C_m}{\partial \alpha}$

C_N normal-force coefficient, $\dfrac{\text{Normal force}}{qS}$

C_{N_α} normal-force-curve slope, $\dfrac{\partial C_N}{\partial \alpha}$

h vertical spacing between upper and lower configuration (see fig. 4), meters

i relative incidence angle between upper and lower configuration, $\alpha_2 - \alpha_1$ (see fig. 4), degrees

L reference length or mean geometric chord based on projected planform (see table I), meters

l overall length of configuration, meters

M free-stream Mach number

q free-stream dynamic pressure, newtons/meter^2

R base radius, meters

r nose radius, meters

S reference area or projected planform area (see table I), meter^2

x_{cp} location of center of pressure forward of base, meters

α angle of attack referenced to flat surface of configuration (see fig. 4), degrees

Subscripts:

1 lower configuration

2 upper configuration

Component designations:

$B_1, B_2, B_3, B_4, B_5, B_6$ body designations (see fig. 1)

W_1 70° swept delta wing for B_1

W_2 70° swept delta wing for B_2

APPARATUS AND TESTS

Wind Tunnel

The wind-tunnel investigation was conducted in the 2-foot hypersonic facility at the Langley Research Center. The 2-foot hypersonic facility, described in reference 3, is a continuous-flow closed-circuit ejector-type wind tunnel. The tunnel has a 60.96-cm by 60.96-cm by 137.16-cm test section and provides a Mach number range of 3 to 6 at relatively low free-stream densities.

Configurations

The configurations were 10° half-cone bodies that varied in length and were tested with and without flat-plate 70° swept delta wings. The configurations had both sharp and blunted body noses. Drawings of the configurations are shown in figure 1, and photographs of some of the lower configurations mounted in the presence of upper configurations are shown in figure 2. The geometric characteristics of the various configurations are presented in table I.

Support Mechanism

Separate sting supports were provided for the lower and upper configurations, with the vertical movement between the configurations being provided by the support system to which the stings were attached. (See fig. 3.) Incidence angle between the configurations was varied by using sting adapters on the upper sting support. The complete support apparatus was attached to an arc strut that varied the angle of attack of the configurations.

Tests

The wind-tunnel tests were conducted at nominal Mach numbers of 3 and 6. The vertical spacing h was varied from 2.03 cm to 10.16 cm, and the incidence angle i was 0° (parallel), 2^O, or 5° for an angle-of-attack range of -9° to 12°. (See fig. 4.) The tests were conducted with the flat surfaces of the configurations adjacent. Tests were also conducted at interference-free conditions $\left(h/l_1 = \infty \right)$; that is, when the configurations were not in proximity to each other.

Static longitudinal aerodynamic force and moment data were simultaneously obtained for the upper and lower configuration by using individual internal six-component strain-gage balances. All data were reduced to standard coefficient form, and the individual angles of attack of the upper and lower configurations were corrected for their respective balance and sting deflection under load. No axial-force corrections were made, and no corrections were made to the incidence angle since these corrections were found to be at most $\pm 0.1^O$. All data were obtained with the configurations aerodynamically smooth, and, at the Reynolds numbers of these tests, laminar flow probably existed over almost the entire configuration.

The average test conditions and Reynolds numbers were as follows:

Mach number	Stagnation pressure, kN/m^2	Stagnation temperature, ^OK	Reynolds number per meter
3	50.6	322	2.6×10^6
6	303.6	422	3.2

PRESENTATION OF RESULTS

Although longitudinal aerodynamic data were simultaneously obtained for both the upper and lower configuration, the data are presented as if they were only obtained for a lower configuration in the presence of an upper configuration. These data are presented in figures 5 to 19 with some of the results summarized in figures 20 and 21. In addition, interference regions are shown in figure 22 and schlieren photographs are presented in figures 23 to 25. An outline of the contents of the data figures is as follows:

Longitudinal aerodynamic characteristics of various lower configurations in presence of various upper configurations —

Lower configuration	Upper configuration	i, deg	l_2/l_1	Figure
B_4	B_1	0	0.60	5
B_2	B_1	0	.75	6
B_2	B_3	0	1.00	7
B_1	B_2	0	1.33	8
B_1	B_4	0	1.67	9
B_2	B_1	2	0.75	10
B_1	B_2	2	1.33	11
B_2	B_1	5	.75	12
B_1	B_2	5	1.33	13
B_2W_2	B_1	0	0.75	14
B_2W_2	B_1W_1	0	.75	15
B_1	B_2W_2	0	1.33	16
B_1W_1	B_2W_2	0	1.33	17
B_6	B_5	5	0.75	18
B_5	B_6	5	1.33	19

RESULTS AND DISCUSSION

The data of figures 5 to 19 show that the proximity of the upper configurations at different vertical spacings and incidence angles produced marked changes in the basic longitudinal aerodynamic coefficients of the lower configurations. The longitudinal aerodynamic characteristics of the lower configurations are compared with the interference-free longitudinal aerodynamic characteristics, and it can be seen that the region of significant influence of the upper configurations generally extended beyond the maximum values of the test spacing h/l_1.

Effects of Upper Configuration Size

Figure 20 illustrates the effect of the relative size of the upper configuration on the longitudinal aerodynamic characteristics of the lower configuration. The relative-size parameter used in figure 20 is l_2/l_1, the ratio of the length of the upper configuration to that of the lower configuration. The data shown in figure 20 were obtained from figures 5 to 9 for $l_2/l_1 = 0.60$ to $l_2/l_1 = 1.67$. The data for $l_2/l_1 = 0$ are for interference-free conditions.

The figure shows that increasing the size of the upper configuration at $M = 3$ (figs. 20(a) to 20(d)) causes a progressive decrease in the normal-force-curve slope $\left(C_{N\alpha}\right)_1$ as well as a similar decrease in the static longitudinal stability $\left(C_{m\alpha}\right)_1$ of the lower configuration. Similar results are also indicated at $M = 6$ for $h/l_1 \leqq 0.10$ (figs. 20(e) and 20(f)). For $h/l_1 > 0.10$ at $M = 6$ (figs. 20(g) and 20(h)), the lower configuration appears to have almost achieved interference-free conditions since the curves approach the interference-free curves.

The data in figure 20 indicate some form of progressive blanketing at angles of attack less than about 3° for the upper configuration larger than the lower configuration

$\left(l_2/l_1 = 1.33 \quad \text{and} \quad l_2/l_1 = 1.67\right)$. This effect is illustrated by the decrease in $\left(C_{N_\alpha}\right)_1$ to approximately zero and even negative values at the smaller vertical spacings. (See figs. 20(a), 20(b), 20(e), and 20(f).) This blanketing is probably caused by the fact that the lower configuration is in the downwash field of the upper configuration, which causes a reduction in the effective angle of attack of the lower configuration together with a reduction in the energy of the flow (low local dynamic pressures) from free-stream conditions.

Effects of Incidence Angle

Upper configuration smaller than lower configuration.- Although the data presented in figures 21(a) to 21(h) are only for $l_2/l_1 = 0.75$, the data are representative for an upper configuration smaller than a lower configuration. These data indicate that at $M = 3$ and $h/l_1 = 0.05$ or $h/l_1 = 0.10$ (figs. 21(a) and 21(b)), increasing the incidence angle of the upper configuration from 0° to 5° caused positive increments in the pitching-moment coefficient (nose up) and negative increments in the normal-force coefficient (decreased normal force) of the lower configuration with little change in the slope of these curves. For h/l_1 greater than 0.10 (figs. 21(c) and 21(d)), increasing the incidence angle had little effect on either the normal-force or pitching-moment curves. Similar results are also indicated at $M = 6$ with the critical spacing being 0.05 instead of 0.10 as it was at $M = 3$.

Upper configuration larger than lower configuration.- Although the data in figures 21(i) to 21(p) are only for $l_2/l_1 = 1.33$, the data are representative for an upper configuration larger than a lower configuration. Similar aerodynamic results are indicated in these figures as were indicated in figures 21(a) to 21(h) of the preceding section. However, at $M = 3$ and $h/l_1 = 0.05$ (fig. 21(i)), increasing the incidence angle caused a decrease in the static longitudinal stability $\left(C_{m_\alpha}\right)_1$ from that at $i = 0^\circ$. Similar results are also shown at $M = 6$ and $h/l_1 = 0.05$ (fig. 21(m)). At both $M = 3$ and $M = 6$ and at the other spacings, the static stability did not change appreciably.

Effects of Nose Bluntness

Blunting the nose of the upper and lower configuration 10 percent of the base radius $(r/R = 0.10)$ had little effect on the longitudinal aerodynamic characteristics of the lower configuration when compared with the data for the pointed-nose configurations at similar geometric conditions; that is, at similar values of h/l_1 and i (fig. 21). It should not be concluded from these few data that nose bluntness will not affect the longitudinal aerodynamic characteristics of a vehicle when in the presence of another vehicle. The bluntness effect has not been thoroughly examined in this investigation and is probably dependent on configuration as well as the amount of bluntness.

Effects of Lifting Surface

Adding a delta wing to just an upper configuration (fig. 16) or to just a lower configuration (fig. 14) or to both the upper and lower configuration (figs. 15 and 17) did not appreciably affect the changes in the characteristics previously discussed for the wingless configurations. Compare, for example, figure 15 with figure 6 or figure 16 with figure 8. However, the changes in the force and moment coefficients could have been significantly altered if the wings had had a different planform shape and had been positioned differently on the configurations.

Comments on Interference Effects

Both references 1 and 2 concluded that the observed changes in forces and moments of the lower configuration were primarily caused by the bow shock wave generated by the upper configuration for an upper configuration smaller than a lower configuration. (See fig. 22(a).) For an upper configuration larger than a lower configuration, the changes in forces and moments were primarily caused by the flow field from the upper configuration, to which must be added the effects of the bow shock wave generated by the lower configuration impinging on the upper configuration and then reflecting back on the lower configuration. (See fig. 22(b).) These interference effects are further substantiated from analysis of schlieren data, some of which are presented in figures 23, 24, and 25.

Some further comments on the nature of the shock interaction effects need to be made. At high supersonic speed (M = 3), figure 23(a) shows that the bow shock wave generated by the upper configuration at $\alpha_1 \approx 0^O$ is relatively weak. At both $\alpha_1 \approx 3^O$ and $\alpha_1 \approx 6^O$ (figs. 23(b) and 23(c)), the bow shock wave is stronger and the classical shock—boundary-layer interaction effects are illustrated. At the highest test angle of attack ($\alpha_1 \approx 12^O$), figure 23(d) indicates similar results; however, one important additional effect should be noted. At this angle of attack, the wake from the lower configuration also interacts strongly with the bow shock wave from the upper configuration and causes the shock wave to bend toward the nose of the lower configuration.

As the Mach number is increased from 3 to 6, the boundary layer is seen to grow appreciably. (Compare fig. 24(a) with 23(a).) At $\alpha_1 \approx 0^O$, $\alpha_1 \approx 3^O$, and $\alpha_1 \approx 6^O$, both figures 24 and 25 illustrate the shock—boundary-layer interaction effects. However, at $\alpha_1 \approx 12^O$ and M = 6, the flow field of the lower configuration has dissipated the shock interaction effects on the lower configuration. This result is seen very clearly in figure 24(d), in which the bow shock wave from the upper configuration only penetrates approximately one-third of the vertical distance between the upper and lower configuration. At the smaller spacing of $h/l_1 = 0.10$, figure 25(d) shows that the bow shock wave was not even in the schlieren photograph. A complete explanation of this flow phenomenon at the largest angle of attack is not presently known. However, it is possible that the

flow between the configurations at this condition is subsonic and that a single strong bow wave lies ahead of both bodies.

CONCLUDING REMARKS

A wind-tunnel investigation has been conducted to examine the aerodynamic interference effects associated with simple three-dimensional aerodynamic configurations placed parallel and in close proximity to each other. The configurations were 10° half-cone bodies that varied in length and were tested with and without simple delta wings. The flat surfaces of the configurations were adjacent to each other during testing. The effects of vertical spacing and relative incidence angle between the configurations were measured, and the resulting data were used to determine the influence of relative body size, nose bluntness, and lifting surfaces on the longitudinal aerodynamic characteristics of the lower configuration at Mach numbers of 3 and 6.

Increasing the size of the upper configuration generally caused a progressive decrease in the normal-force-curve slope and a progressive decrease in the static longitudinal stability of the lower configuration. For the upper configuration larger than the lower configuration, the data suggest some form of progressive blanketing since the normal-force-curve slope decreases to zero and even negative values at some of the vertical spacings investigated. Increasing the incidence angle of the upper configuration generally caused nose-up increments in the pitching-moment coefficient and negative increments in the normal-force coefficient of the lower configuration.

Blunting the nose of the upper and lower configuration or adding delta wings, with a root chord equal to the body length, to either configuration or both the upper and lower configuration had little effect on the longitudinal aerodynamic characteristics of the lower configuration when compared with the data for the pointed-nose configurations or the wingless configurations. However, these effects, which probably depend upon configuration, amount of bluntness, and the wing planform shape and position, have not been thoroughly investigated in this paper.

Langley Research Center,
National Aeronautics and Space Administration,
Langley Station, Hampton, Va., May 22, 1969,
124-07-05-02-23.

REFERENCES

1. Decker, John P.:   An Exploratory Experimental and Analytical Study of Separating
   Two Parallel Lifting Stages of a Reusable Launch Vehicle at Mach Numbers of 3
   and 6.   M.A.E. Thesis, Univ. of Virginia, 1968.

2. Decker, John P.; and Gera, Joseph: An Exploratory Study of Parallel-Stage Separation
   of Reusable Launch Vehicles.   NASA TN D-4765, 1968.

3. Stokes, George M.:   Description of a 2-Foot Hypersonic Facility at the Langley
   Research Center.   NASA TN D-939, 1961.

TABLE I.- GEOMETRIC CHARACTERISTICS OF CONFIGURATIONS

Configuration B_1:
Length overall, cm 30.48
Reference area, cm^2 . . . . 163.82
Reference length, cm 20.32
Moment reference center (distance from base), cm 10.16
Nose bluntness, percent base radius 0

Configuration B_2:
Length overall, cm 40.64
Reference area, cm^2 . . . . 291.23
Reference length, cm 27.09
Moment reference center (distance from base), cm 13.55
Nose bluntness, percent base radius 0

Configuration B_3:
Length overall, cm 40.64
Reference area, cm^2 . . . . 291.23
Reference length, cm 27.09
Moment reference center (distance from base), cm 13.55
Nose bluntness, percent base radius 0

Configuration B_4:
Length overall, cm 50.80
Reference area, cm^2 . . . . 455.22
Reference length, cm 33.87
Moment reference center (distance from base), cm 16.93
Nose bluntness, percent base radius 0

Configuration B_5:
Length overall, cm 27.43
Reference area, cm^2 . . . . 163.82
Reference length, cm 20.32
Moment reference center (distance from base), cm 10.16
Nose bluntness, percent base radius 10

Configuration B_6:
Length overall, cm 36.58
Reference area, cm^2 . . . . 291.23
Reference length, cm 27.09
Moment reference center (distance from base), cm 13.55
Nose bluntness, percent base radius 10

Configuration B_1W_2:
Length overall, cm 30.48
Reference area, cm^2 . . . . 338.14
Reference length, cm 20.32
Moment reference center (distance from base), cm 10.16
Nose bluntness, percent base radius 0

Configuration B_2W_2:
Length overall, cm 40.64
Reference area, cm^2 . . . . 601.14
Reference length, cm 27.09
Moment reference center (distance from base), cm 13.55
Nose bluntness, percent base radius 0

11
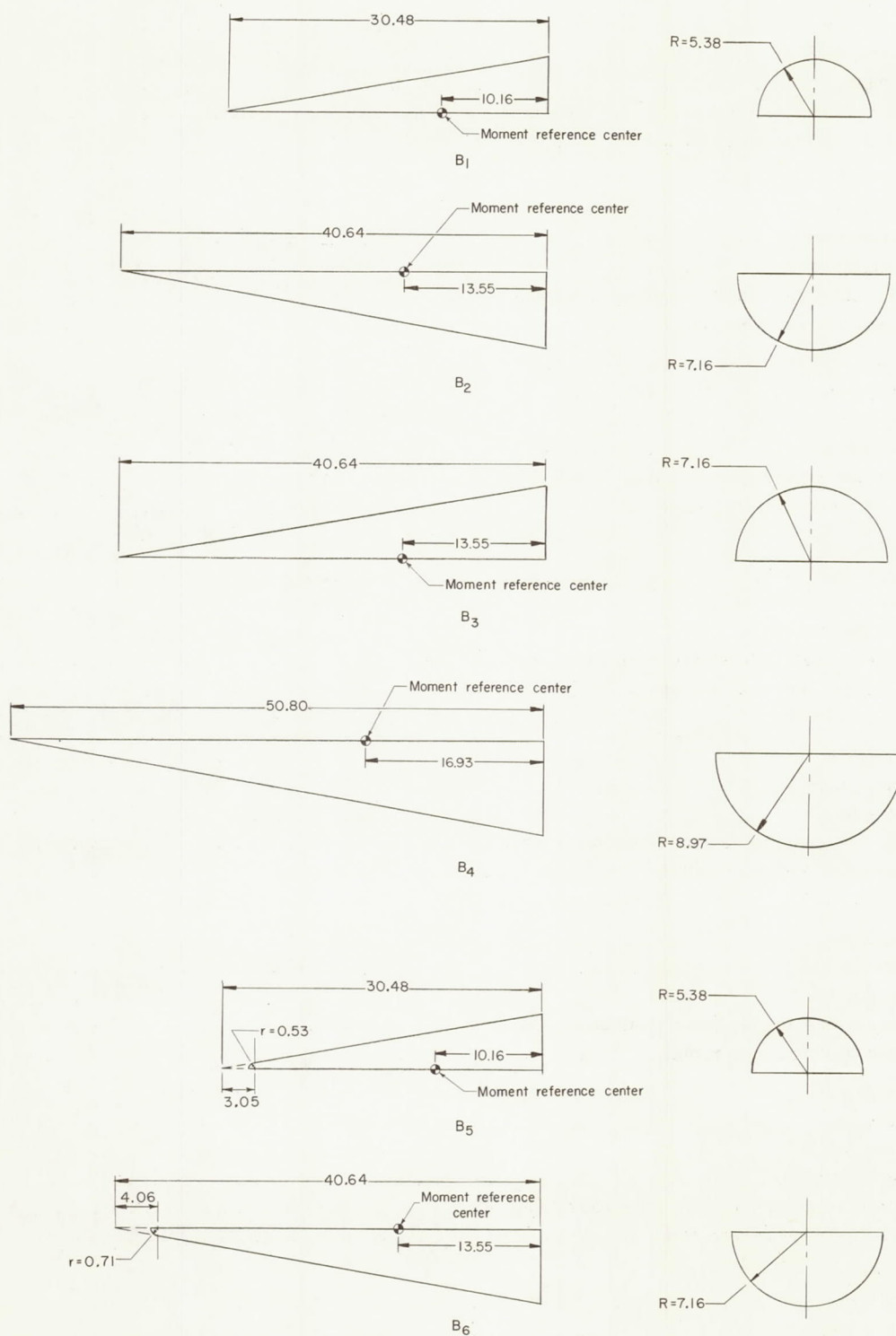
Figure 1.- Drawings of configurations used in wind-tunnel investigation. All dimensions are in centimeters.
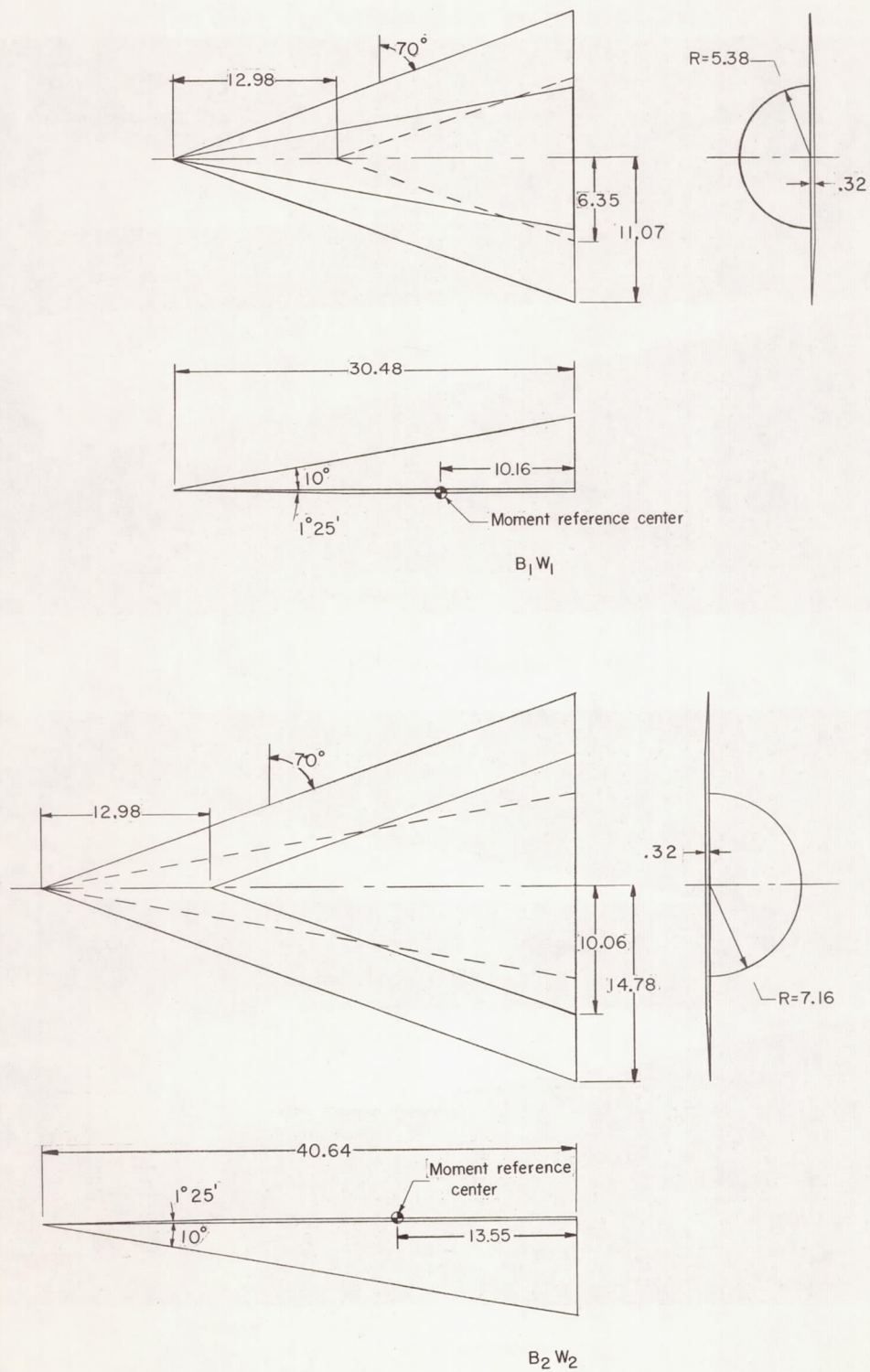
$B_1 W_1$

$B_2 W_2$

Figure 1.- Concluded.
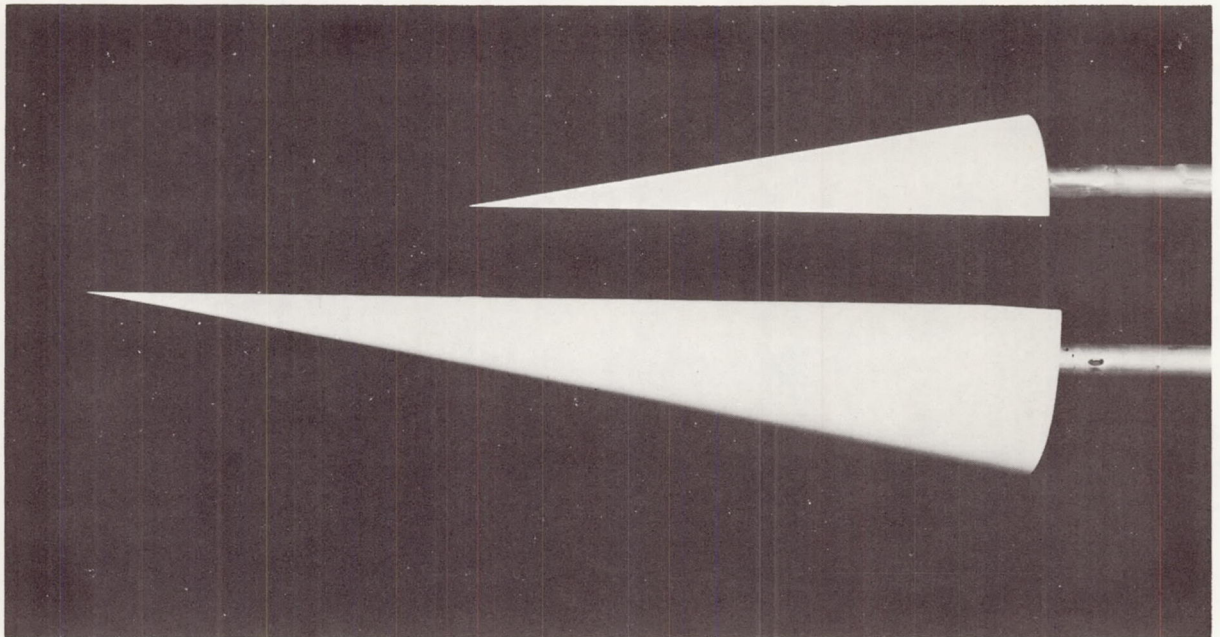
(a) B_4 in presence of B_1.   L-65-5767
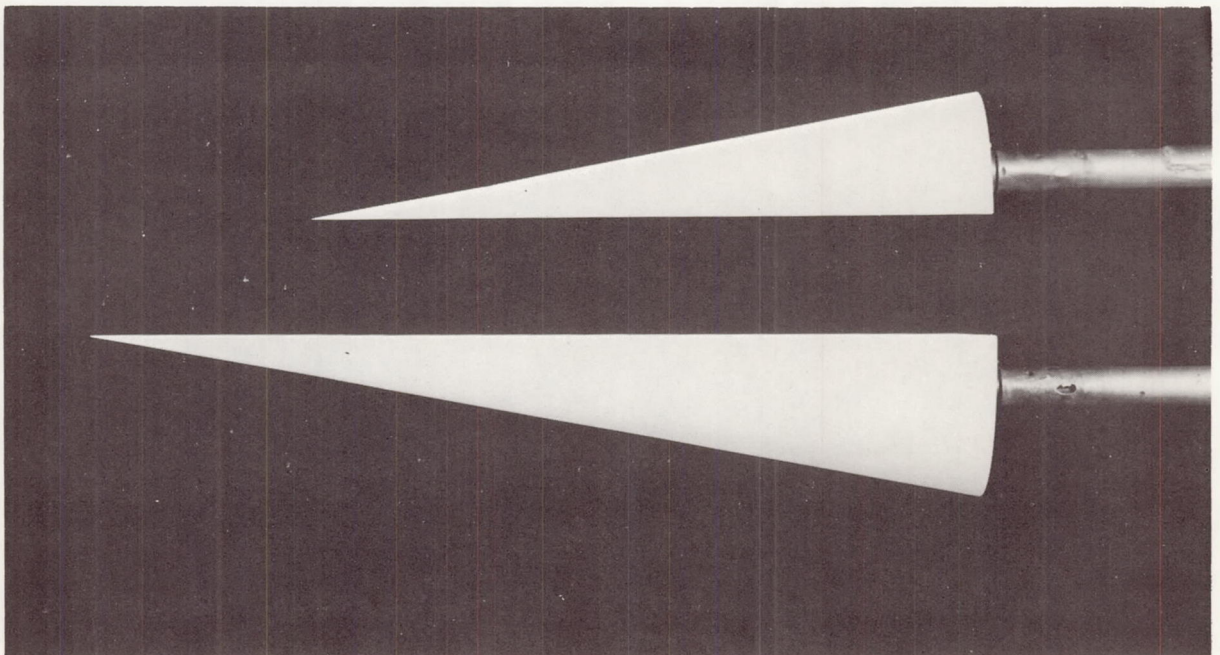
(b) B_2 in presence of B_1.   L-65-5766

Figure 2.- Photographs of lower configurations mounted in presence of upper configurations.
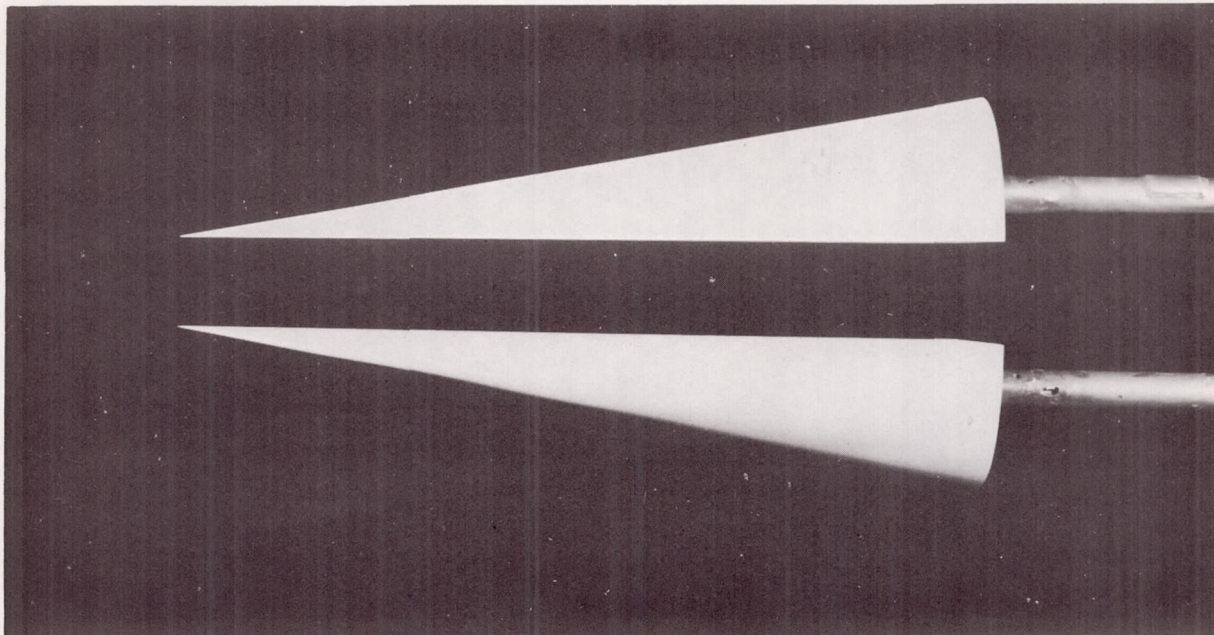
(c) B_2 in presence of B_3. L-65-5772
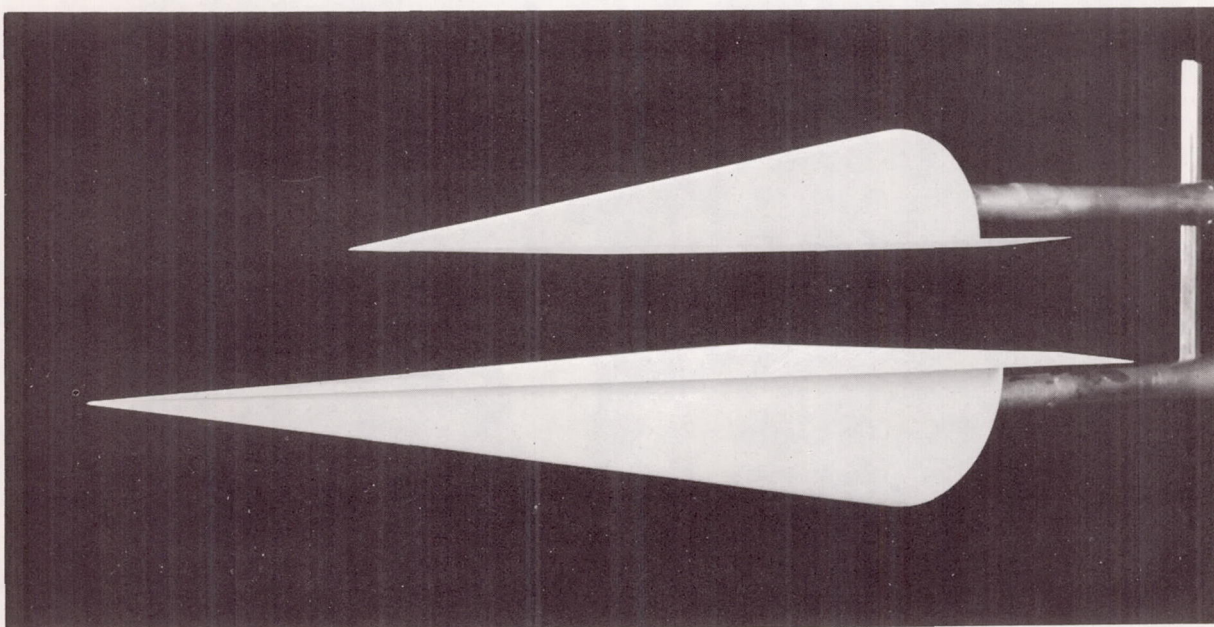
(d) B_2W_2 in presence of B_1W_1. L-65-5759

Figure 2.- Concluded.
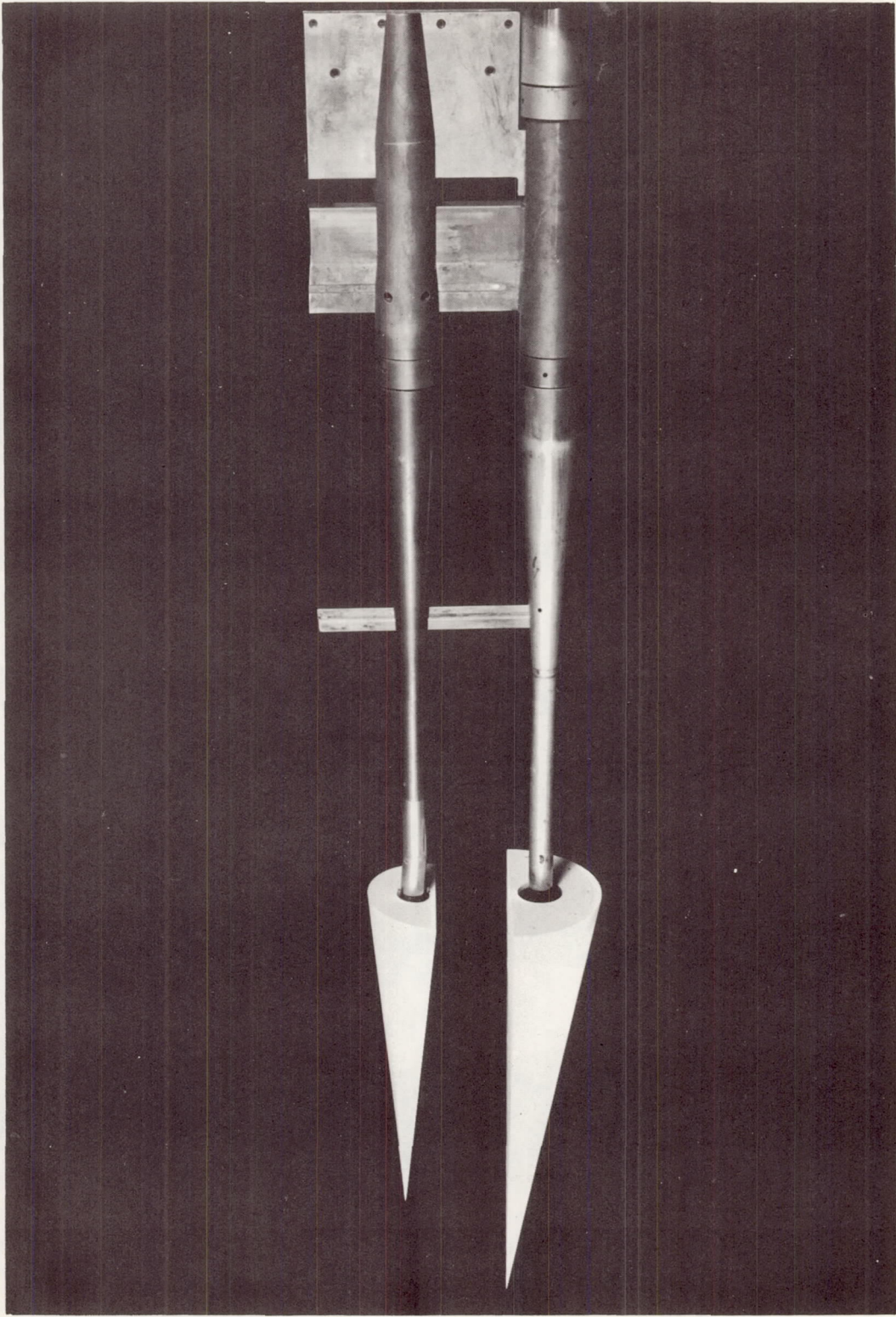
Figure 3.- Photograph of configurations on support mechanism.
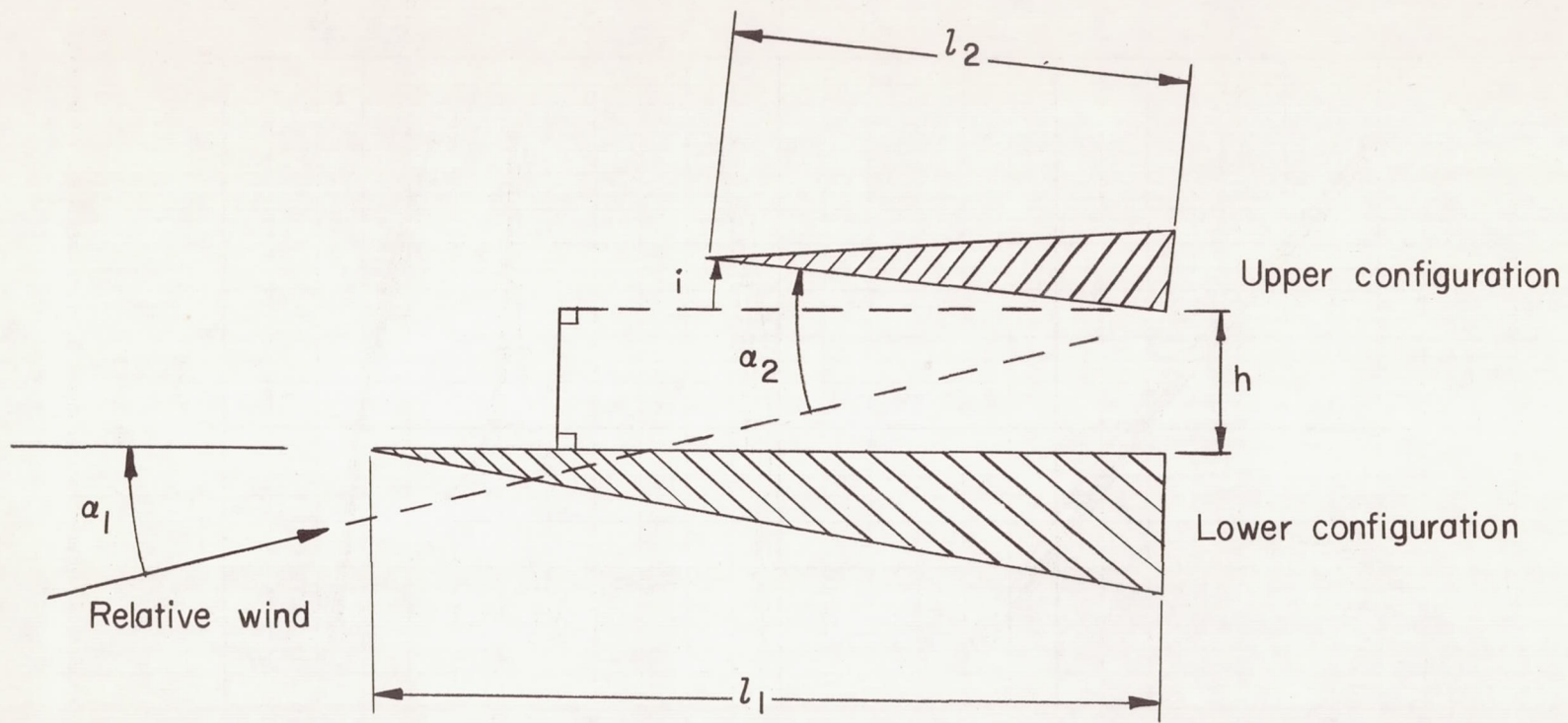
Figure 4.- Nomenclature and general arrangement of upper and lower configurations during wind-tunnel investigation.

(a) M = 3.
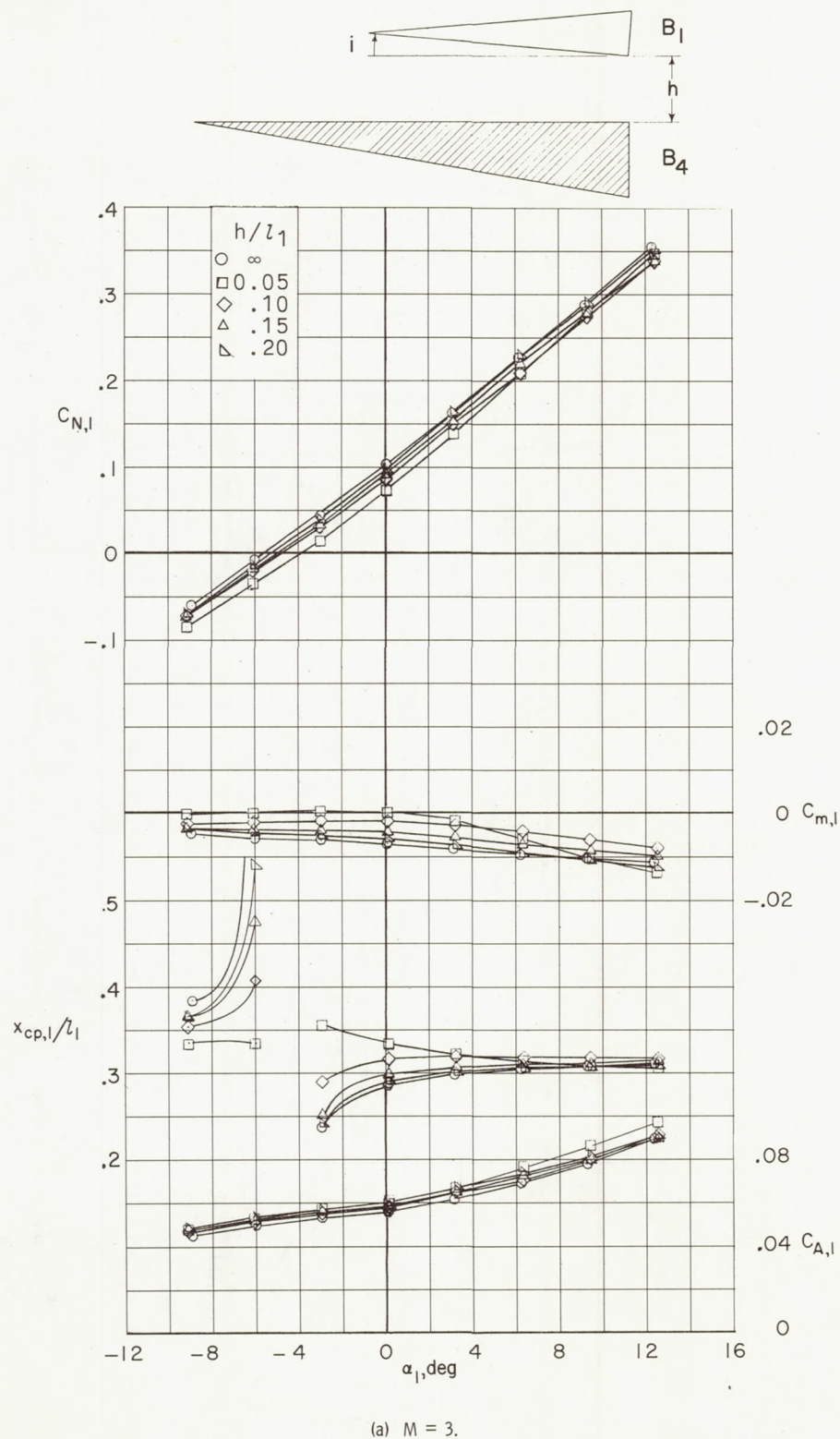
Figure 5.- Longitudinal aerodynamic characteristics of B_4 in presence of B_1. $i = 0^o$; $l_2/l_1 = 0.60$.
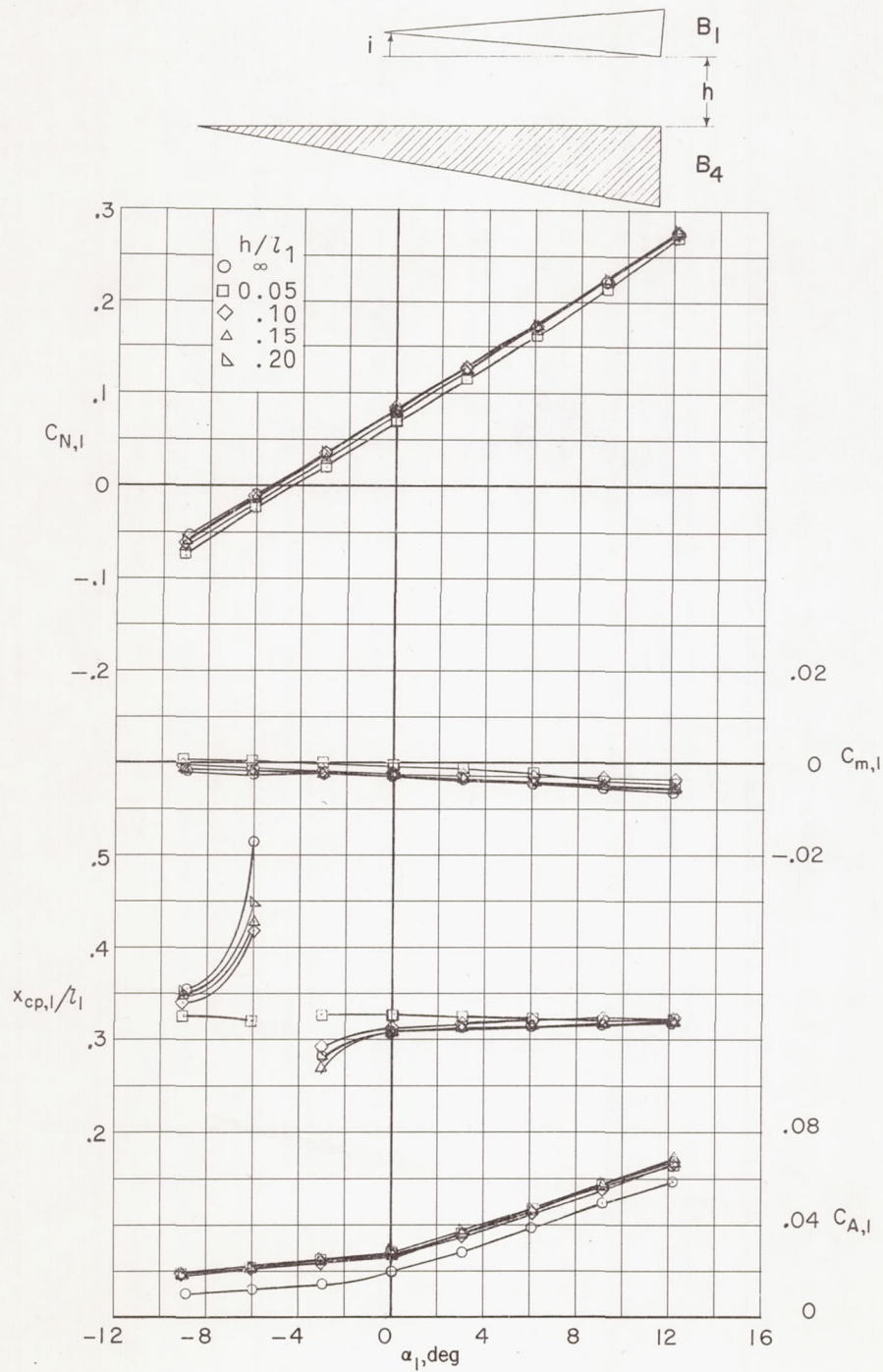
(b) M = 6.

Figure 5.- Concluded.
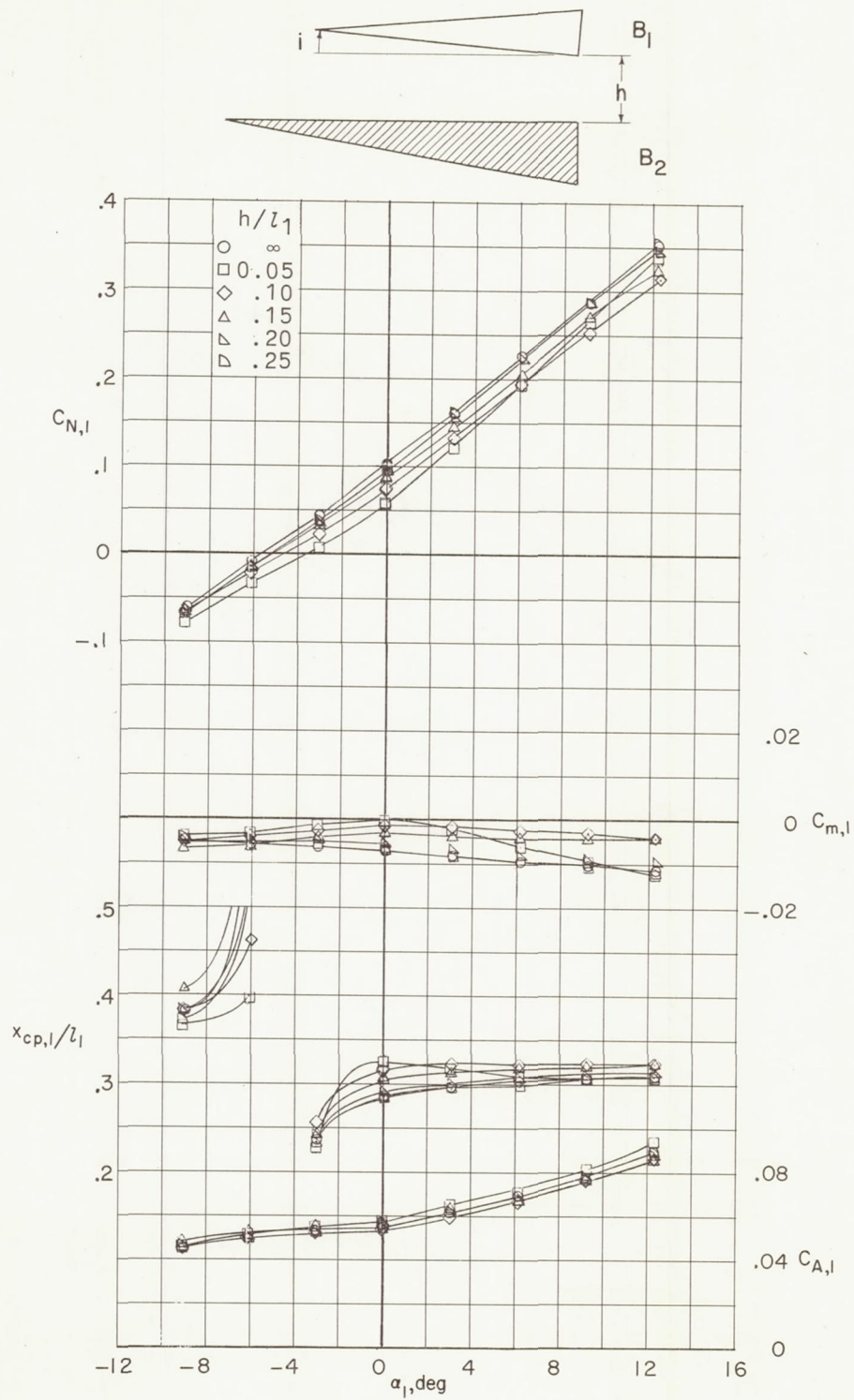
(a) M = 3.

Figure 6.- Longitudinal aerodynamic characteristics of B_2 in presence of B_1. $i = 0^0$; $l_2/l_1 = 0.75$.
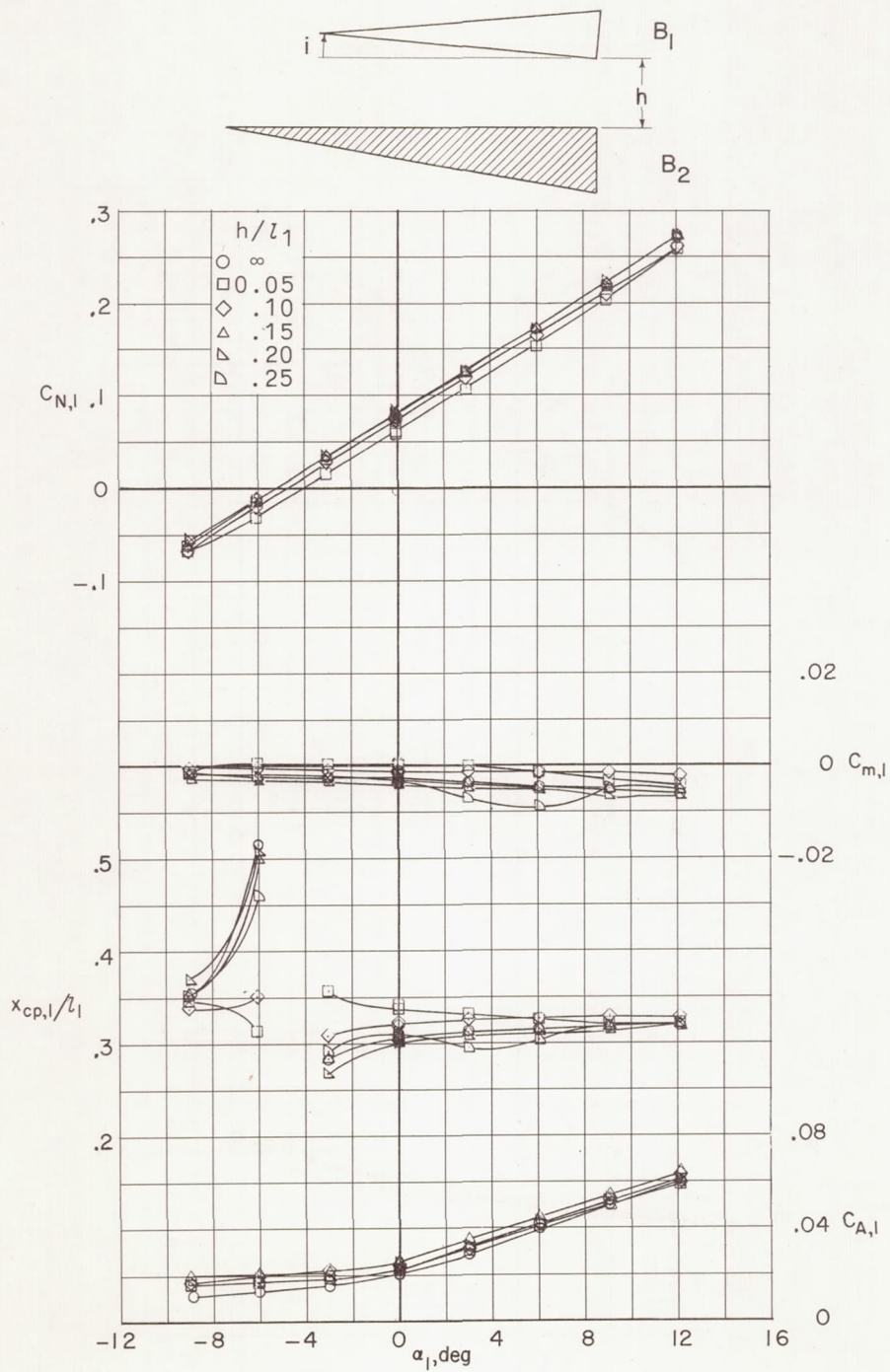
(b) M = 6.

Figure 6.- Concluded.

(a) M = 3.
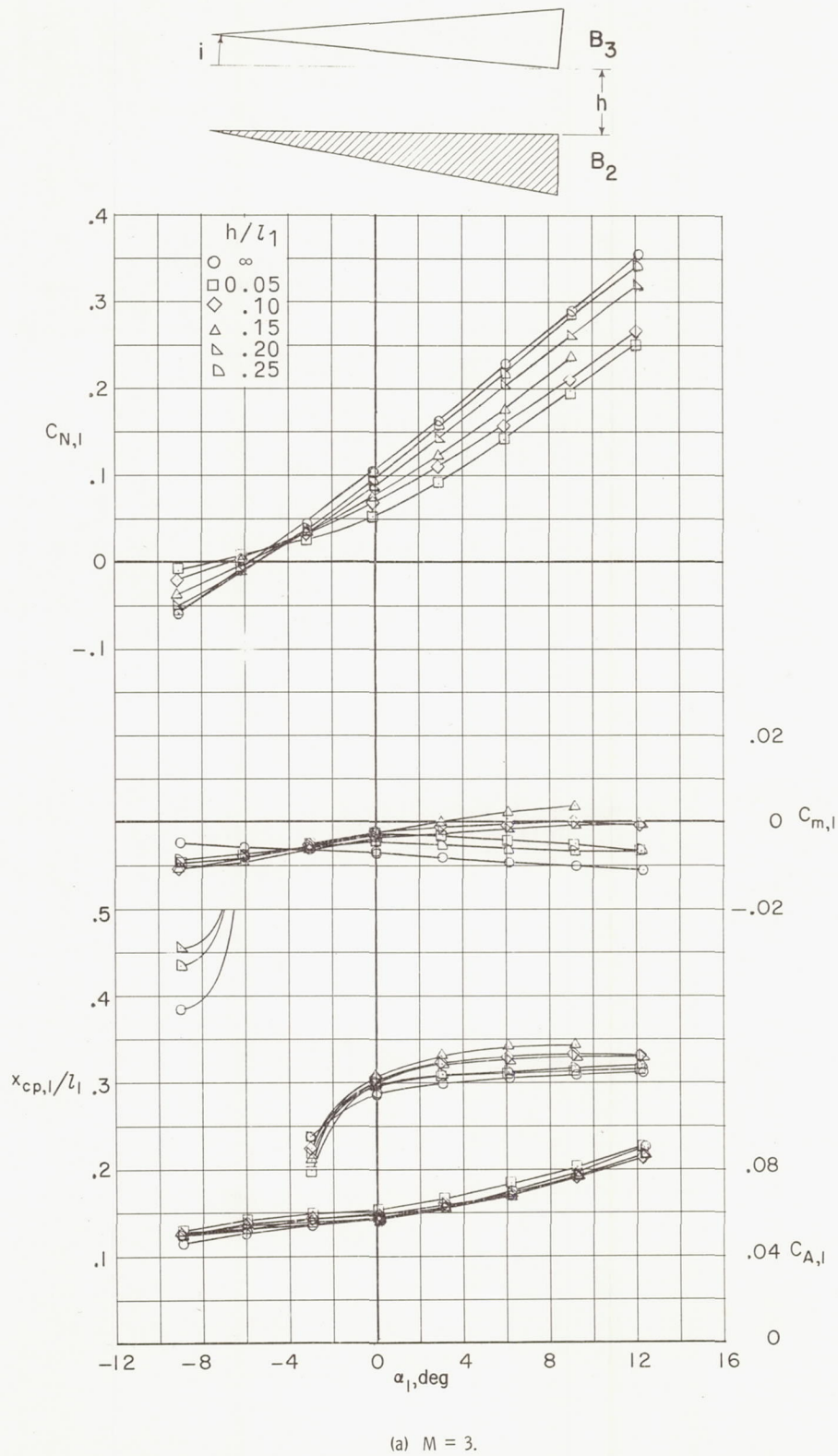
Figure 7.- Longitudinal aerodynamic characteristics of B_2 in presence of B_3. i = 0°; l_2/l_1 = 1.00.

22
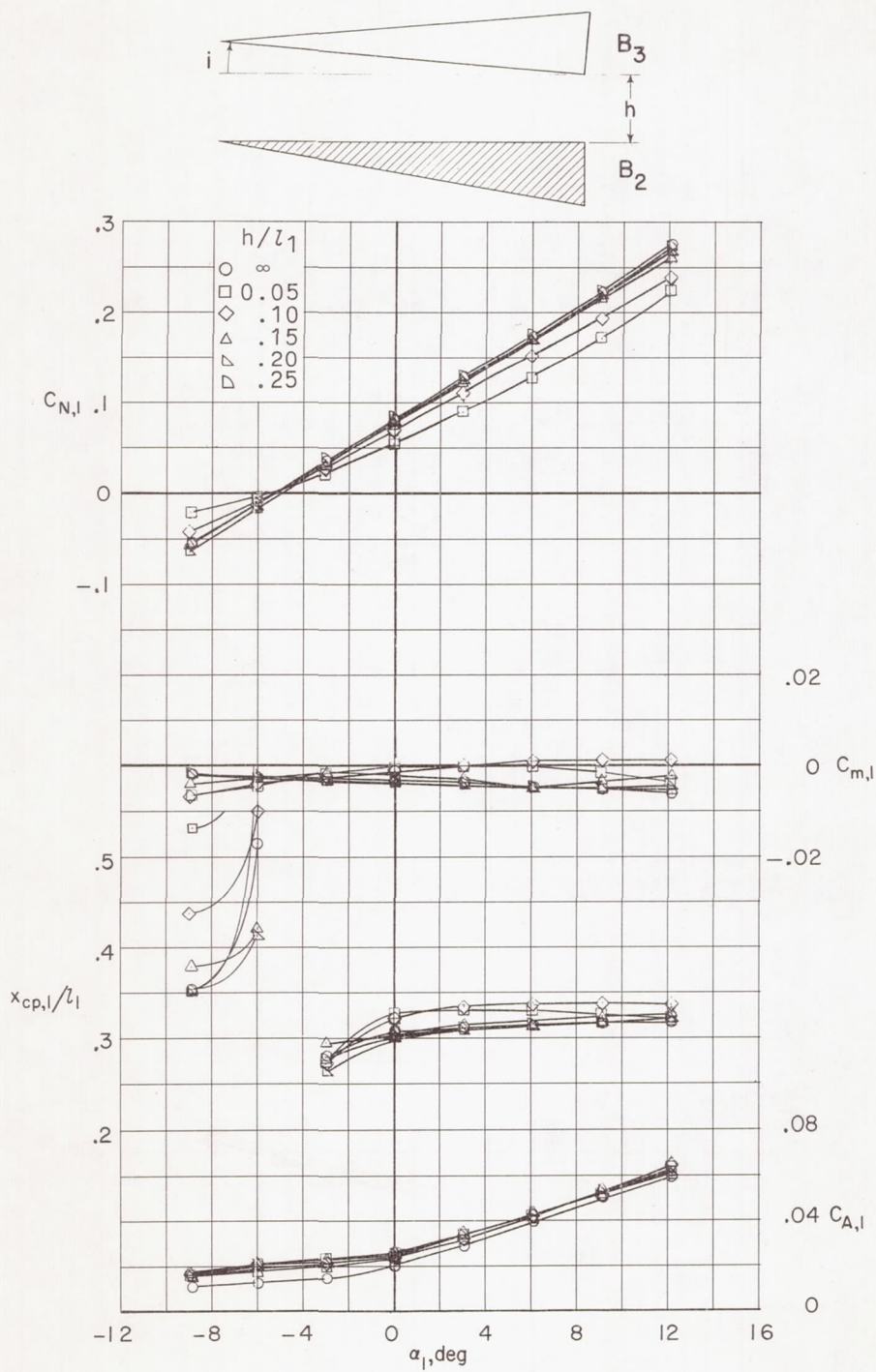
(b) M = 6.

Figure 7.- Concluded.
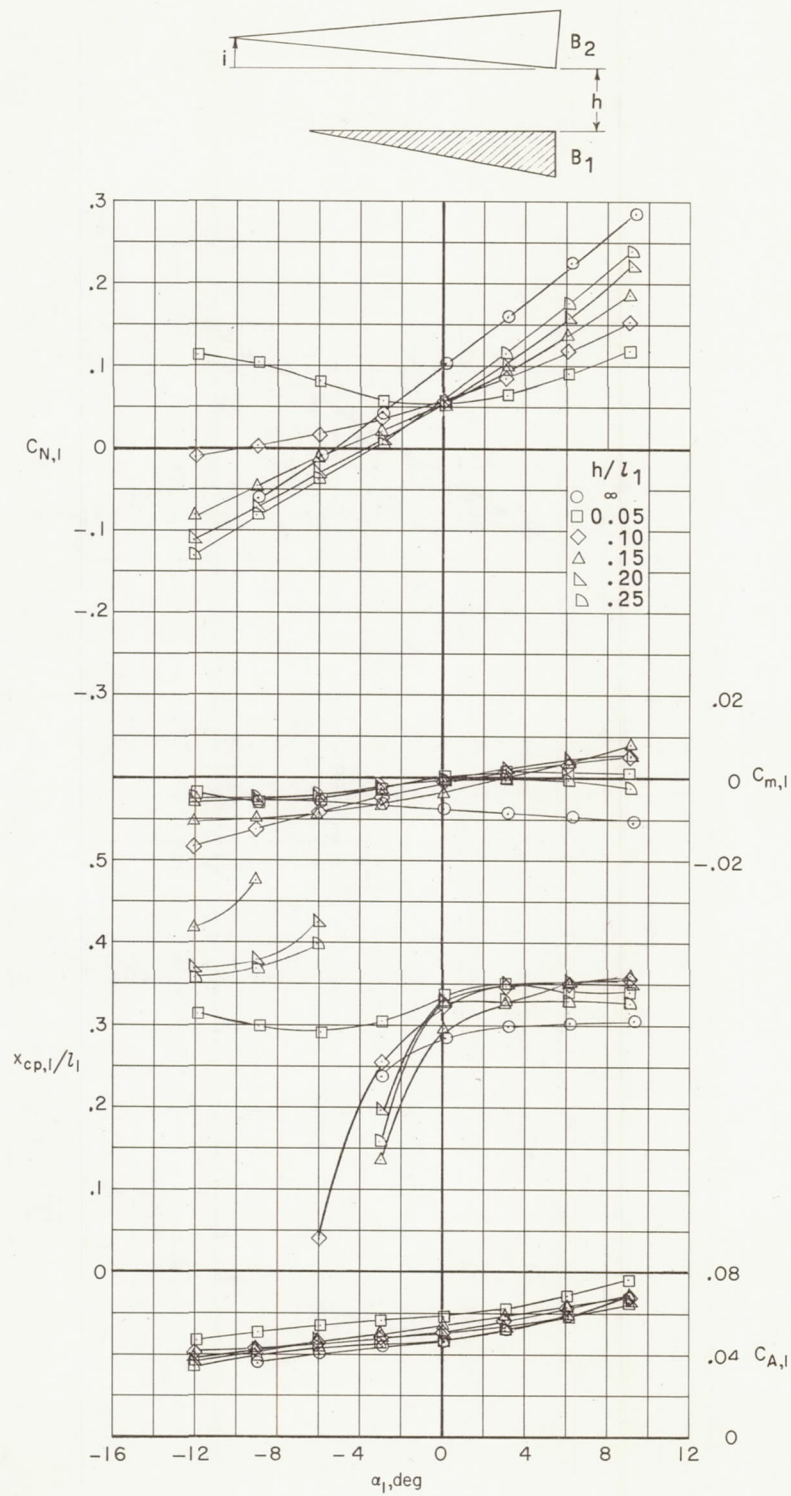
(a) M = 3.

Figure 8.- Longitudinal aerodynamic characteristics of B_1 in presence of B_2. $i = 0^0$; $l_2/l_1 = 1.33$.
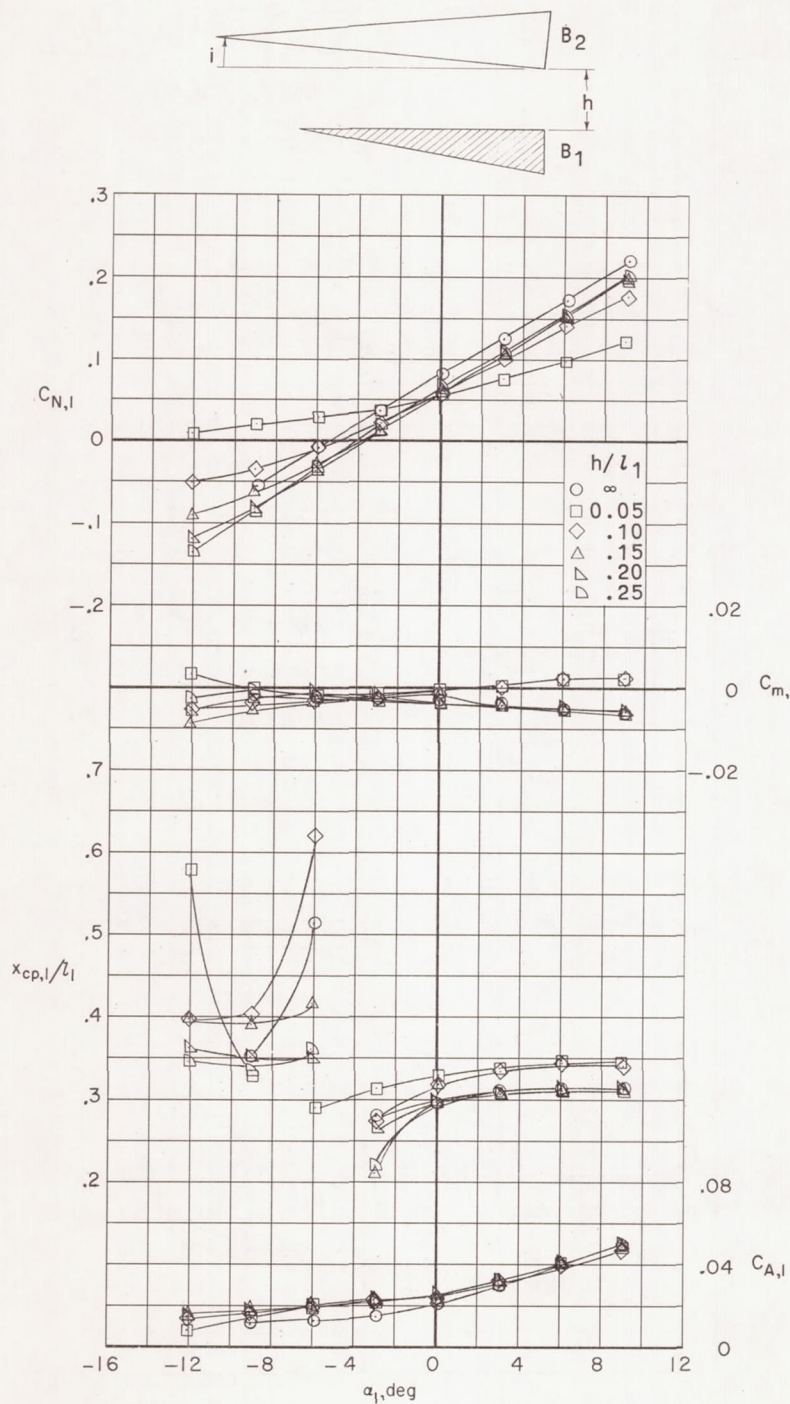
(b) M = 6.

Figure 8.- Concluded.
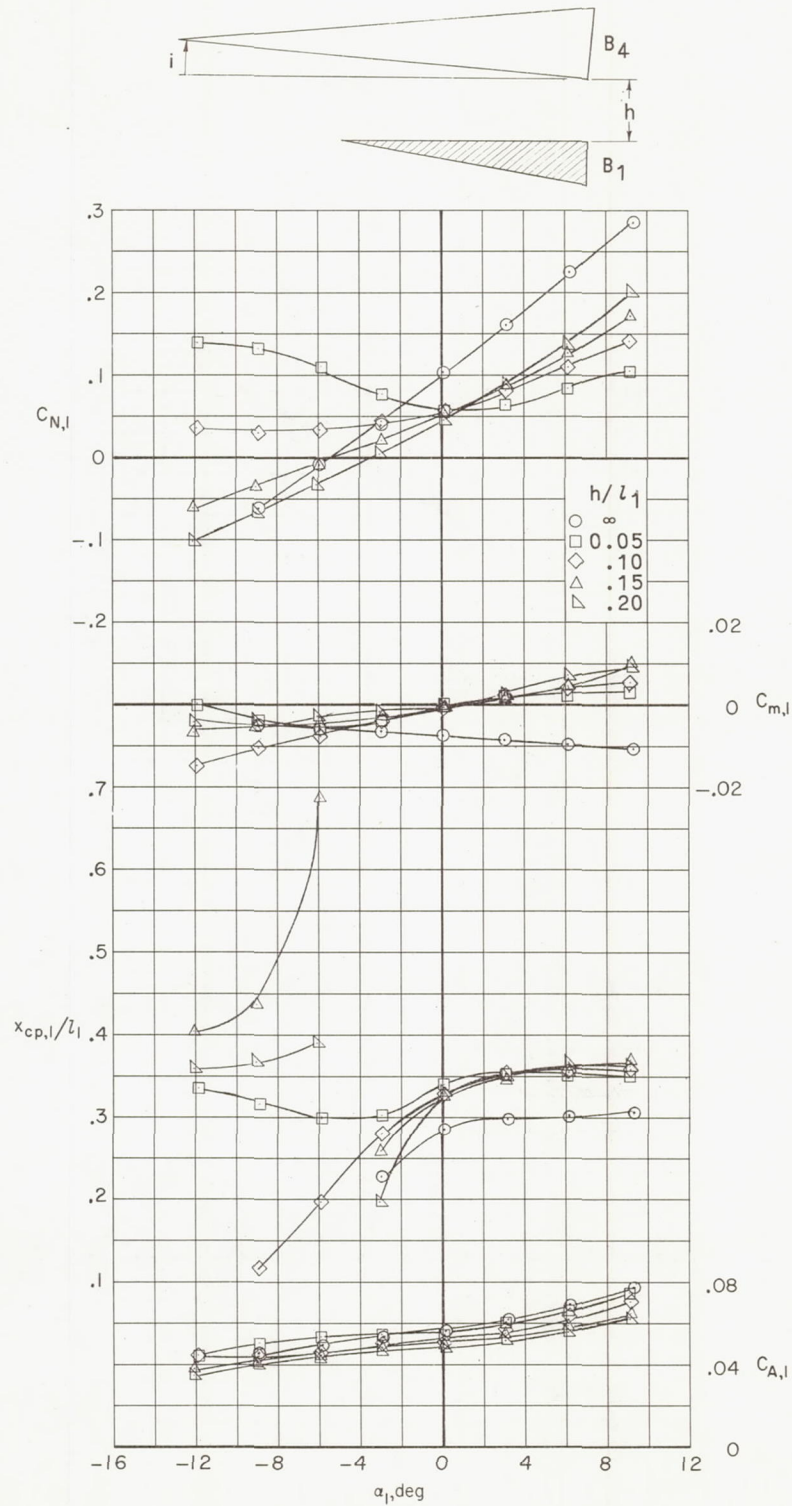
(a) M = 3.

Figure 9.- Longitudinal aerodynamic characteristics of B_1 in presence of B_4. $i = 0^0$; $l_2/l_1 = 1.67$.
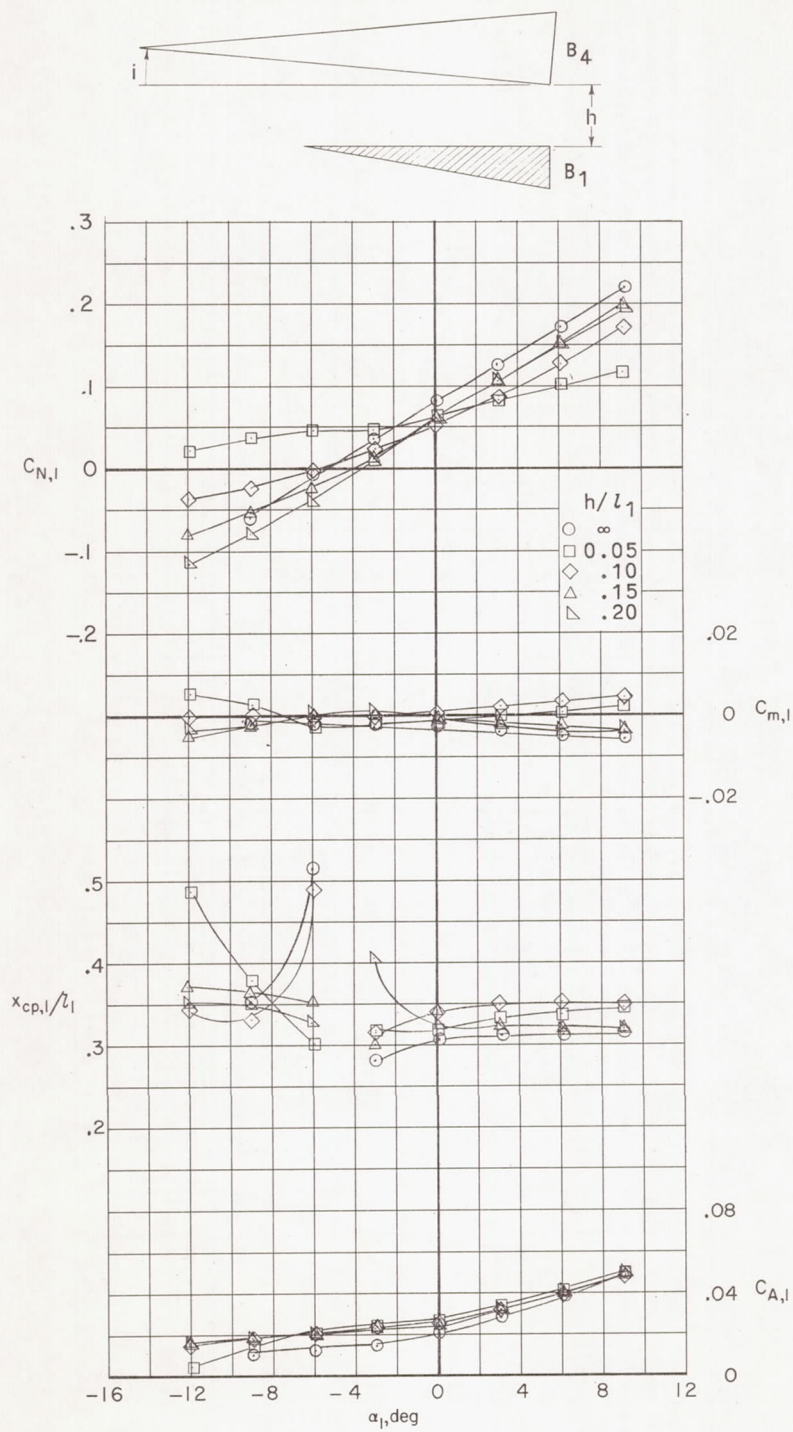
(b) M = 6.

Figure 9.- Concluded.
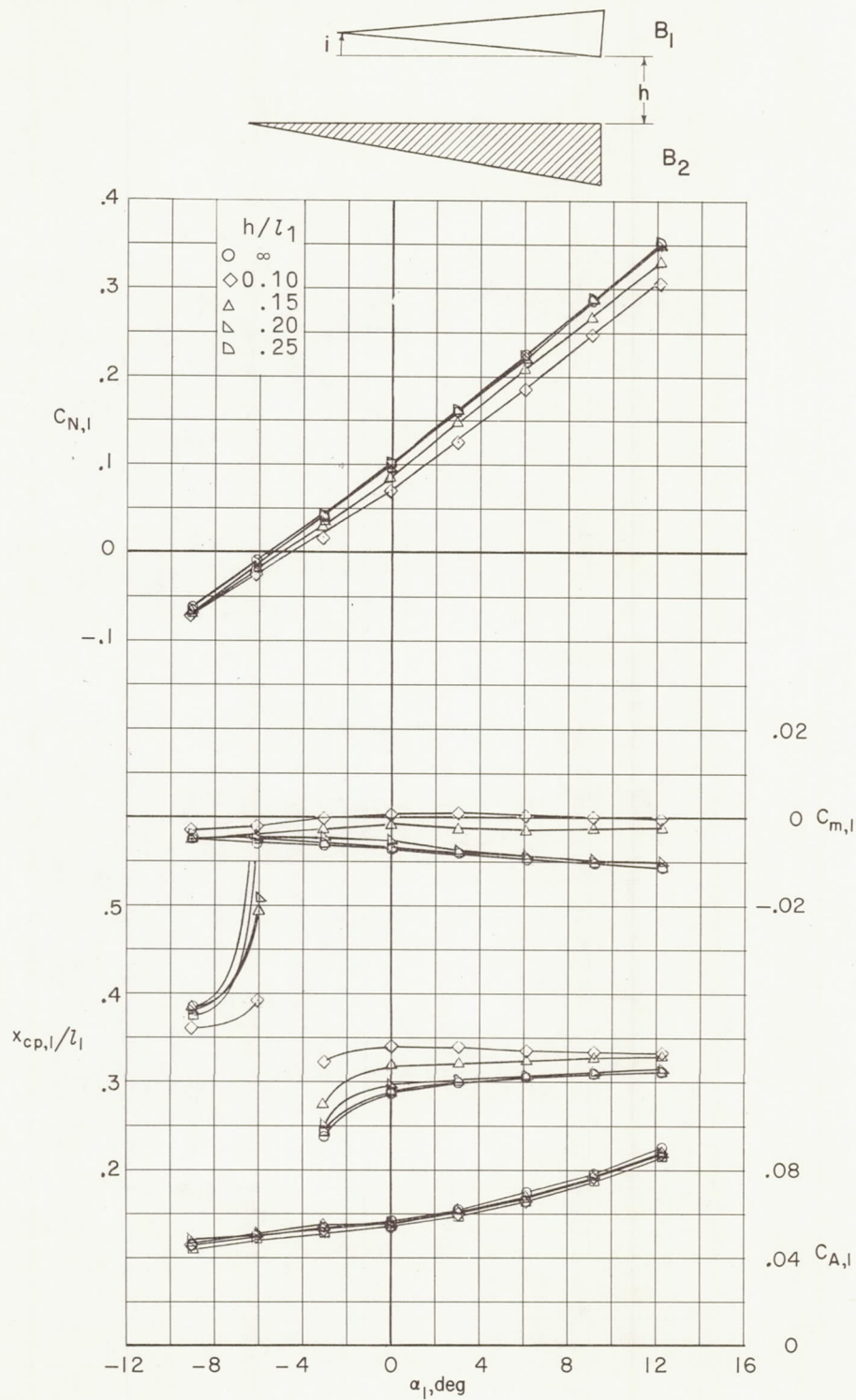
(a) M = 3.

Figure 10.- Longitudinal aerodynamic characteristics of B_2 in presence of B_1. i = 2°; $l_2/l_1 = 0.75$.
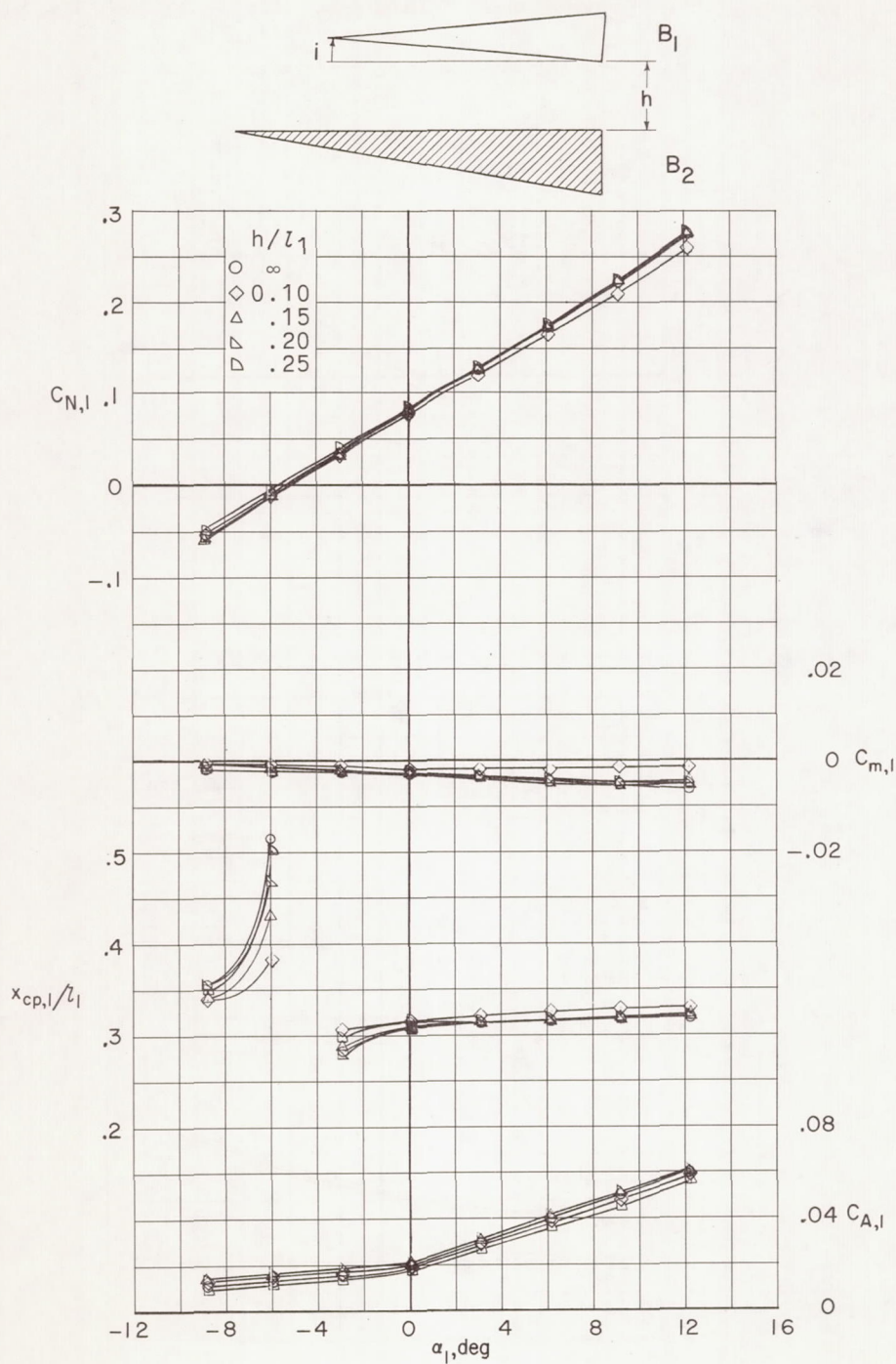
(b) M = 6.

Figure 10.- Concluded.
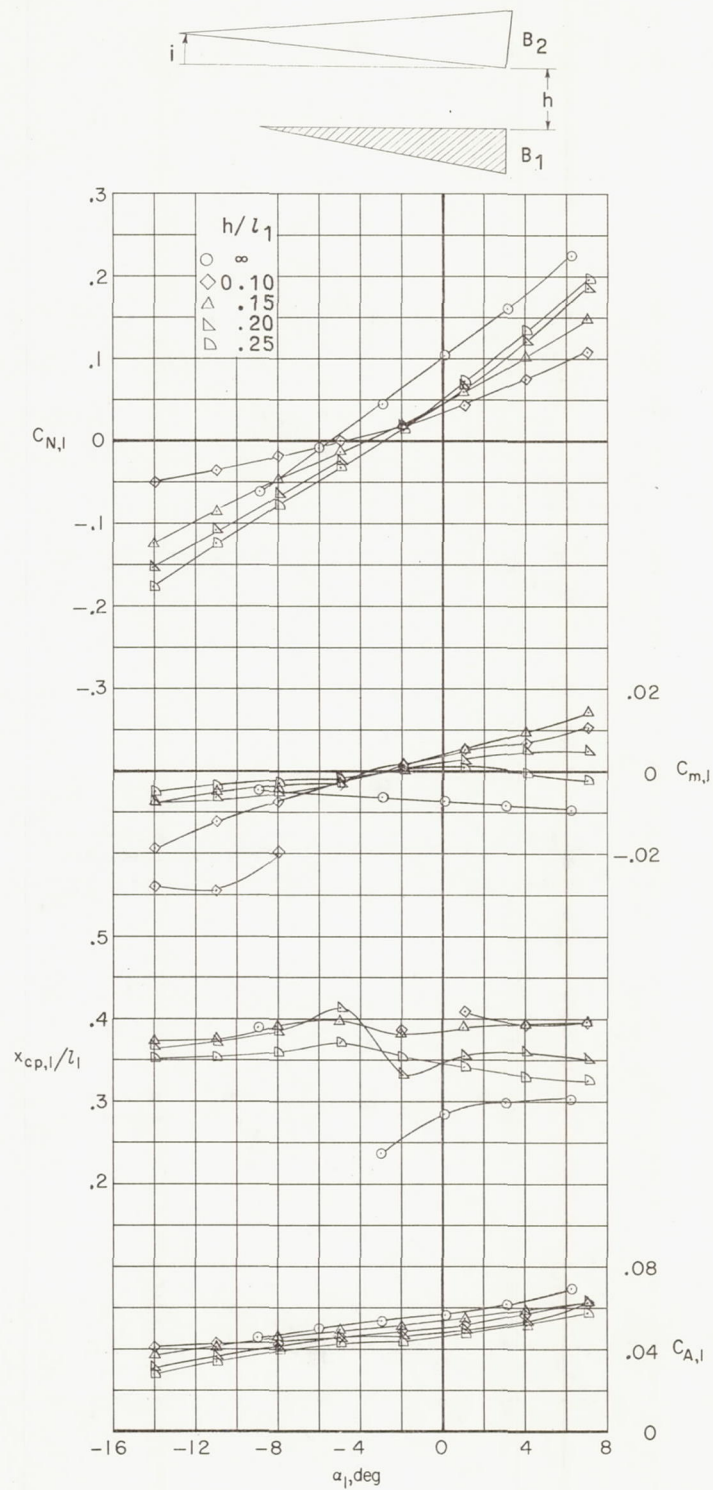
(a) M = 3.

Figure 11.- Longitudinal aerodynamic characteristics of B_1 in presence of B_2. i = 2^0; l_2/l_1 = 1.33.
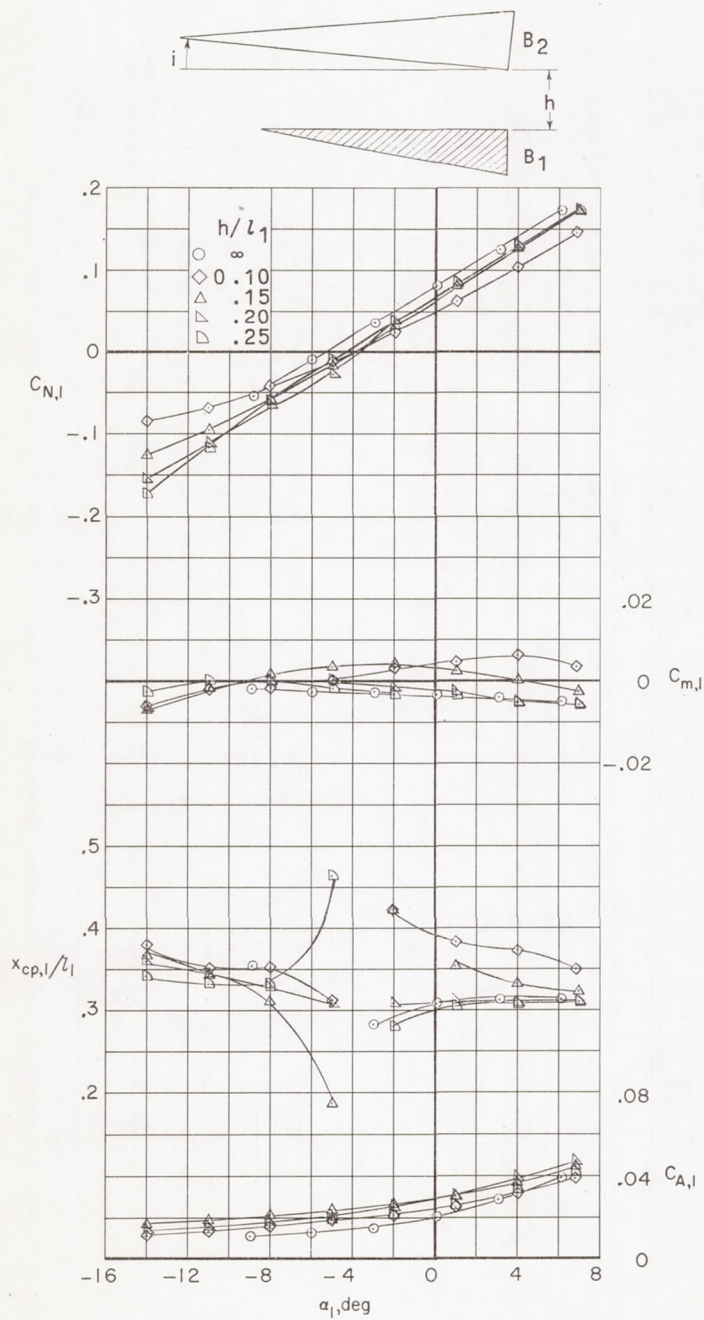
(b) M = 6.

Figure 11.- Concluded.
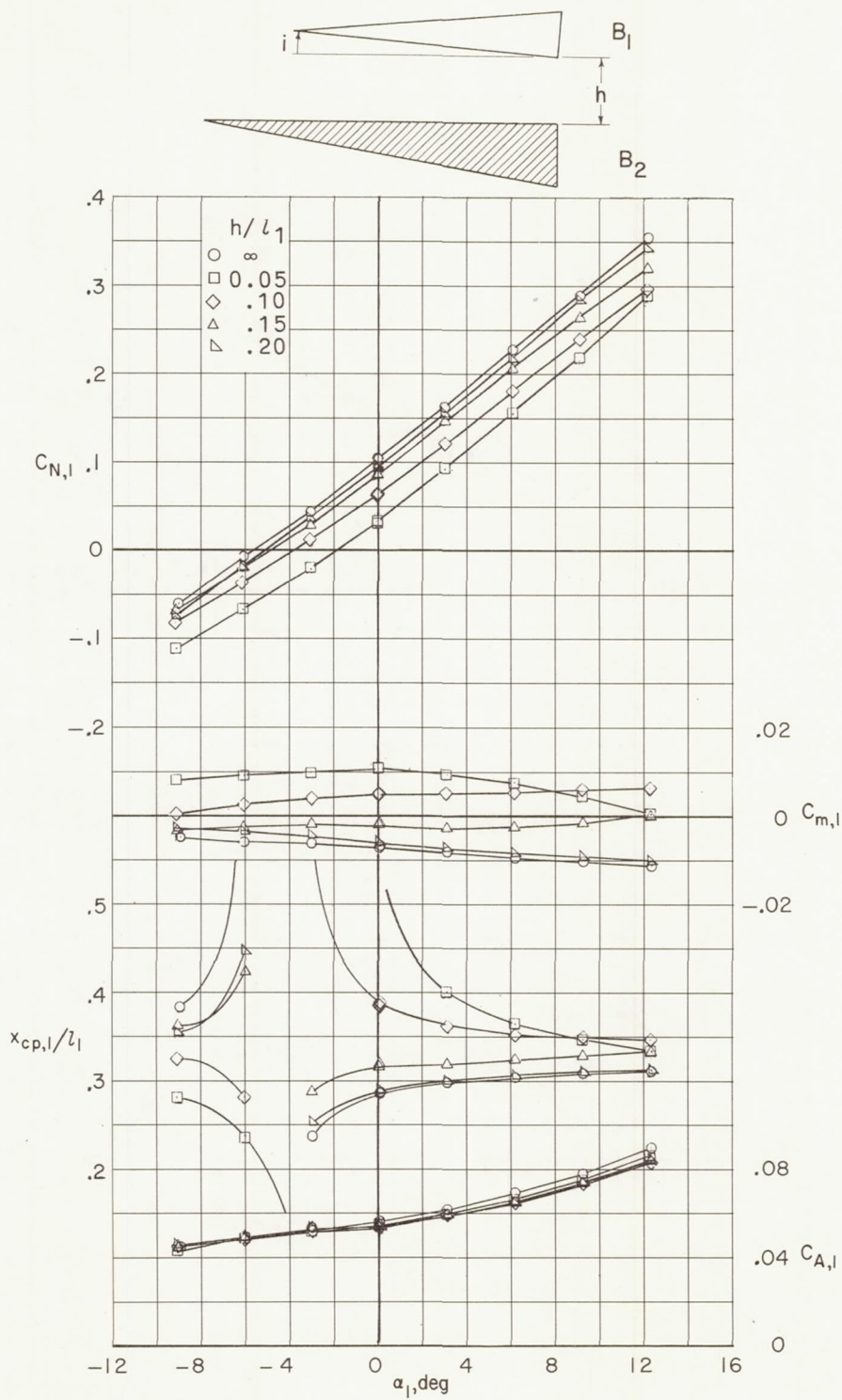
(a) M = 3.

Figure 12.- Longitudinal aerodynamic characteristics of B_2 in presence of B_1. $i = 5^0$; $l_2/l_1 = 0.75$.
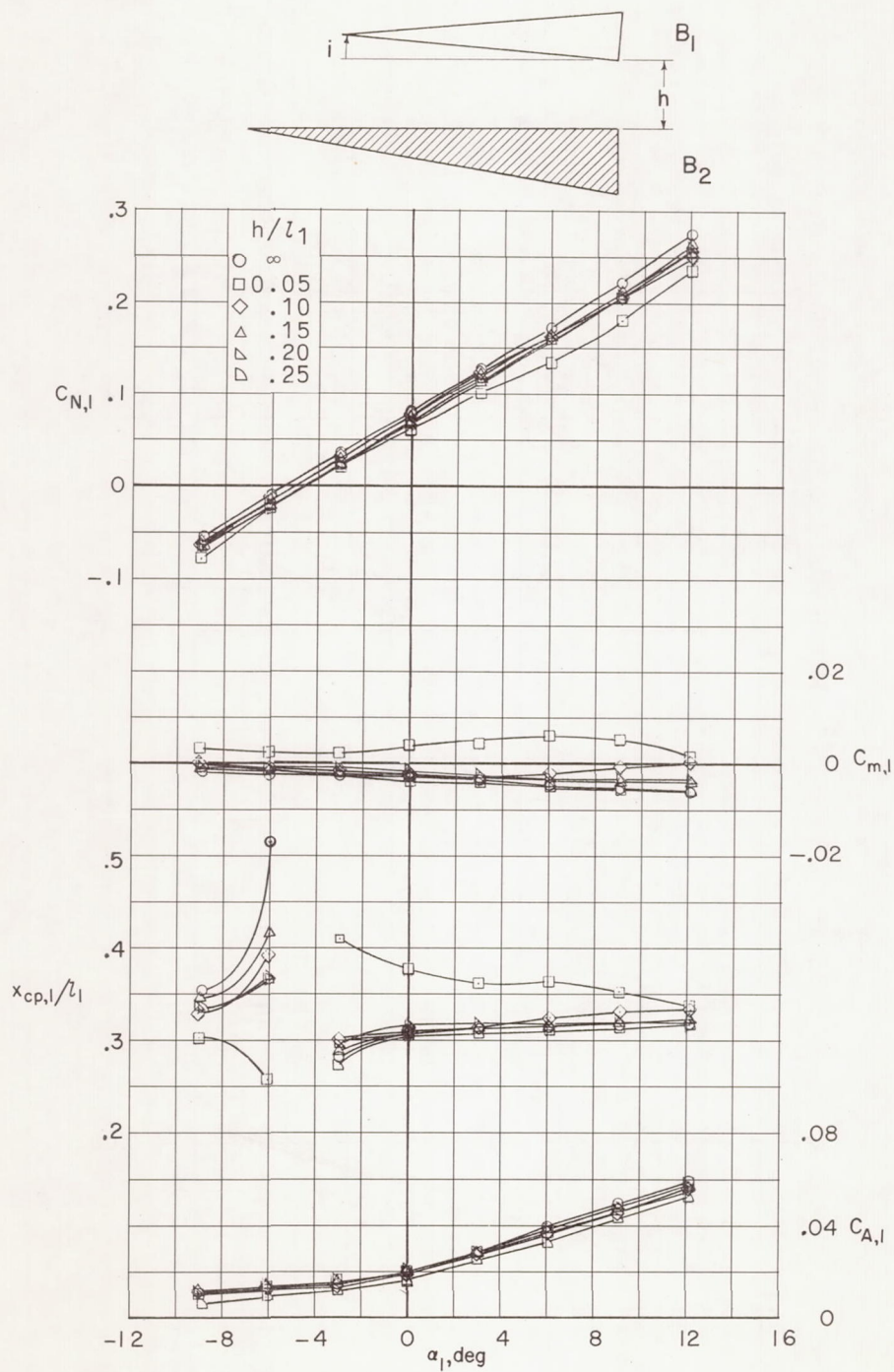
(b) M = 6.

Figure 12.- Concluded.
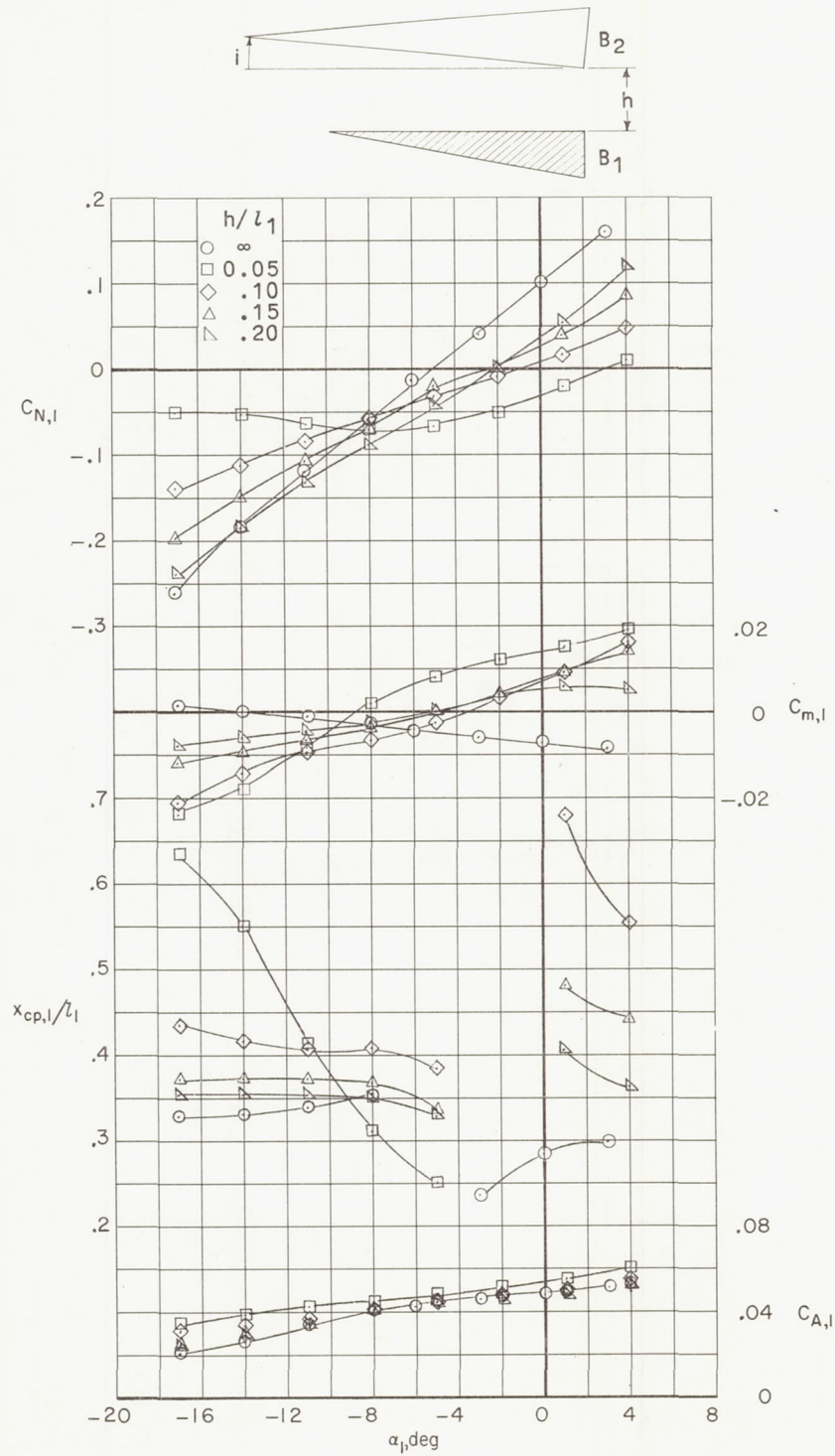
(a) M = 3.

Figure 13.- Longitudinal aerodynamic characteristics of B_1 in presence of B_2. i = 5°; l_2/l_1 = 1.33.
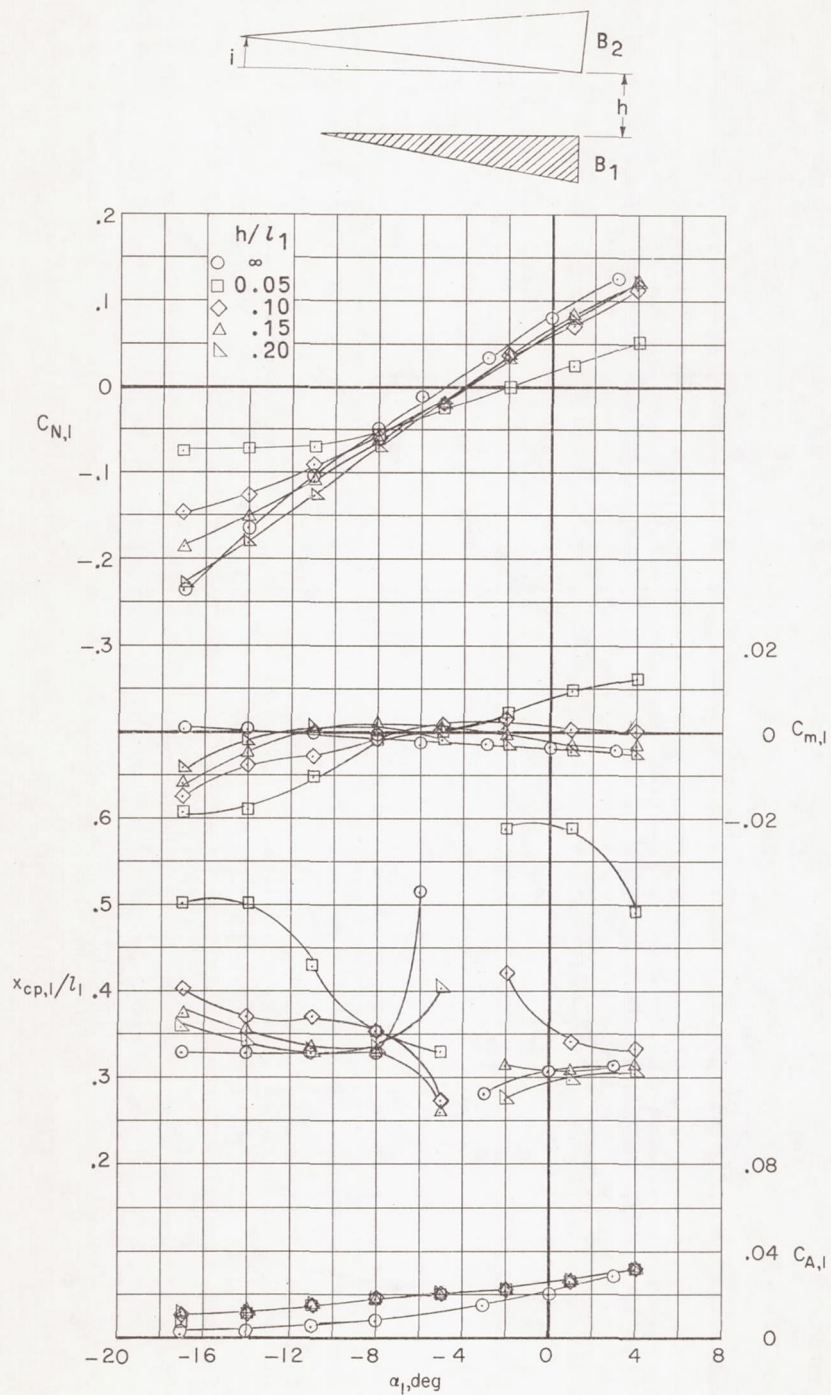
(b) M = 6.

Figure 13.- Concluded.
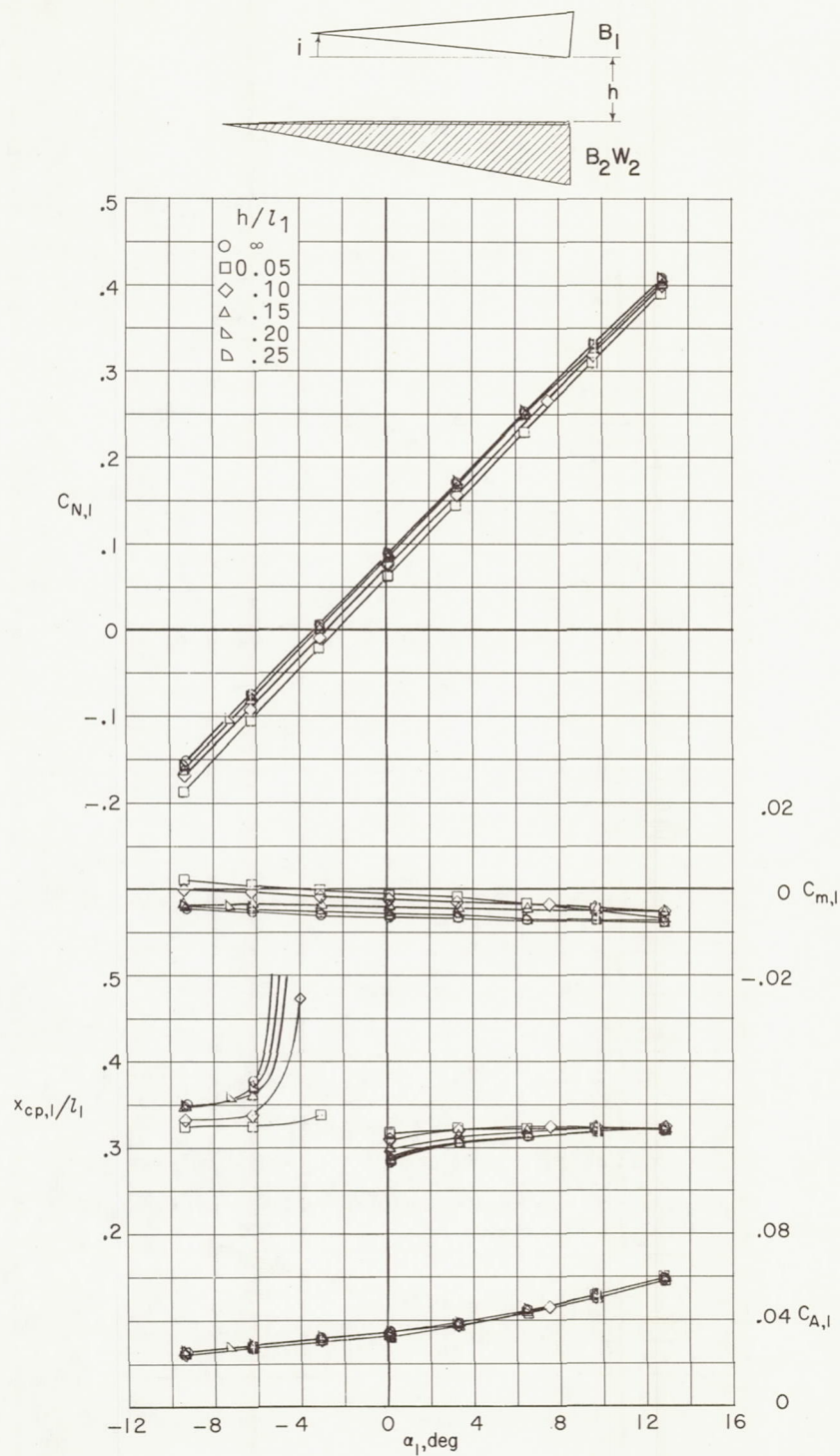
(a) M = 3.

Figure 14.- Longitudinal aerodynamic characteristics of B_2W_2 in presence of B_1. i = 0^0; l_2/l_1 = 0.75.
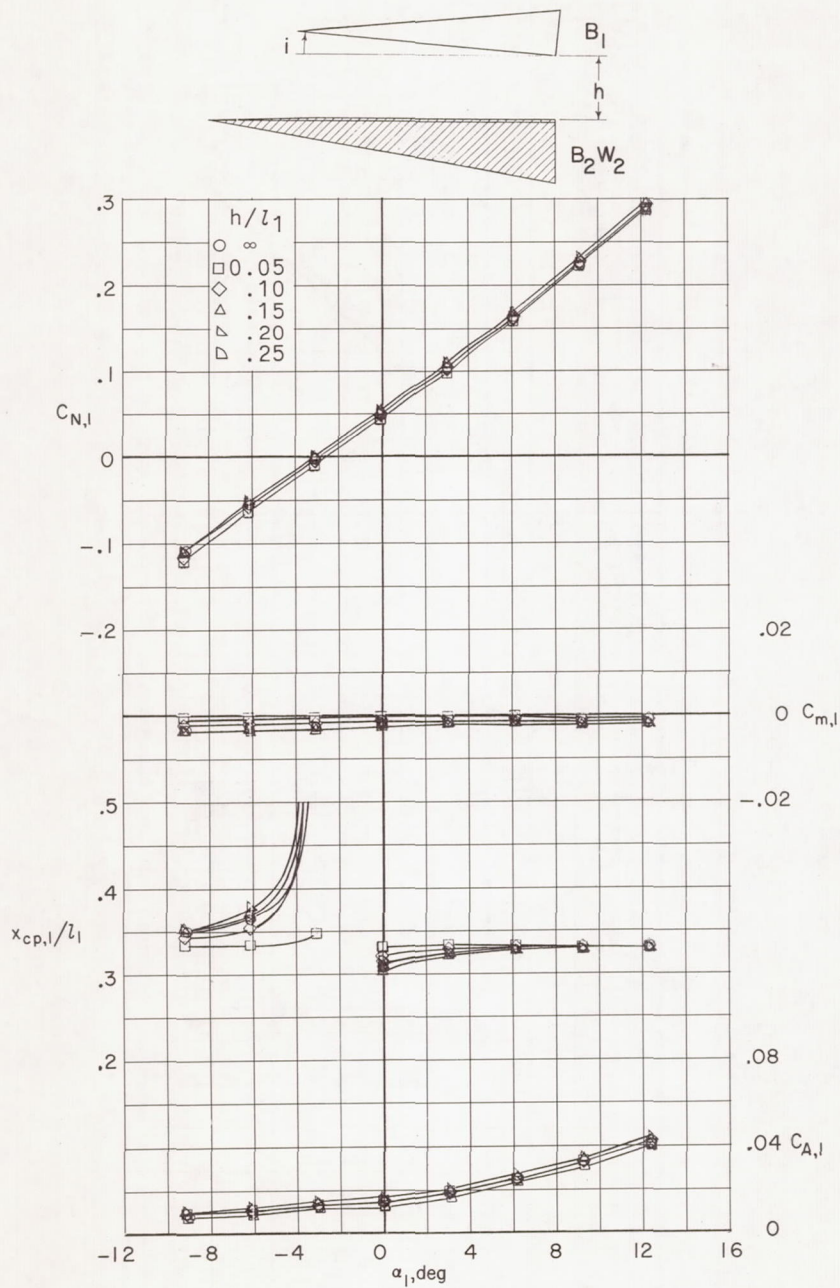
(b) M = 6.

Figure 14.- Concluded.
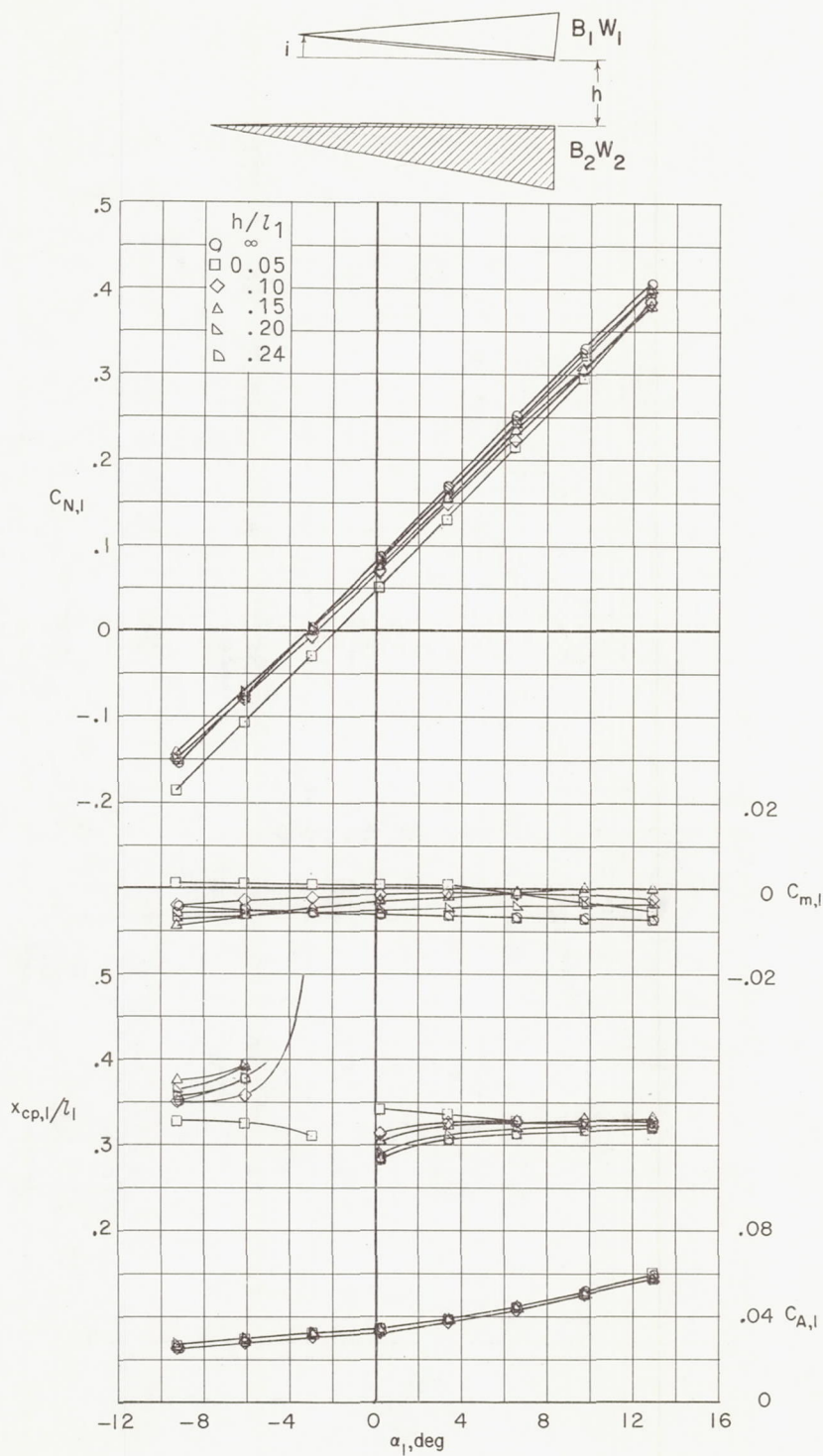
(a) M = 3.

Figure 15.- Longitudinal aerodynamic characteristics of B_2W_2 in presence of B_1W_1. i = 0^0; l_2/l_1 = 0.75.
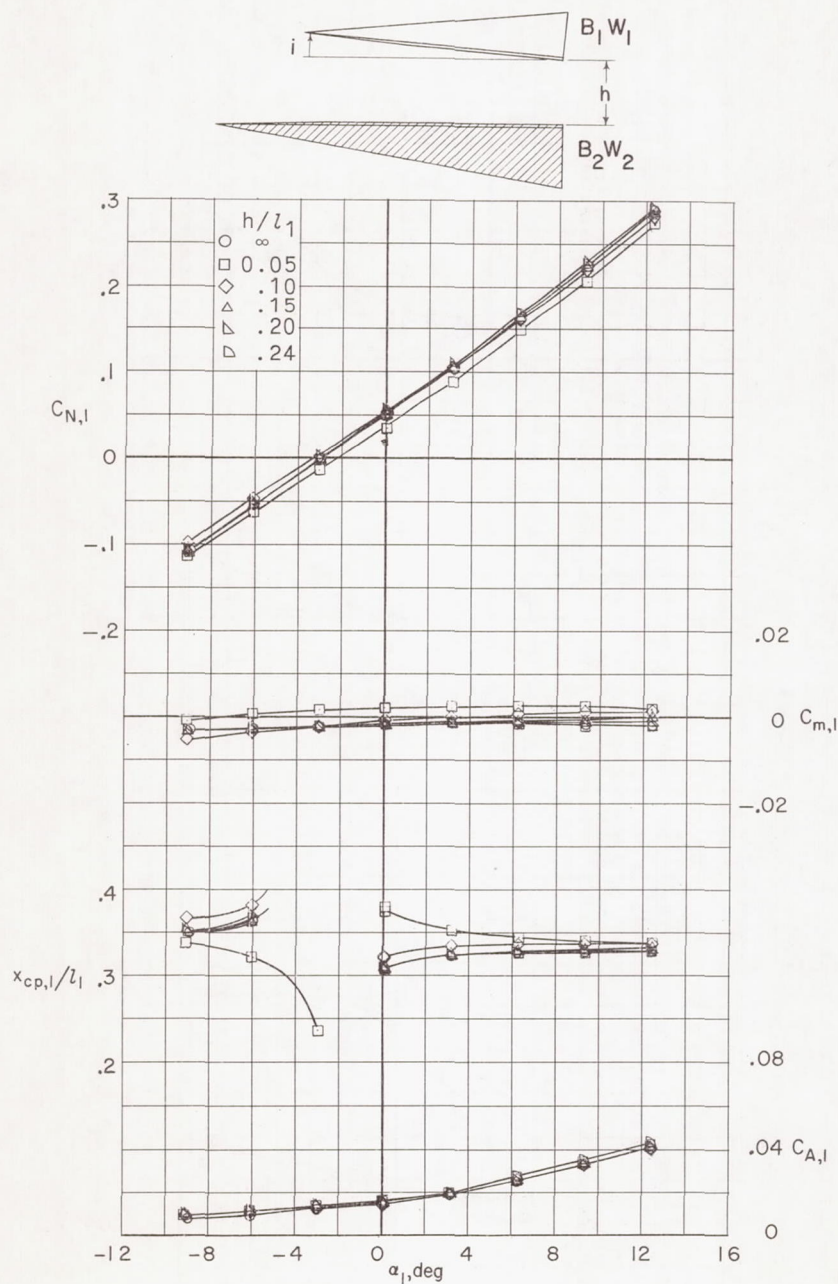
(b) M = 6.

Figure 15.- Concluded.
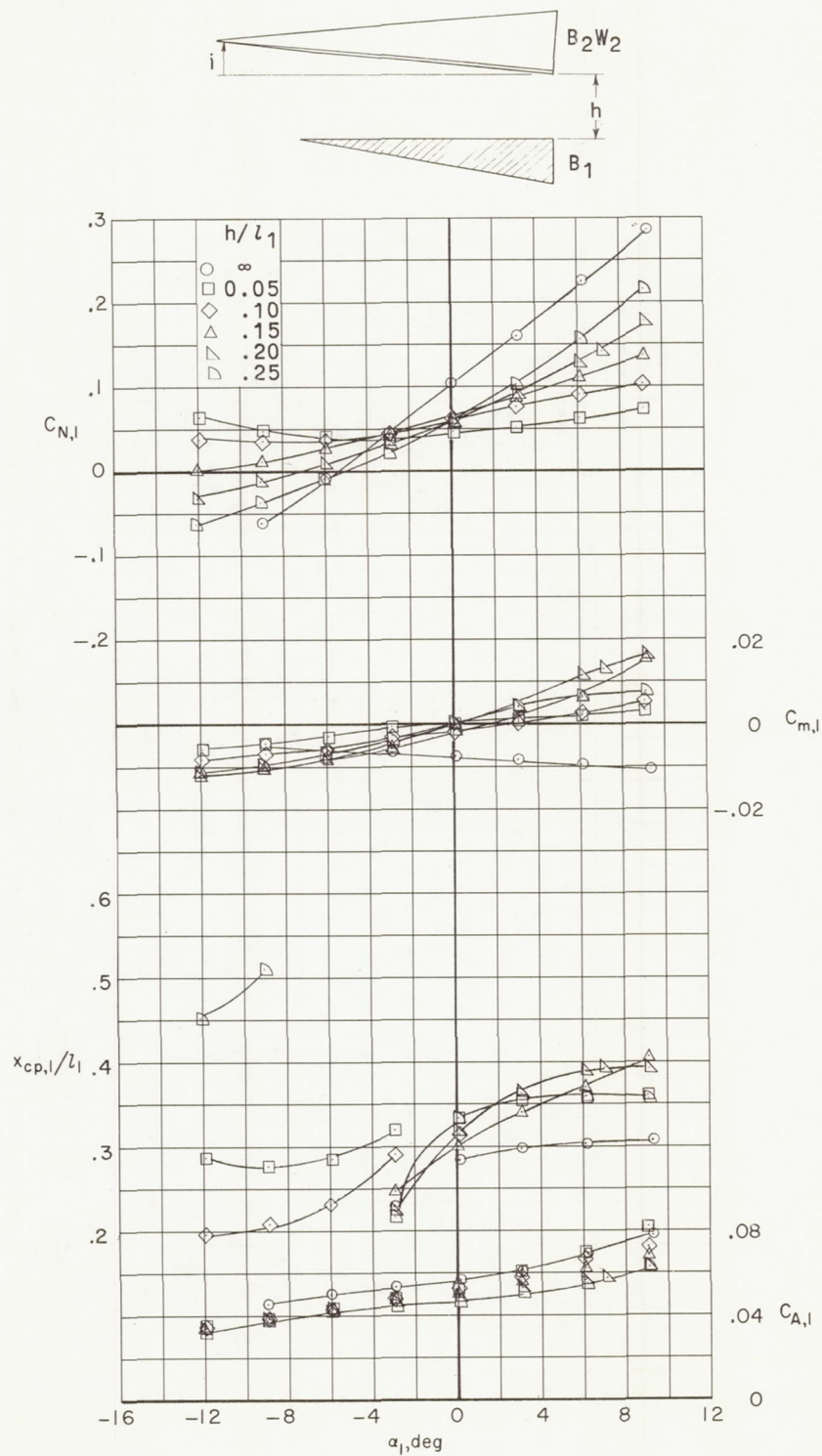
(a) M = 3.

Figure 16.- Longitudinal aerodynamic characteristics of B_1 in presence of B_2W_2. $i = 0°$; $l_2/l_1 = 1.33$.
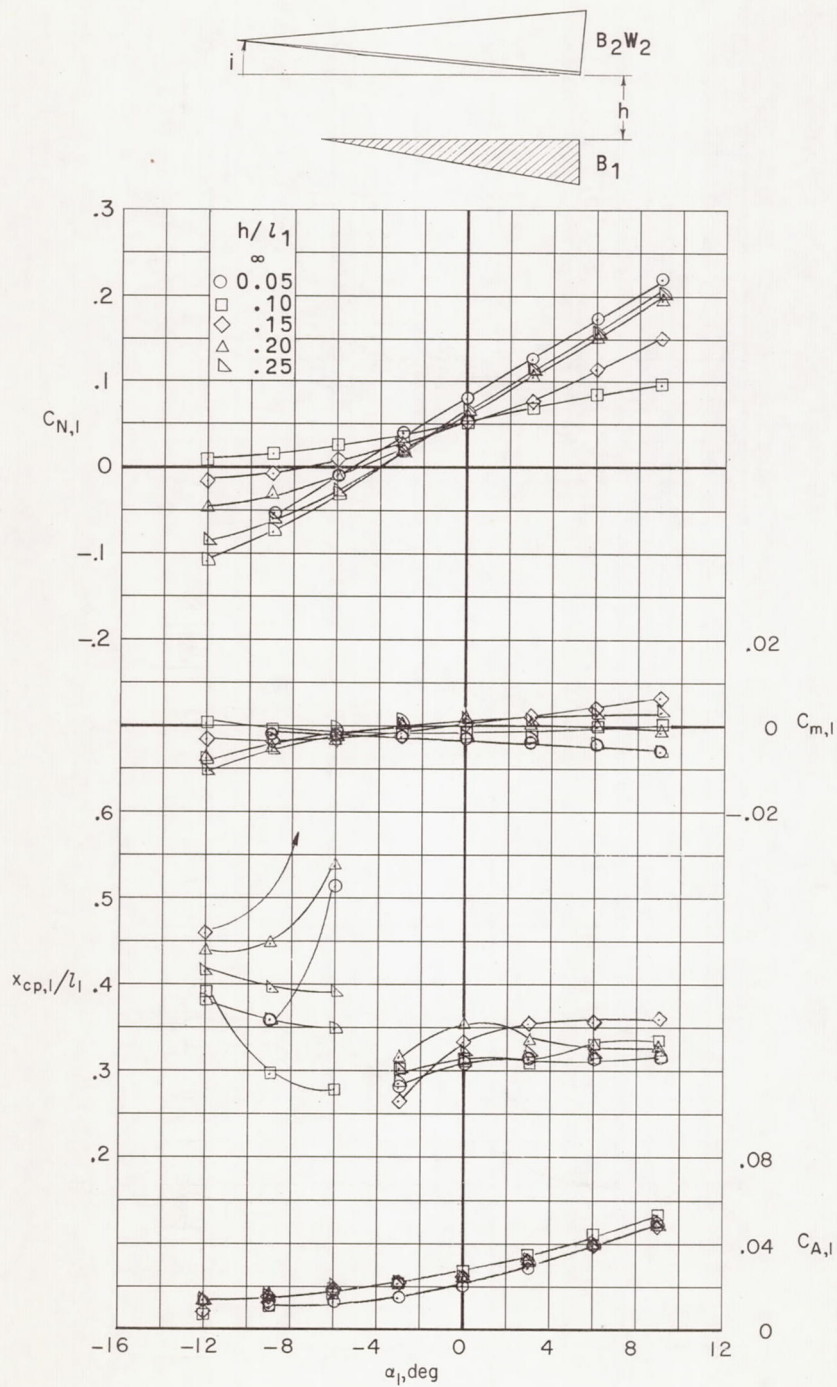
(b) M = 6.

Figure 16.- Concluded.
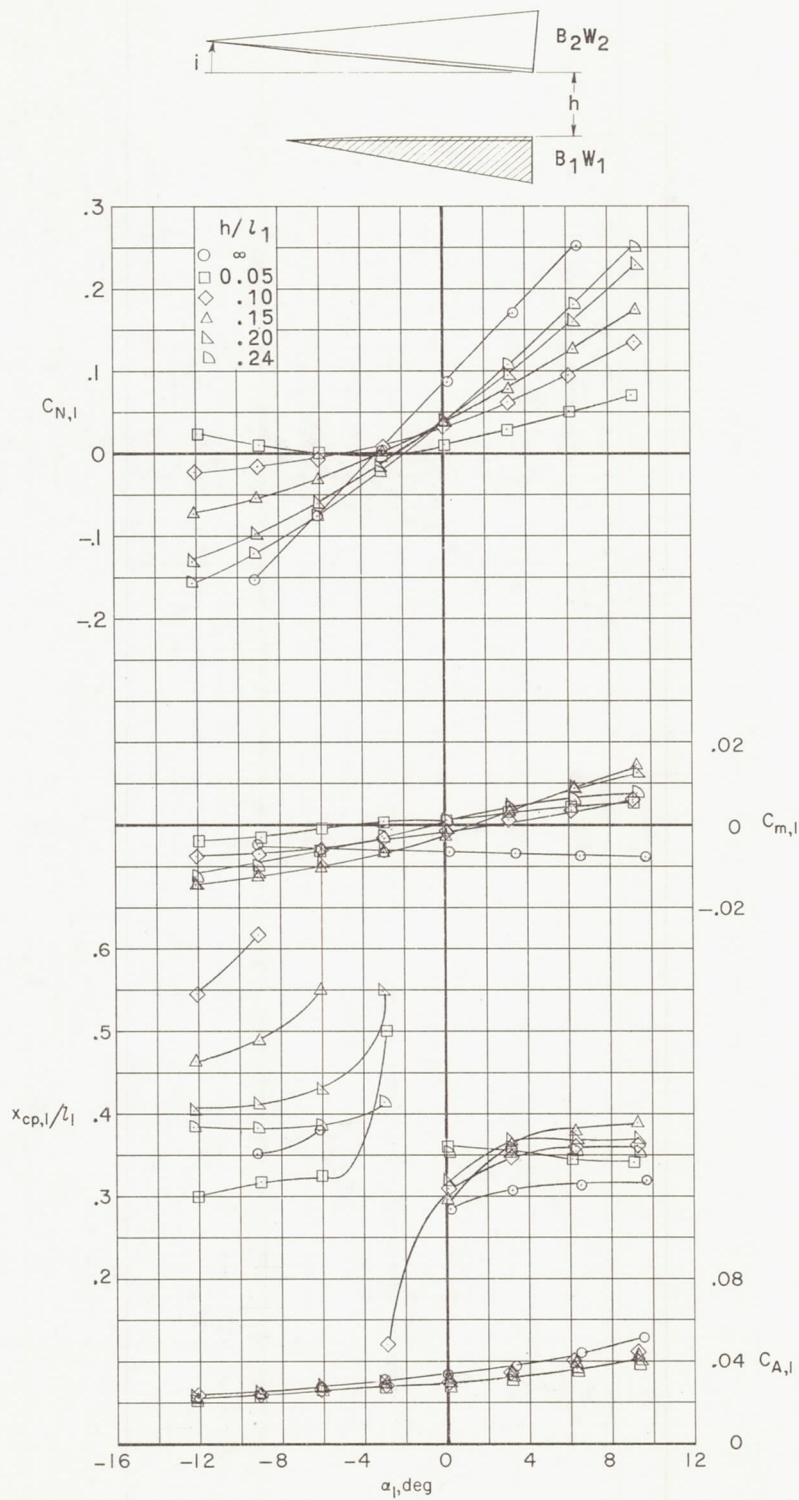
(a) M = 3.

Figure 17.- Longitudinal aerodynamic characteristics of B_1W_1 in presence of B_2W_2. i = 0°; l_2/l_1 = 1.33.
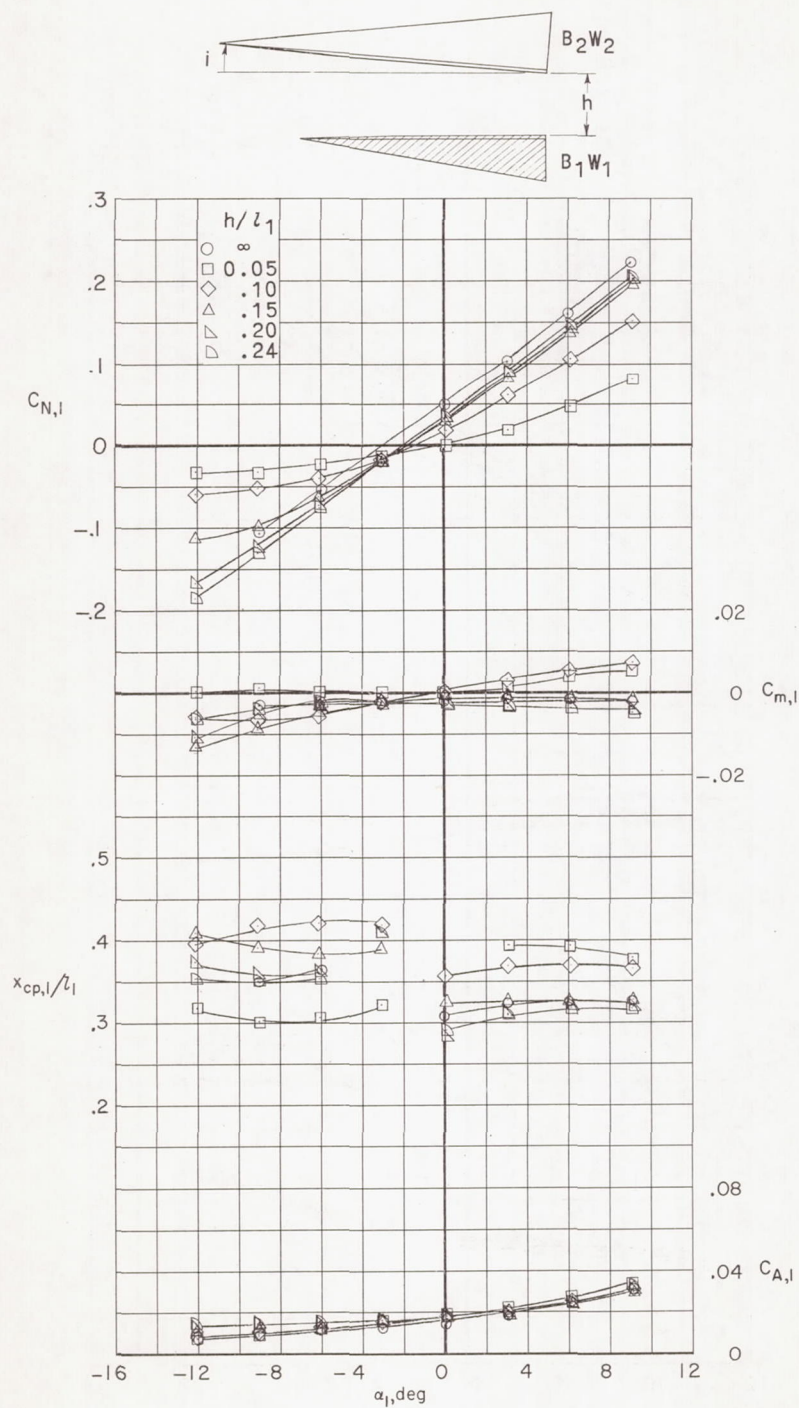
(b) M = 6.

Figure 17.- Concluded.
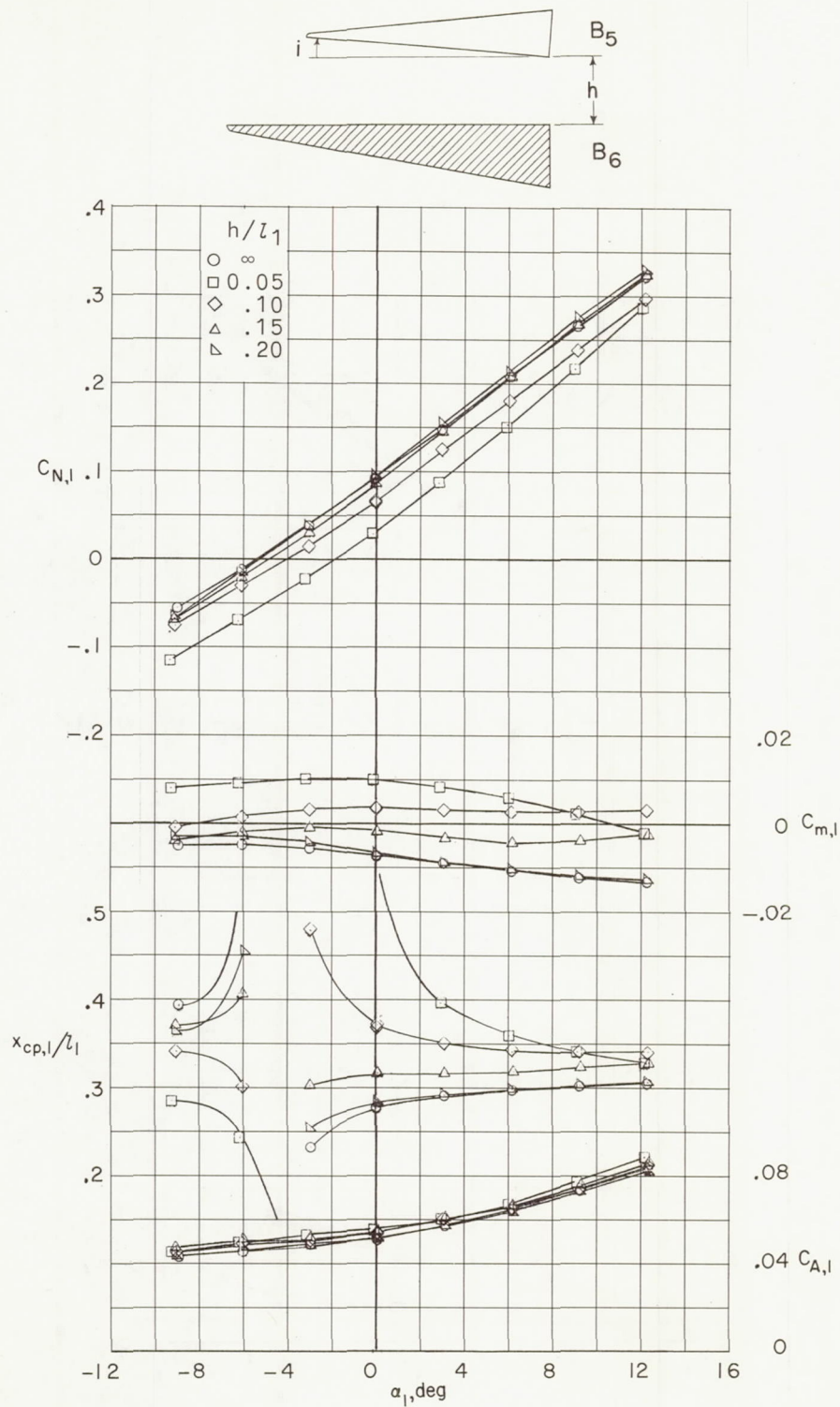
(a) M = 3.

Figure 18.- Longitudinal aerodynamic characteristics of B_6 in presence of B_5. i = 5°; l_2/l_1 = 0.75.
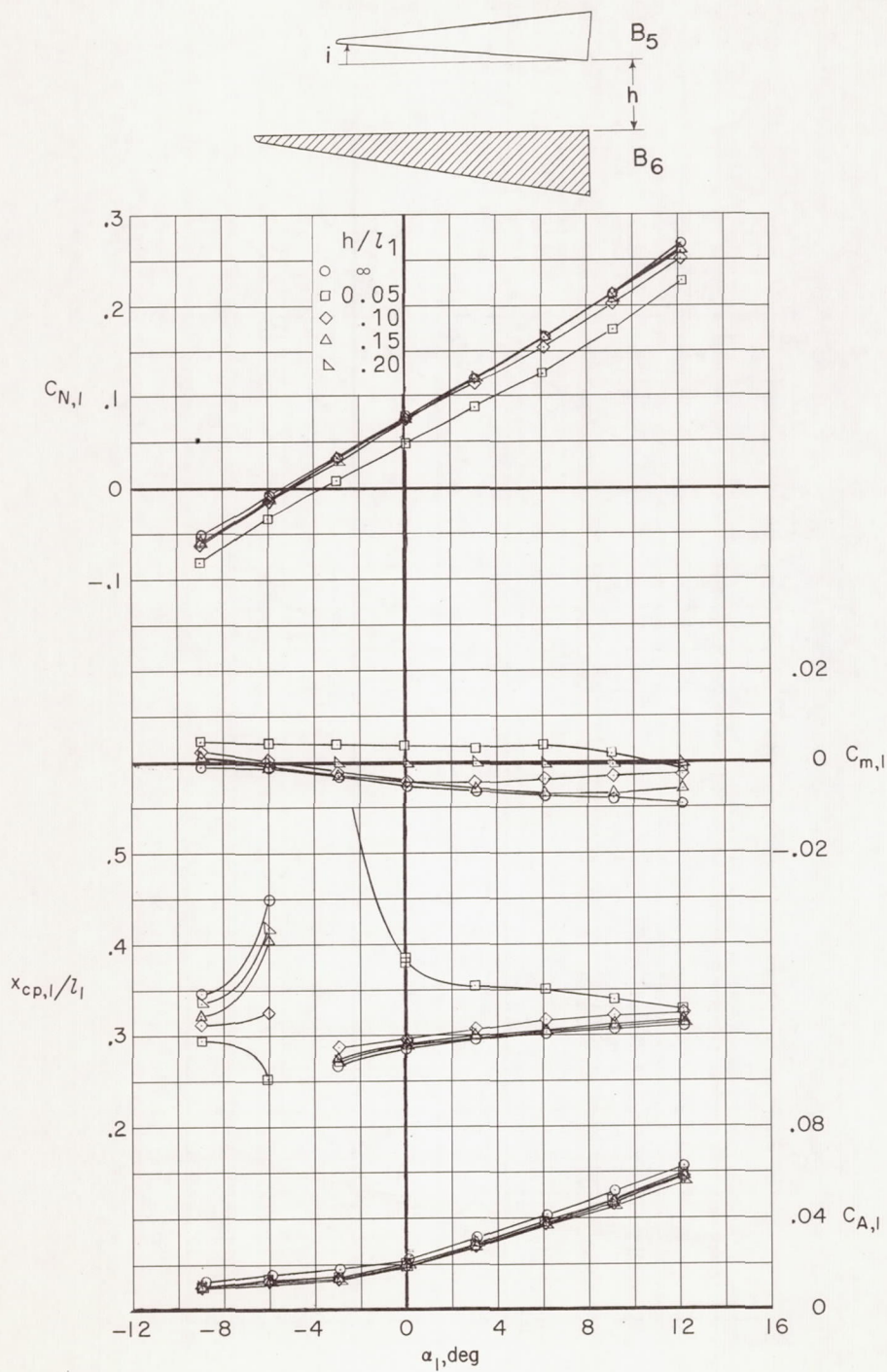
(b) M = 6.

Figure 18.- Concluded.
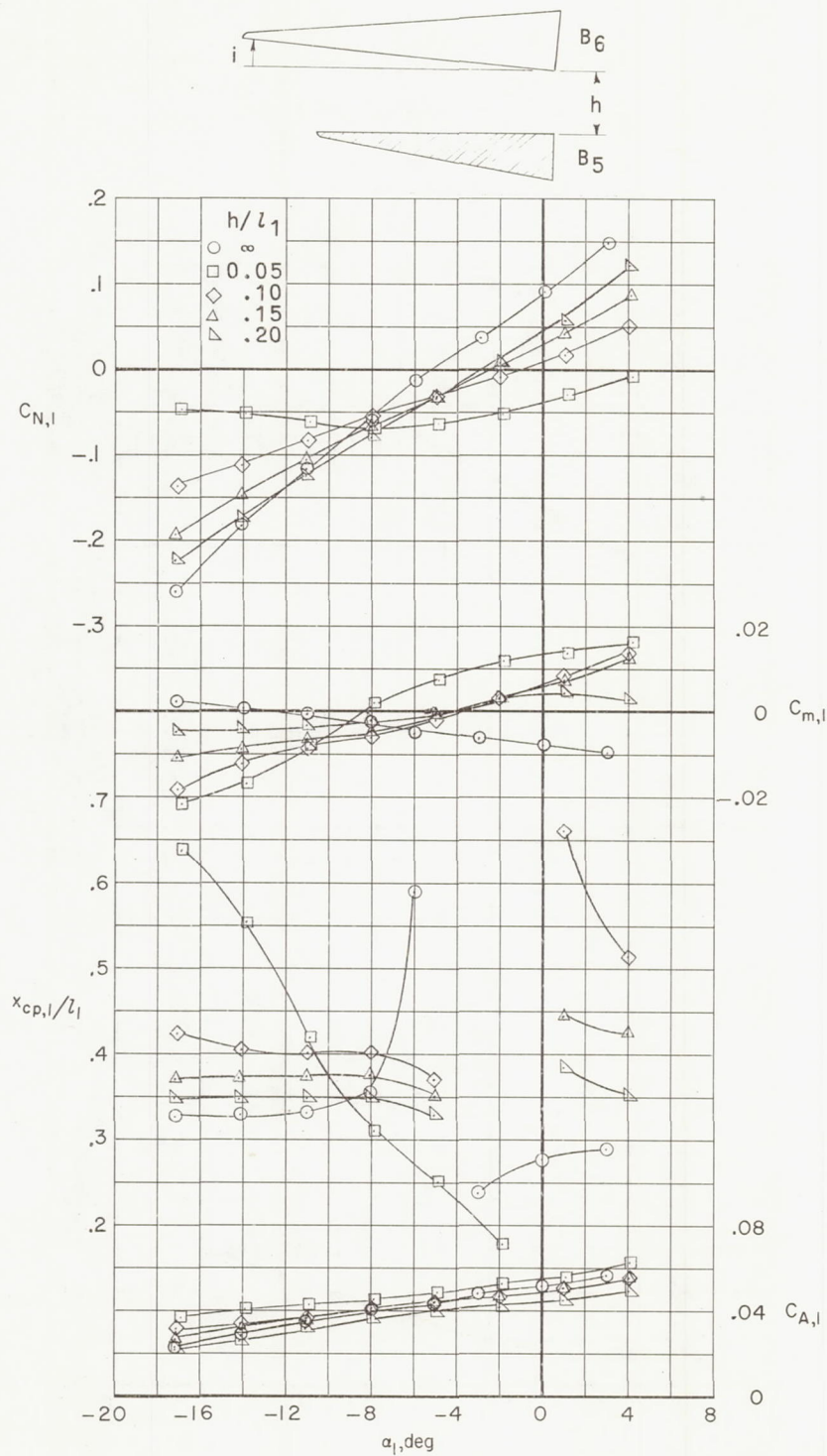
(a) M = 3.

Figure 19.- Longitudinal aerodynamic characteristics of B_5 in presence of B_6. i = 5°; l_2/l_1 = 1.33.
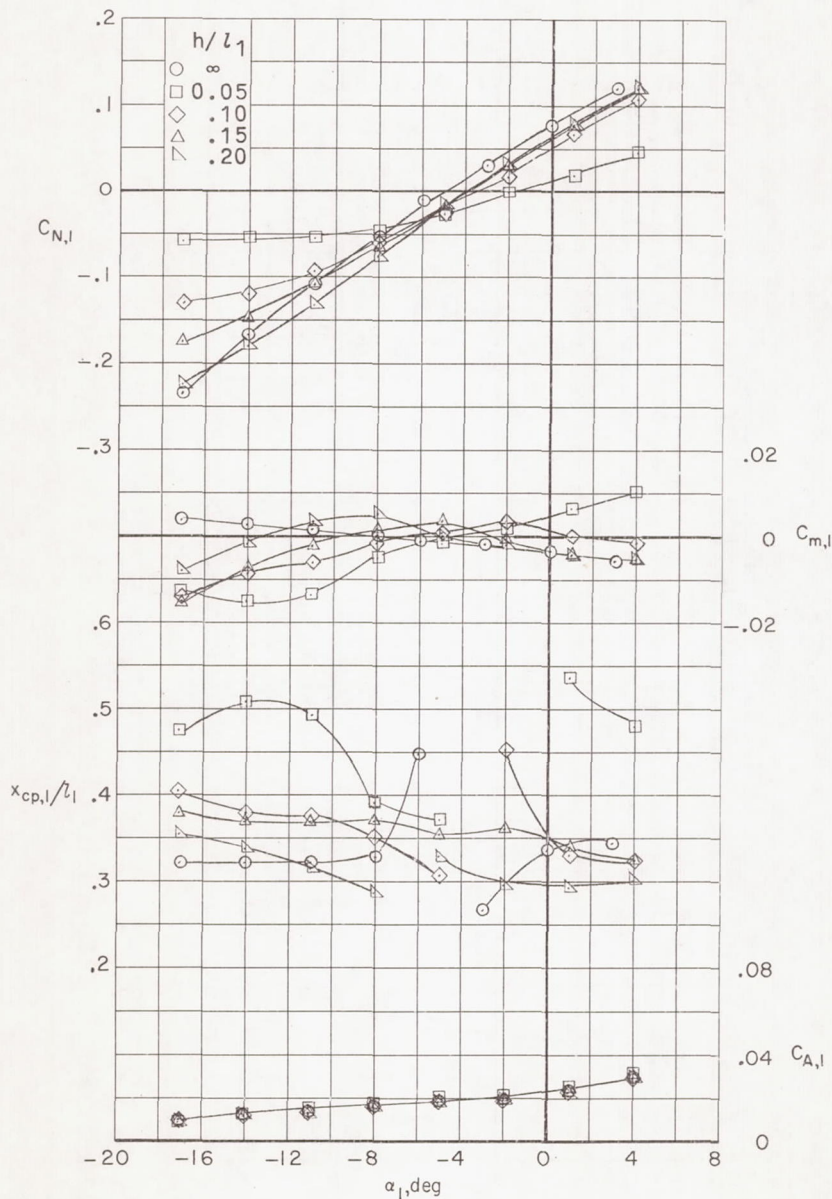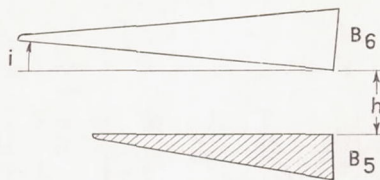
(b) M = 6.

Figure 19.- Concluded.
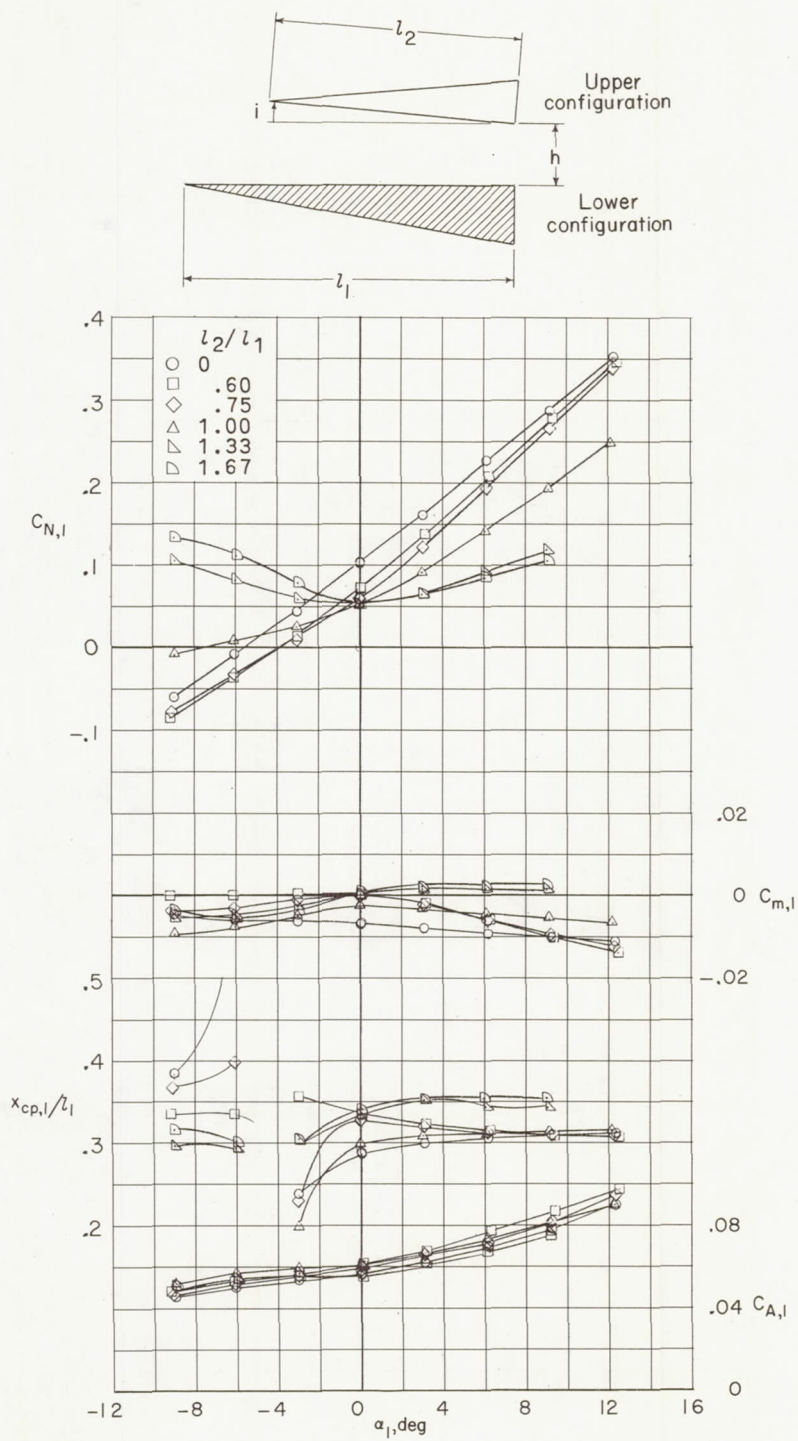
(a) $M = 3$; $i = 0^0$; $h/l_1 = 0.05$.

Figure 20.- Effect of relative size of upper configuration on longitudinal aerodynamic characteristics of lower configuration.
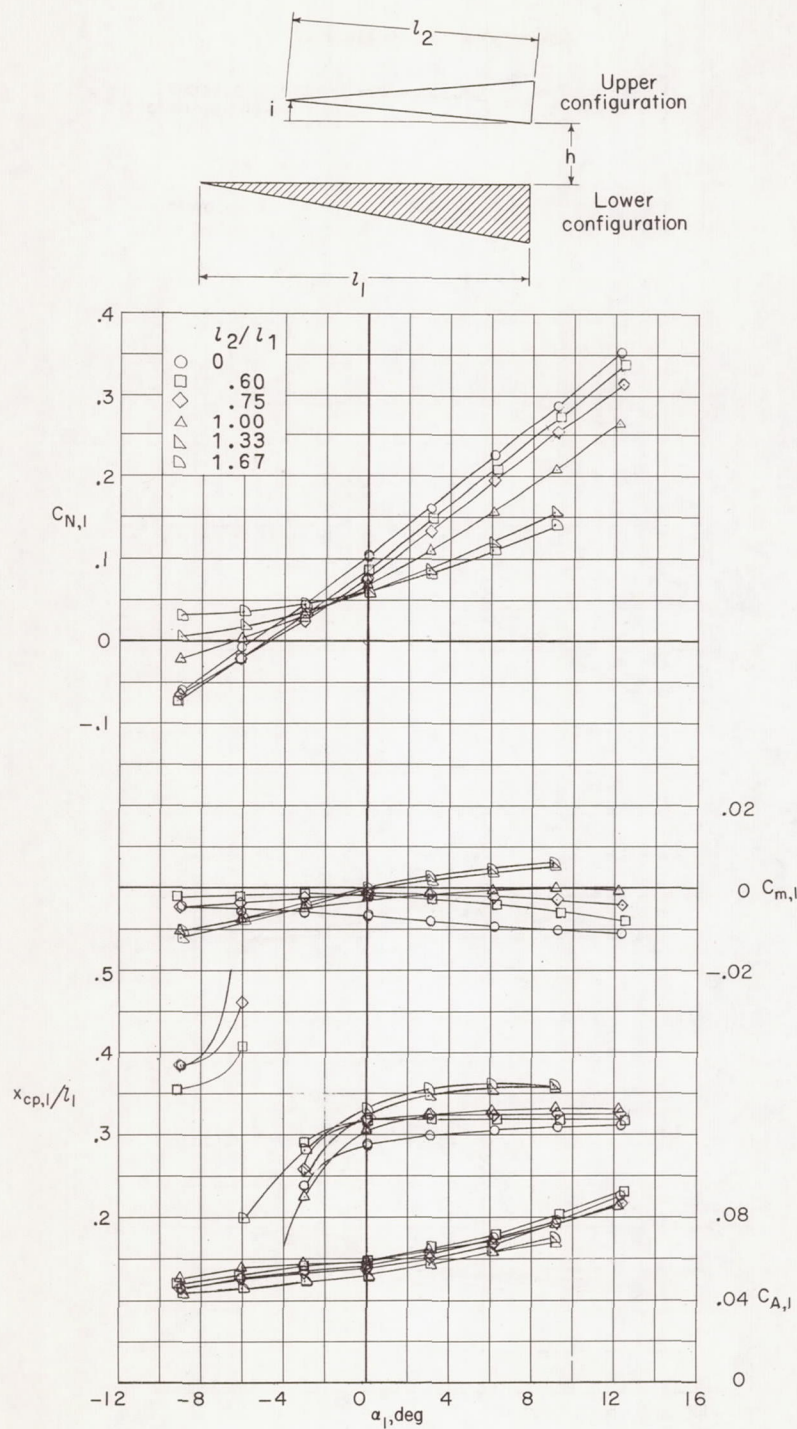
(b) $M = 3$; $i = 0^0$; $h/l_1 = 0.10$.

Figure 20.- Continued.
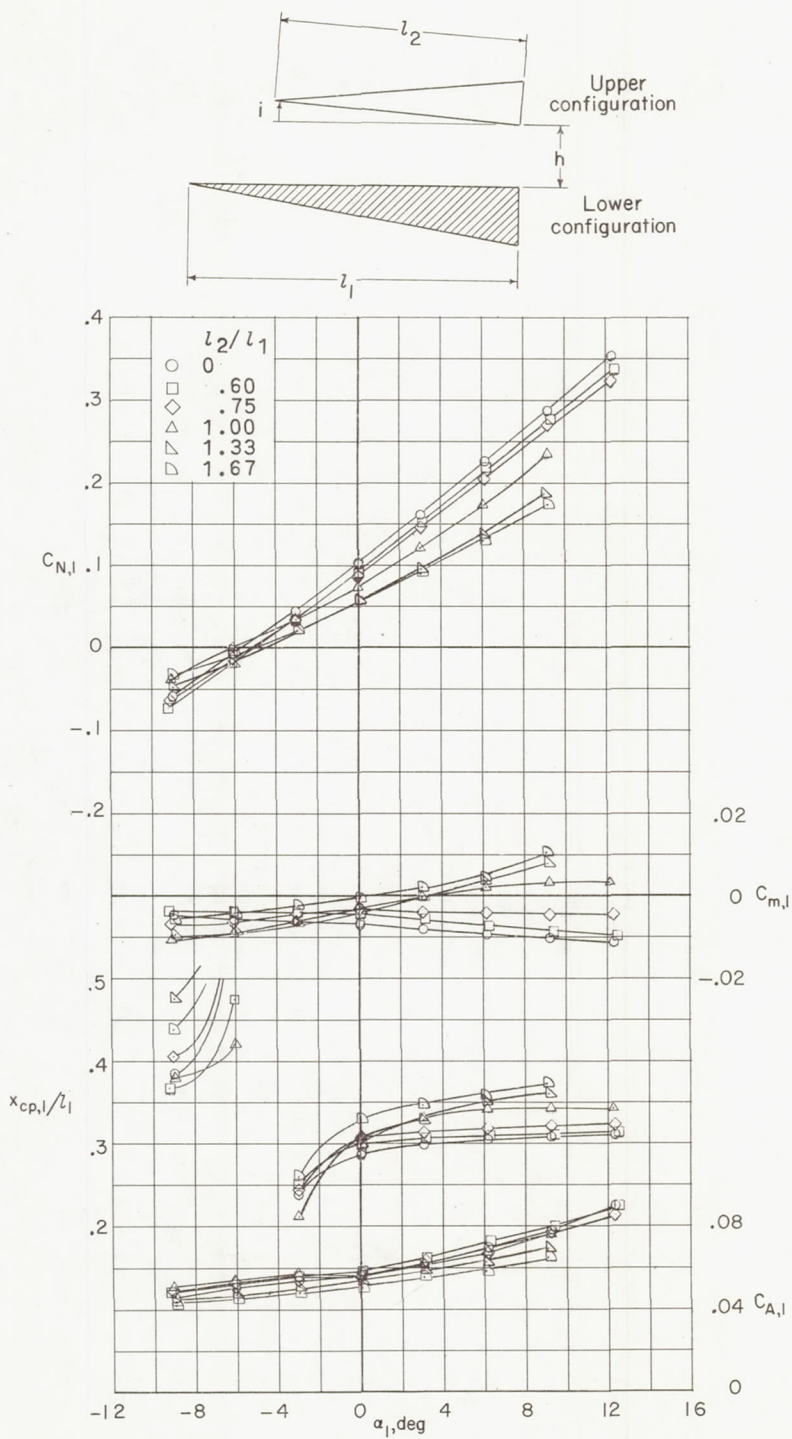
(c) $M = 3$; $i = 0^0$; $h/l_1 = 0.15$.

Figure 20.- Continued.
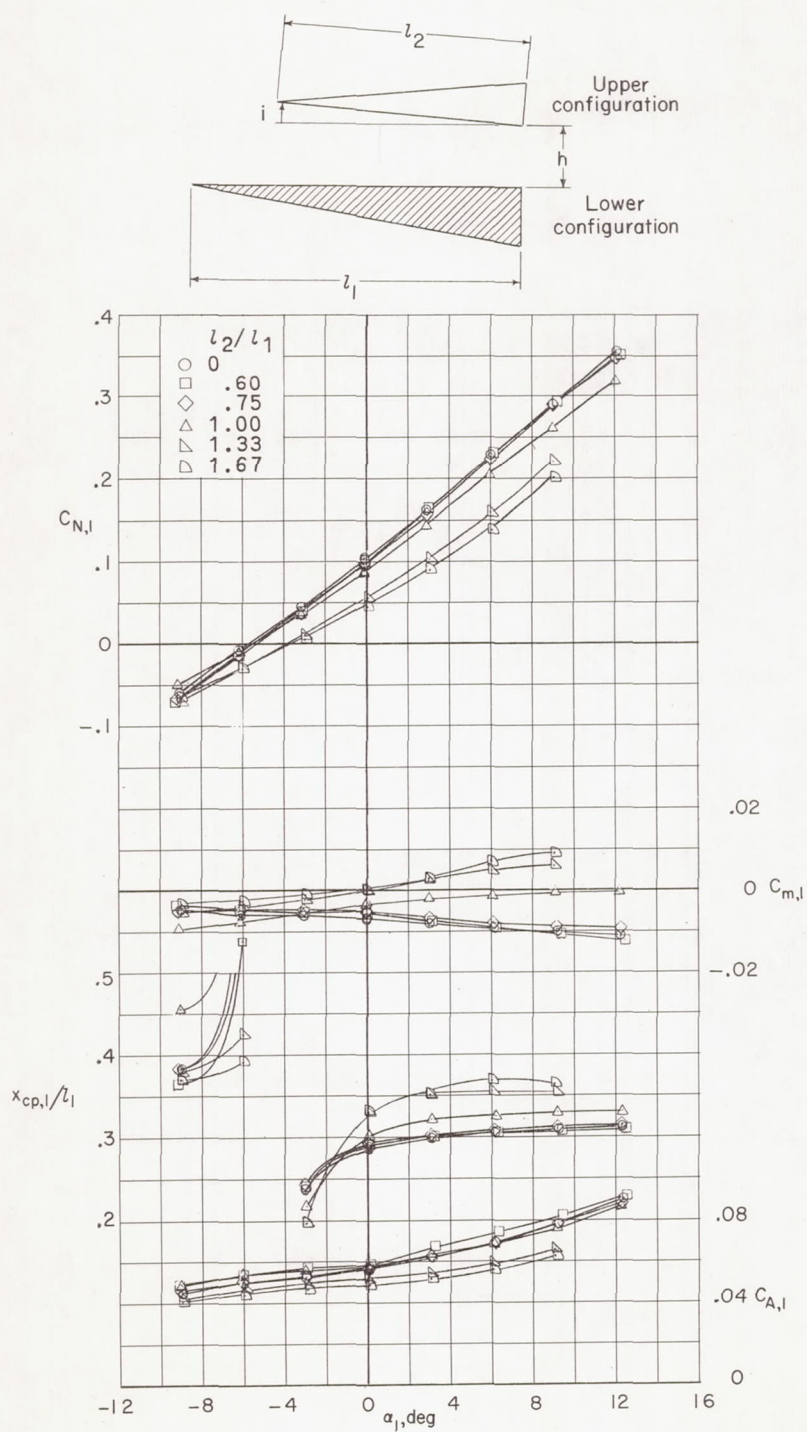
(d) M = 3; i = 0°; h/l_1 = 0.20.

Figure 20.- Continued.
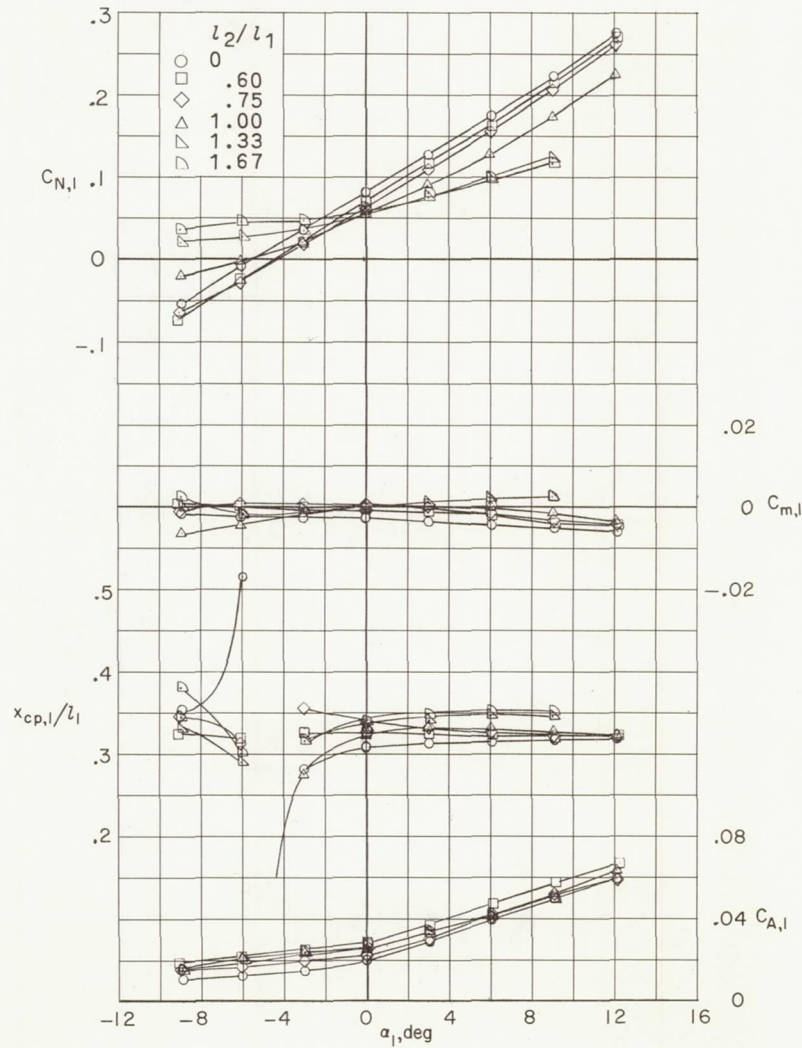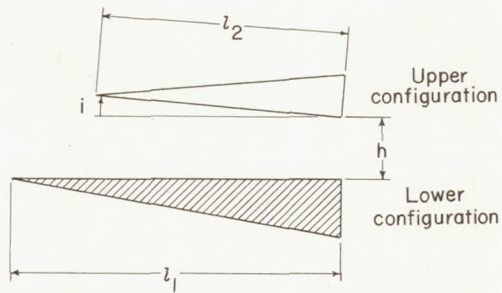
(e) $M = 6$; $i = 0^0$; $h/l_1 = 0.05$.

Figure 20.- Continued.
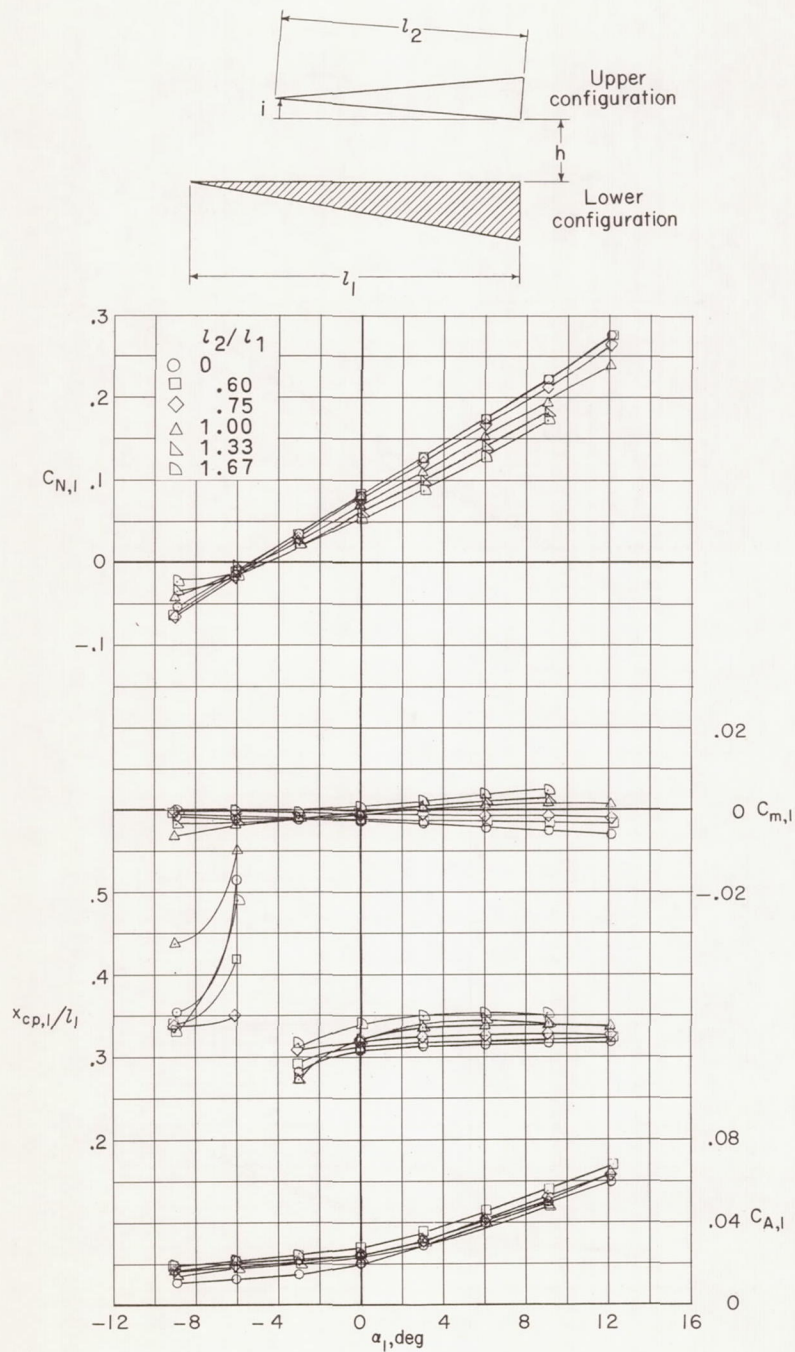
(f) M = 6; i = 0^0; h/l_1 = 0.10.

Figure 20.- Continued.
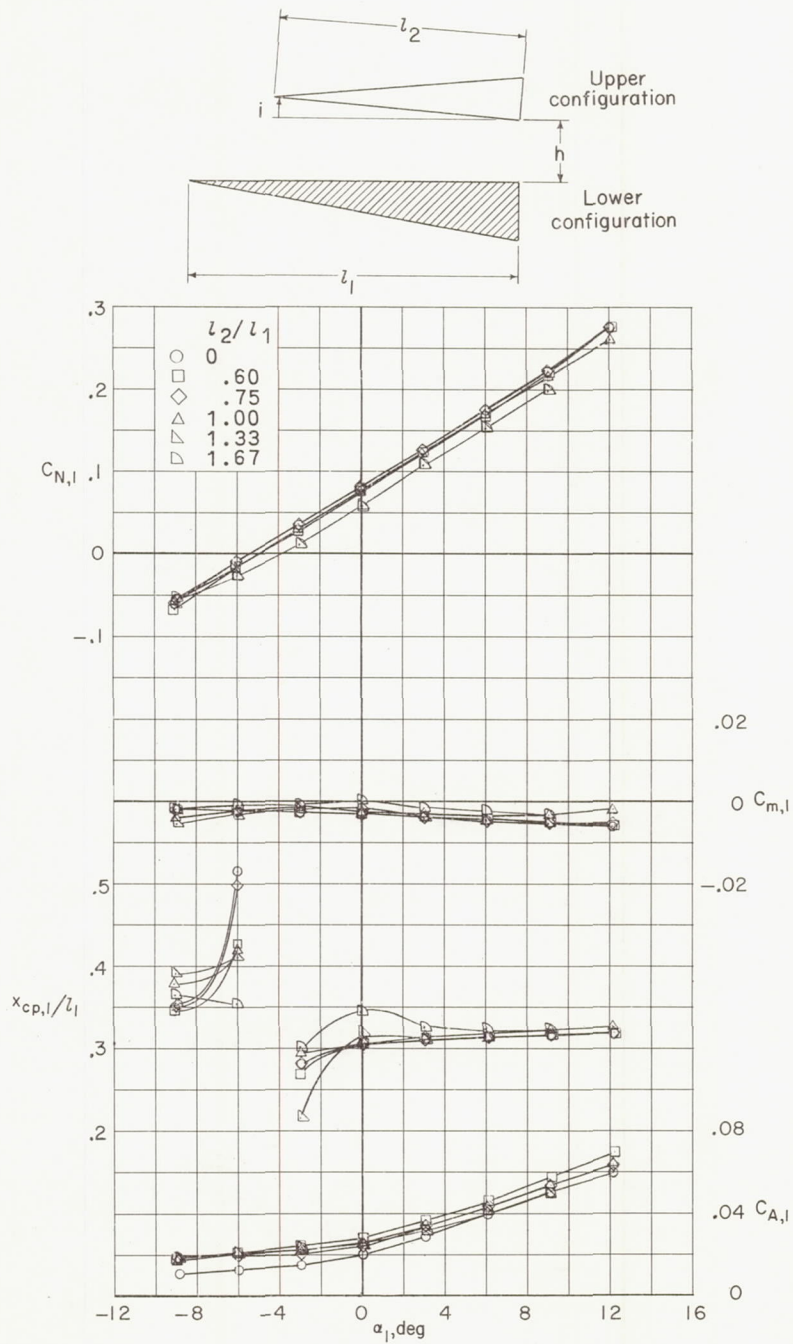
(g) $M = 6$; $i = 0^0$; $h/l_1 = 0.15$.

Figure 20.- Continued.
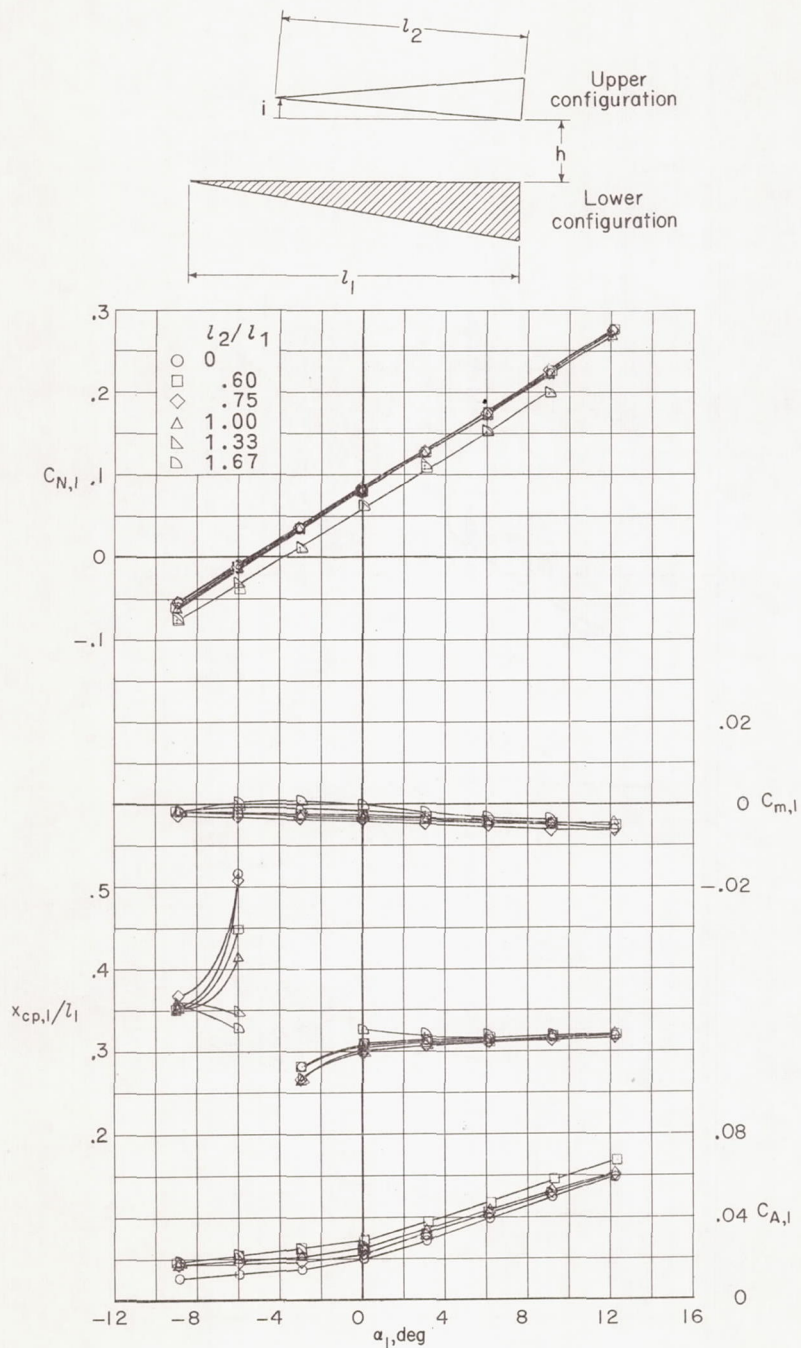
(h) $M = 6$; $i = 0^0$; $h/l_1 = 0.20$.

Figure 20.- Concluded.
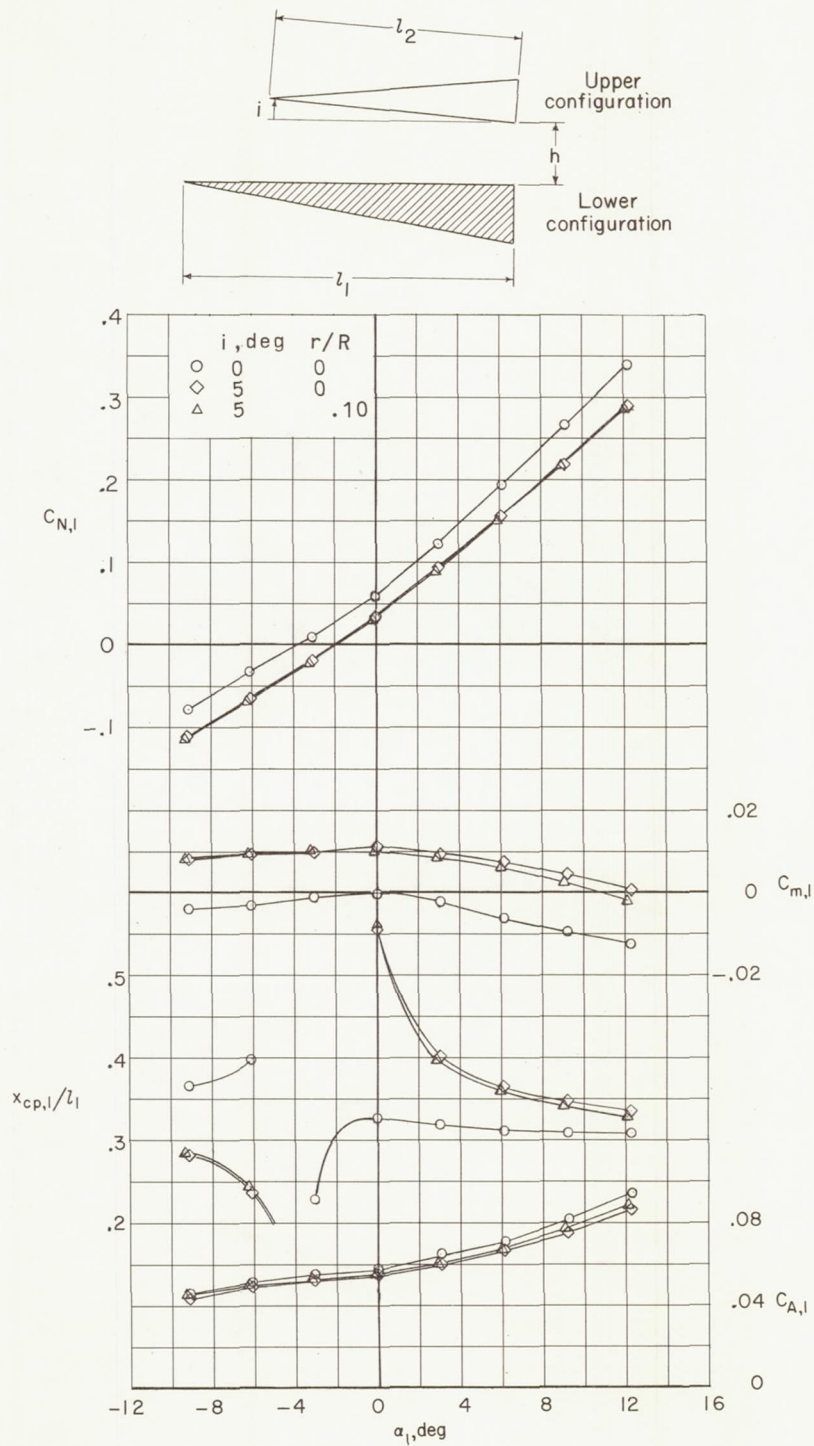
(a) M = 3; $l_2/l_1 = 0.75$; $h/l_1 = 0.05$.

Figure 21.- Effect of incidence angle and nose bluntness of upper configuration on longitudinal aerodynamic characteristics of lower configuration.
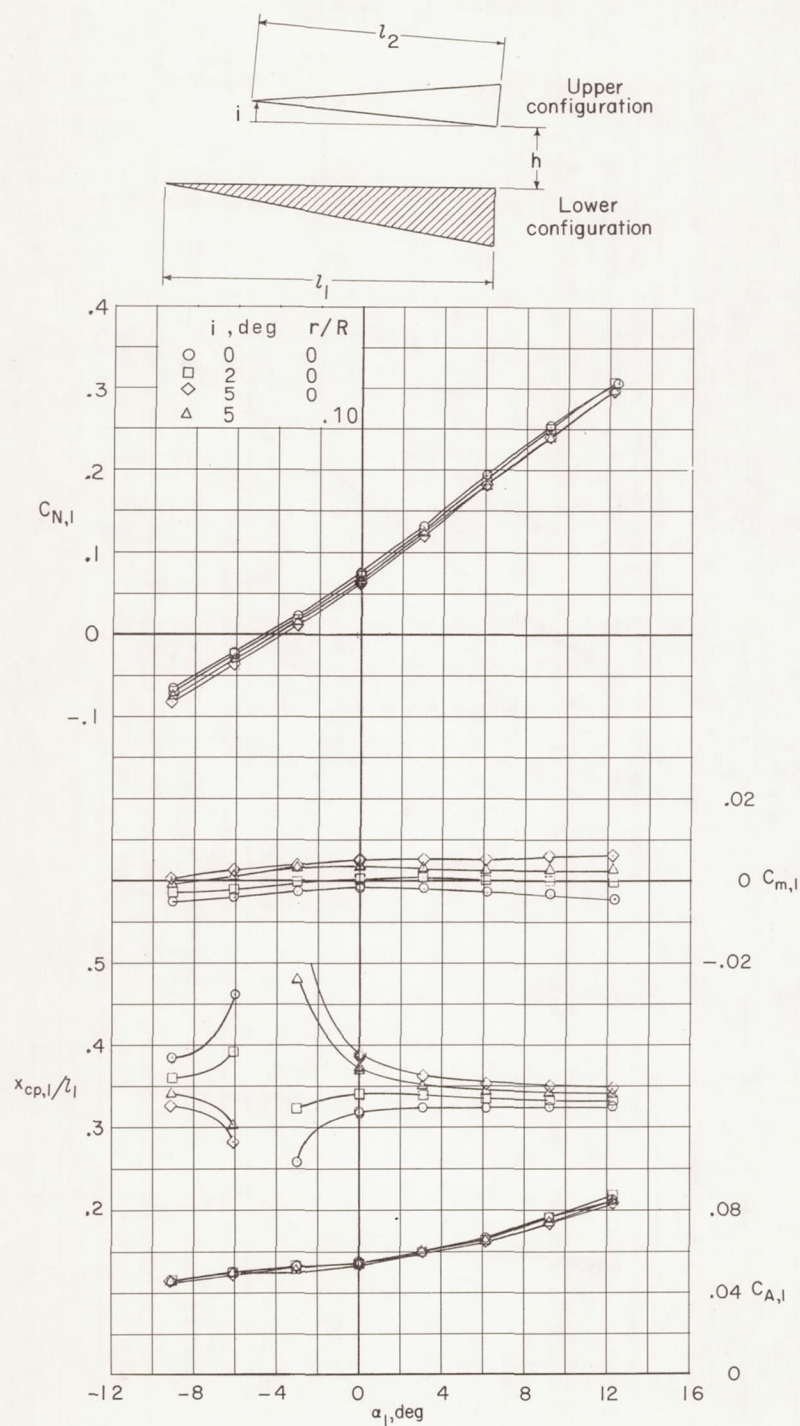
(b) M = 3; l_2/l_1 = 0.75; h/l_1 = 0.10.

Figure 21.- Continued.
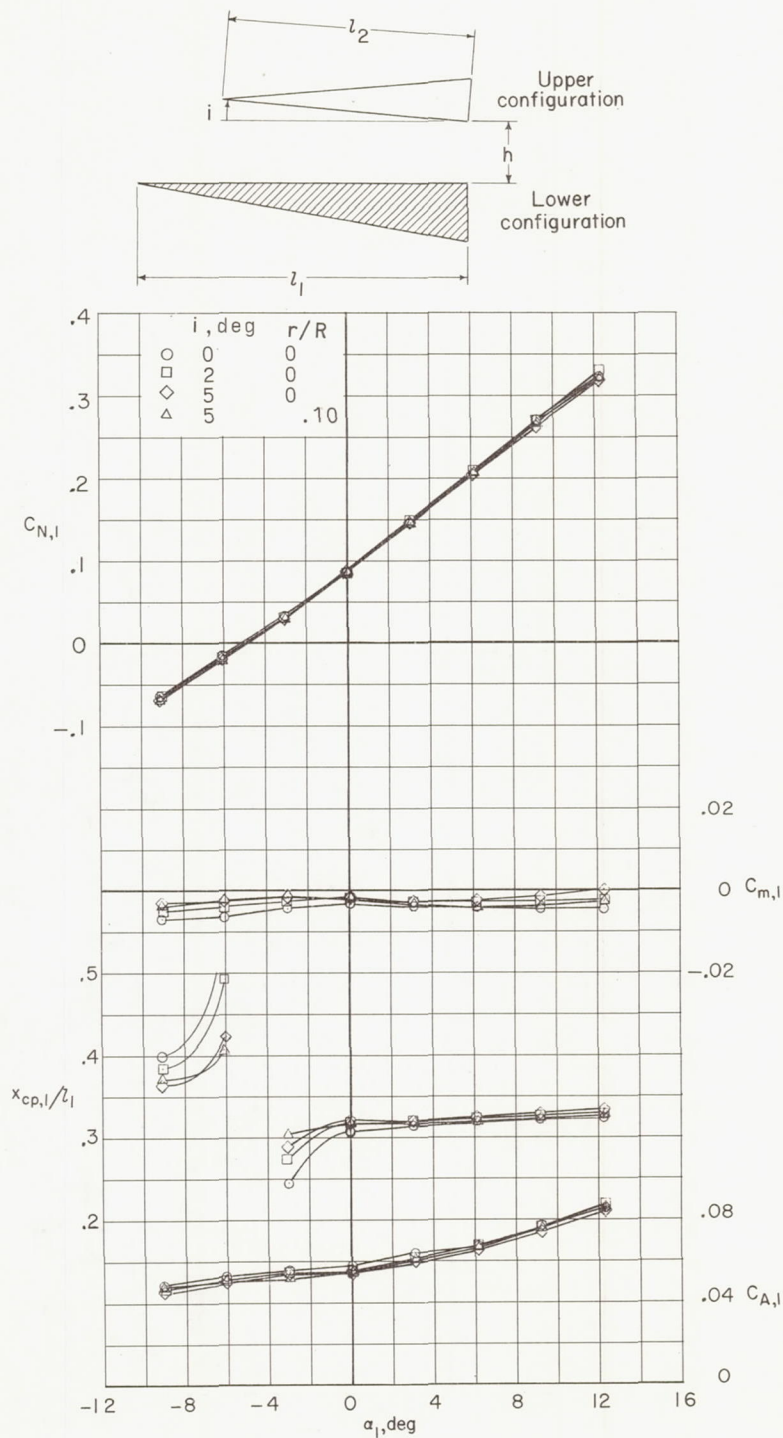
(c) $M = 3$; $l_2/l_1 = 0.75$; $h/l_1 = 0.15$.

Figure 21.- Continued.
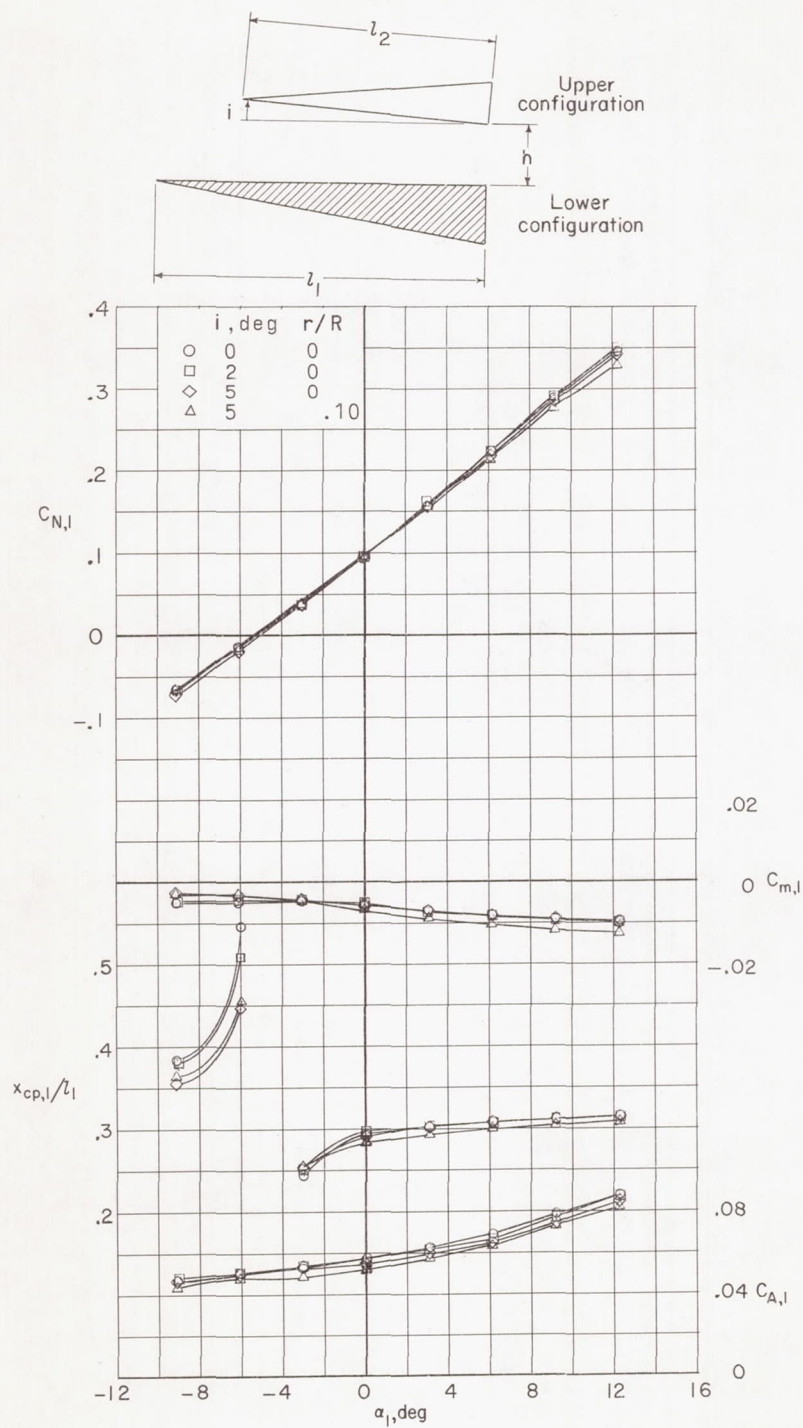
(d) $M = 3$; $l_2/l_1 = 0.75$; $h/l_1 = 0.20$.

Figure 21.- Continued.
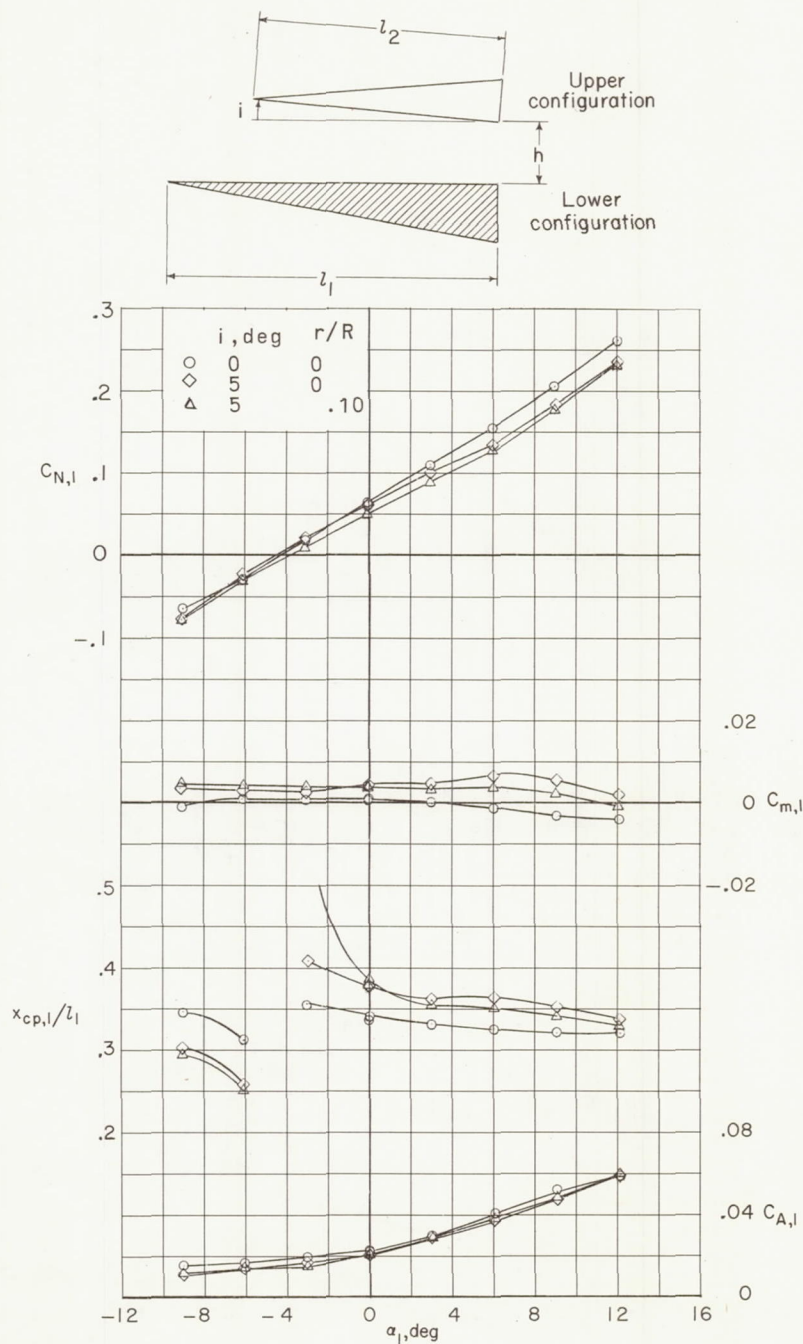
(e) $M = 6$; $l_2/l_1 = 0.75$; $h/l_1 = 0.05$.

Figure 21.- Continued.
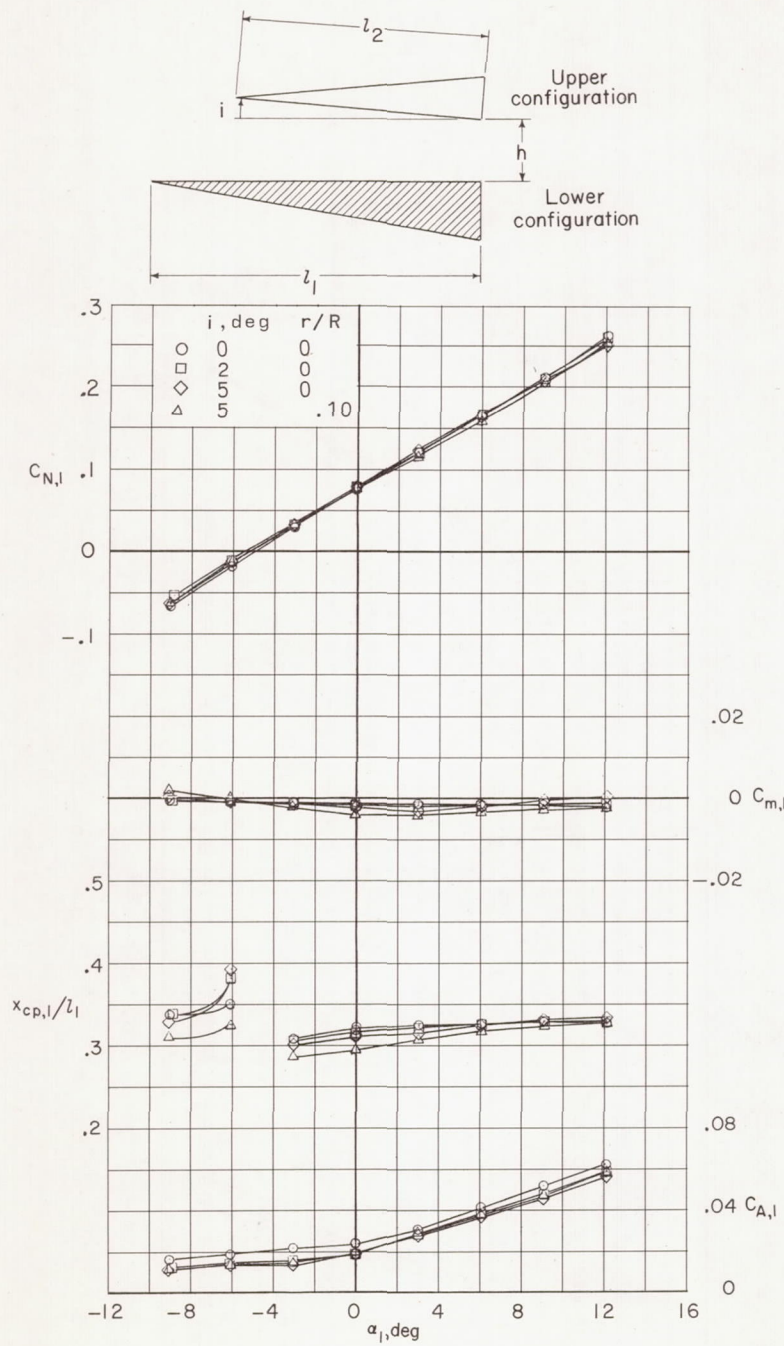
(f) $M = 6$; $l_2/l_1 = 0.75$; $h/l_1 = 0.10$.

Figure 21.- Continued.
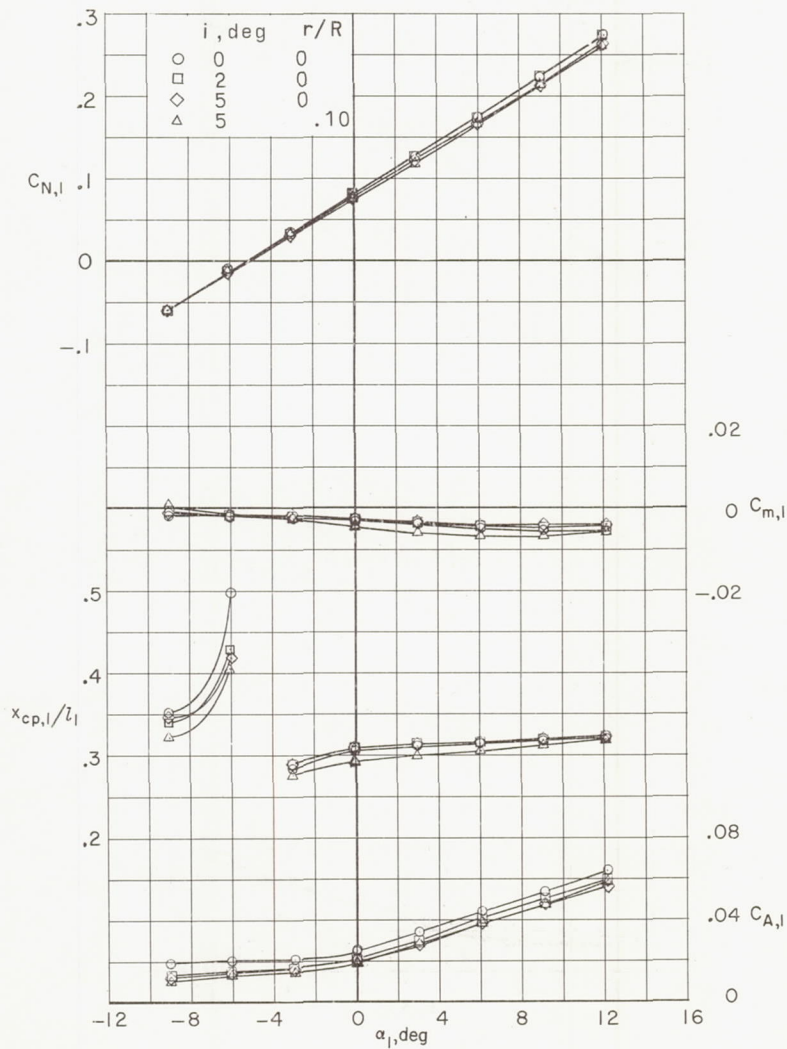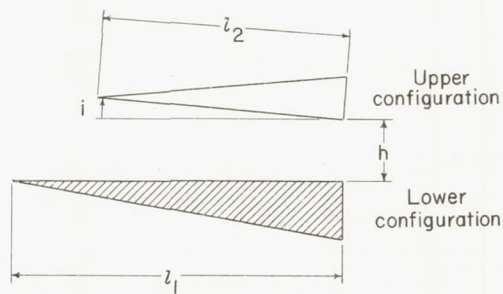
(g) $M = 6$; $l_2/l_1 = 0.75$; $h/l_1 = 0.15$.

Figure 21.- Continued.
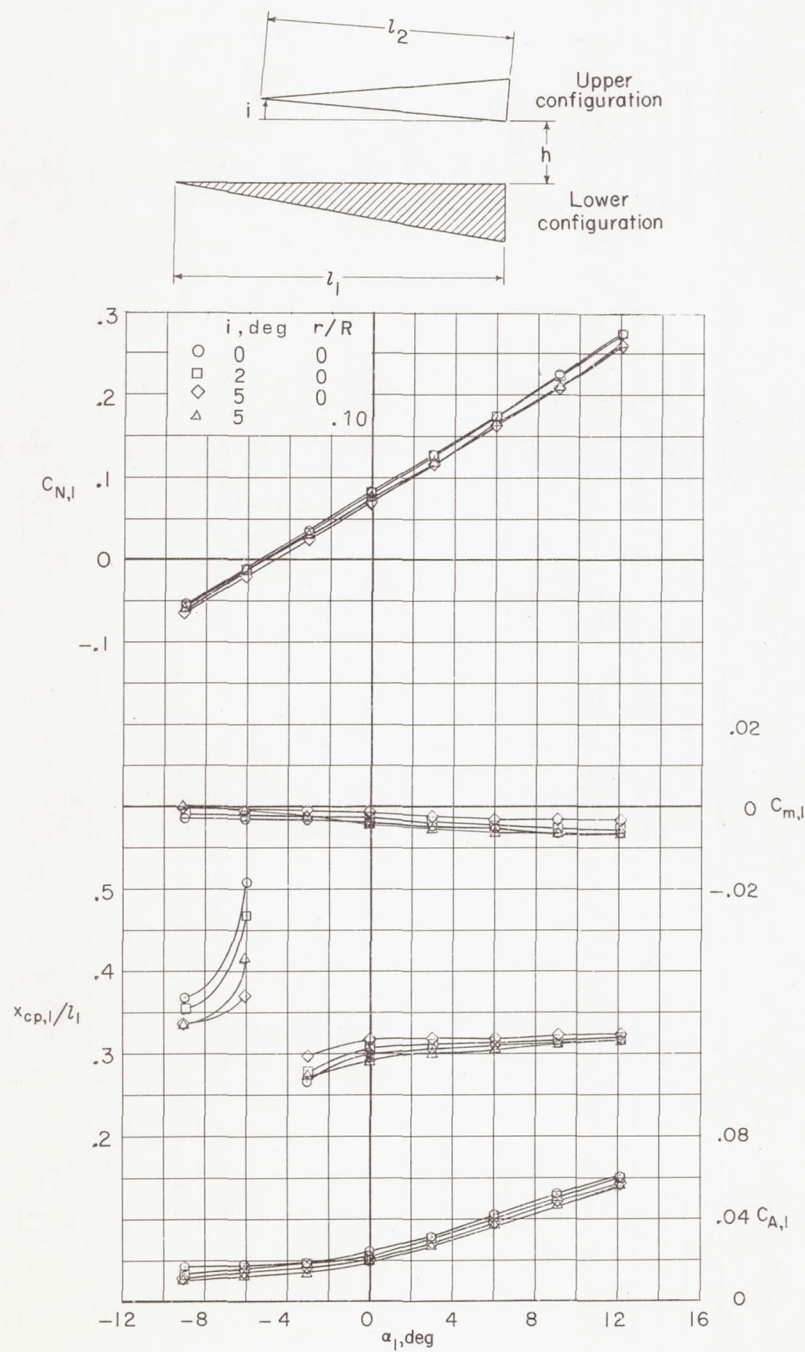
(h) $M = 6$; $l_2/l_1 = 0.75$; $h/l_1 = 0.20$.

Figure 21.- Continued.
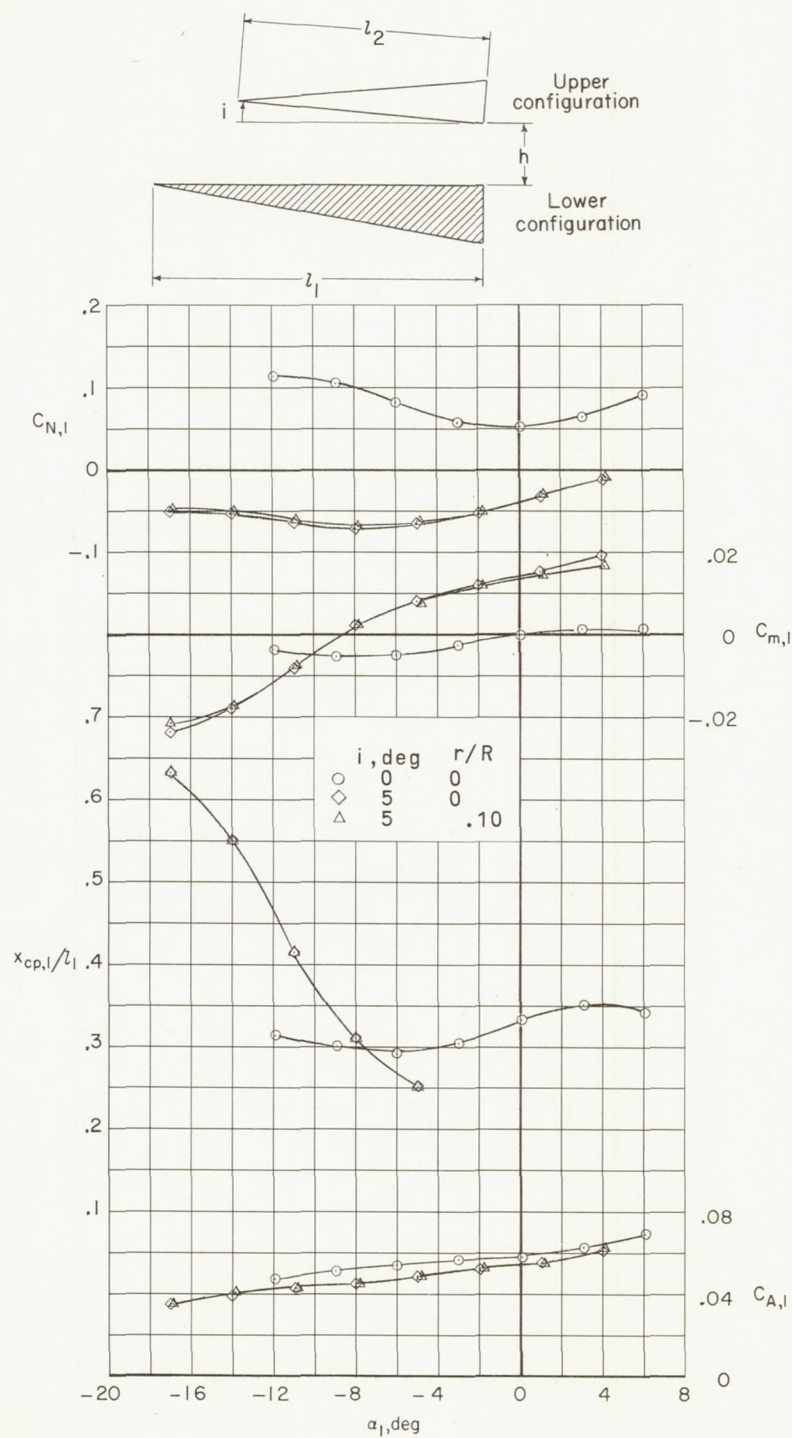
(i) $M = 3$; $l_2/l_1 = 1.33$; $h/l_1 = 0.05$.

Figure 21.- Continued.
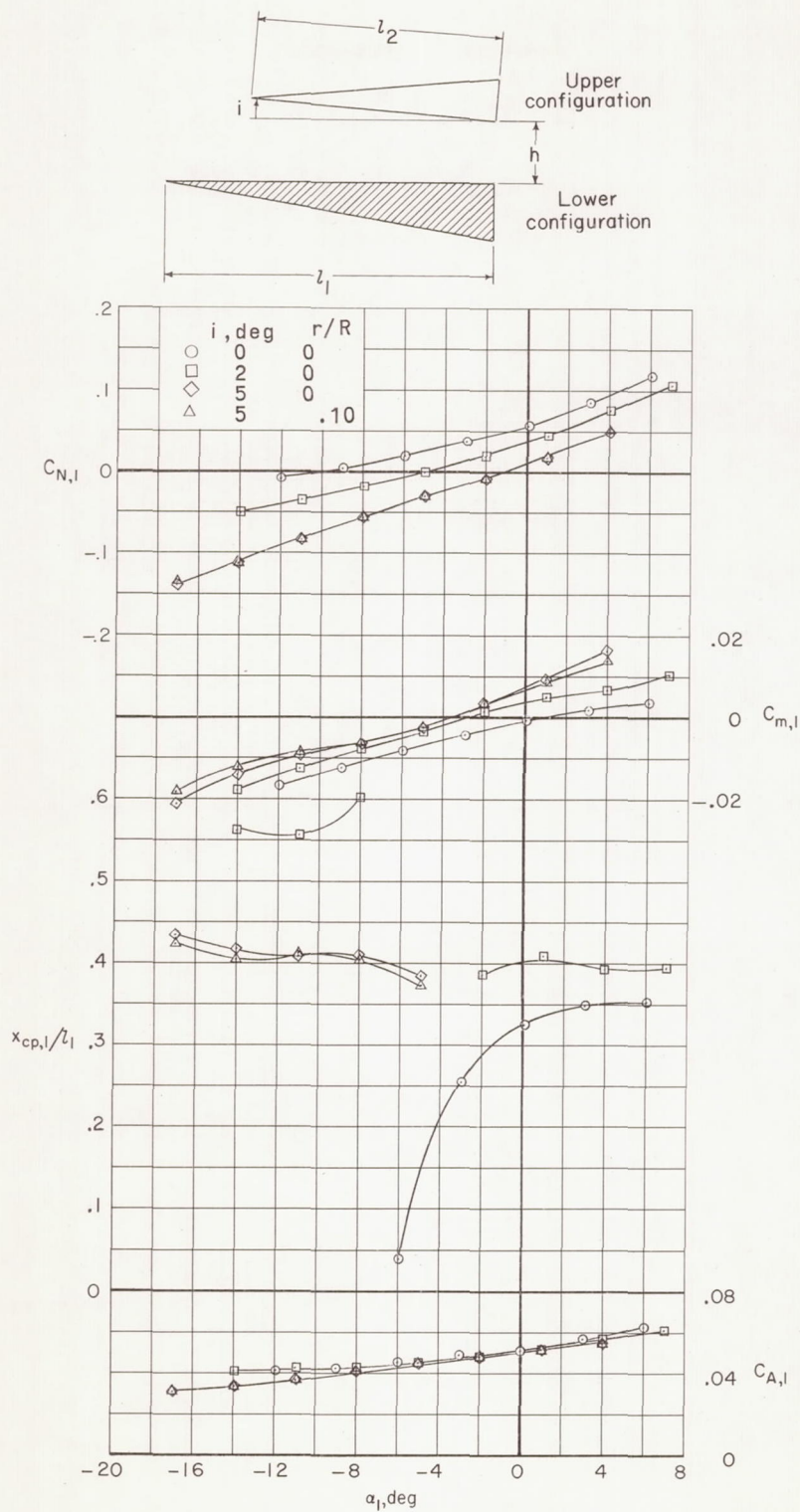
(j) $M = 3$; $l_2/l_1 = 1.33$; $h/l_1 = 0.10$.

Figure 21.- Continued.
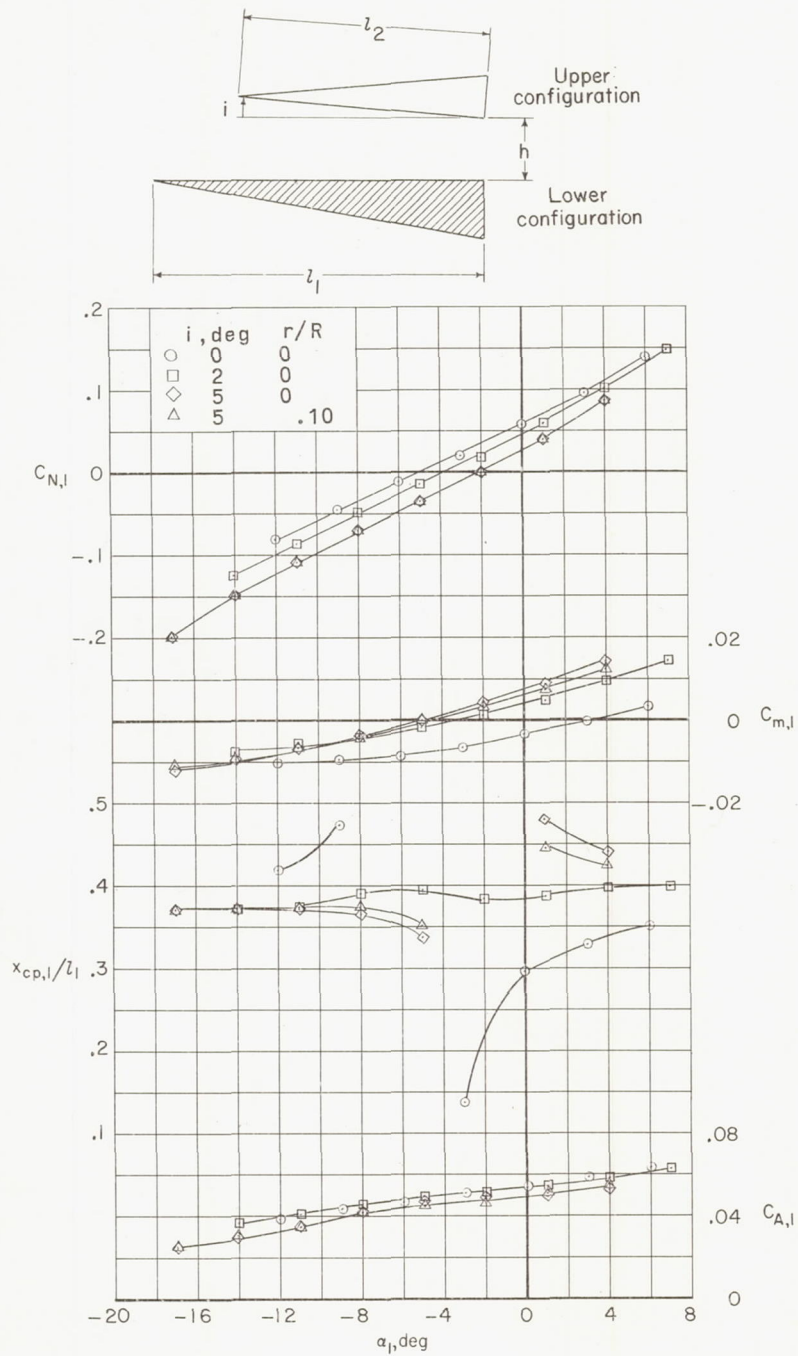
(k) M = 3; $l_2/l_1 = 1.33$; $h/l_1 = 0.15$.

Figure 21.- Continued.
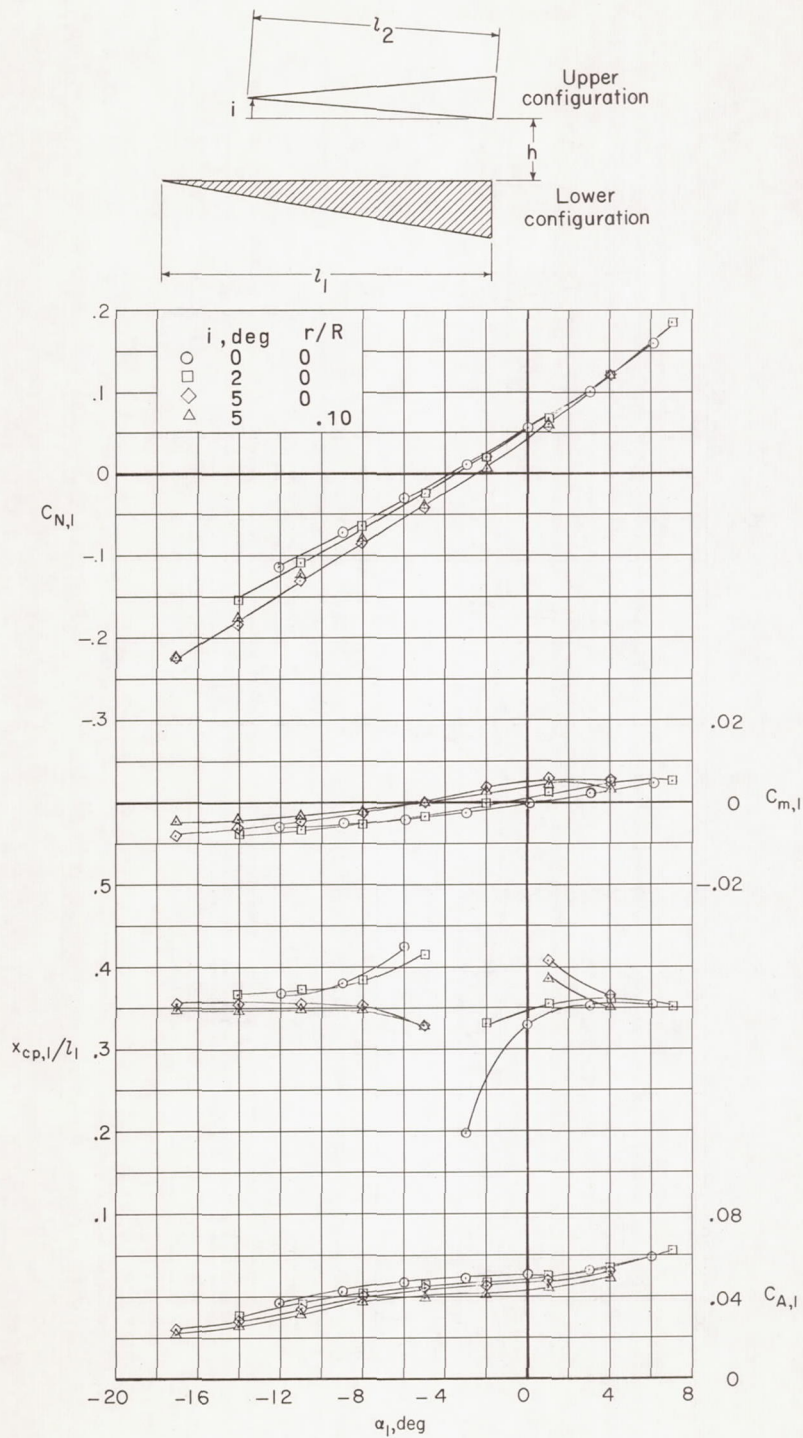
(l) $M = 3$; $l_2/l_1 = 1.33$; $h/l_1 = 0.20$.

Figure 21.- Continued.
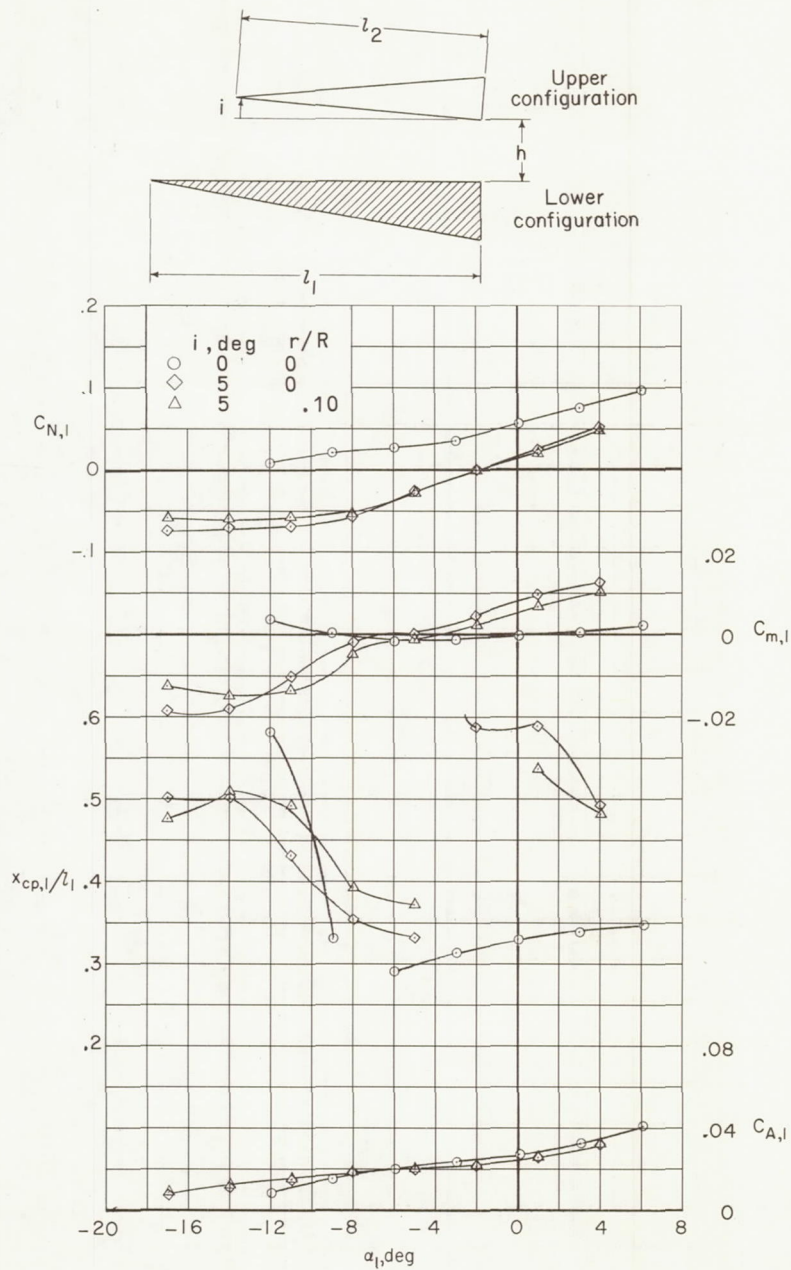
(m) $M = 6$; $l_2/l_1 = 1.33$; $h/l_1 = 0.05$.

Figure 21.- Continued.
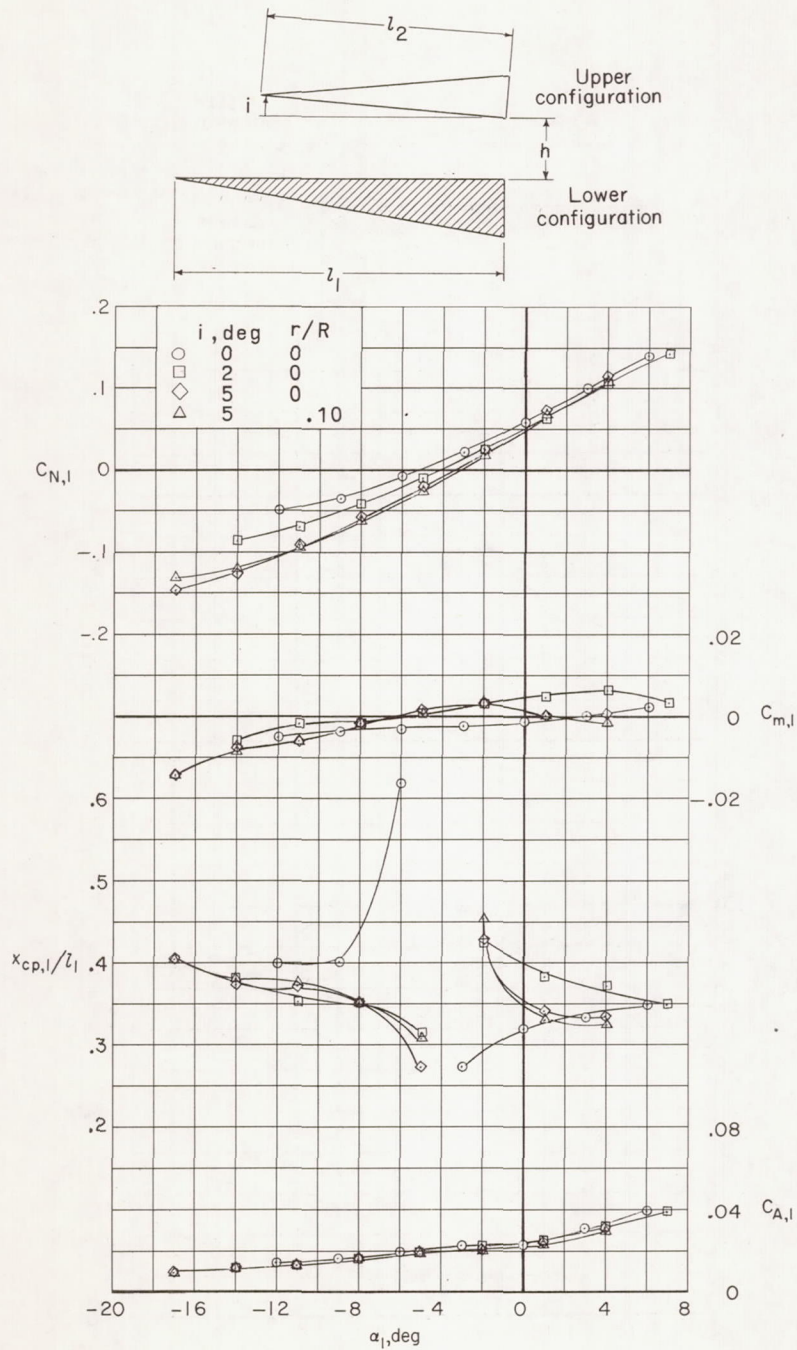
(n) $M = 6$; $l_2/l_1 = 1.33$; $h/l_1 = 0.10$.

Figure 21.- Continued.
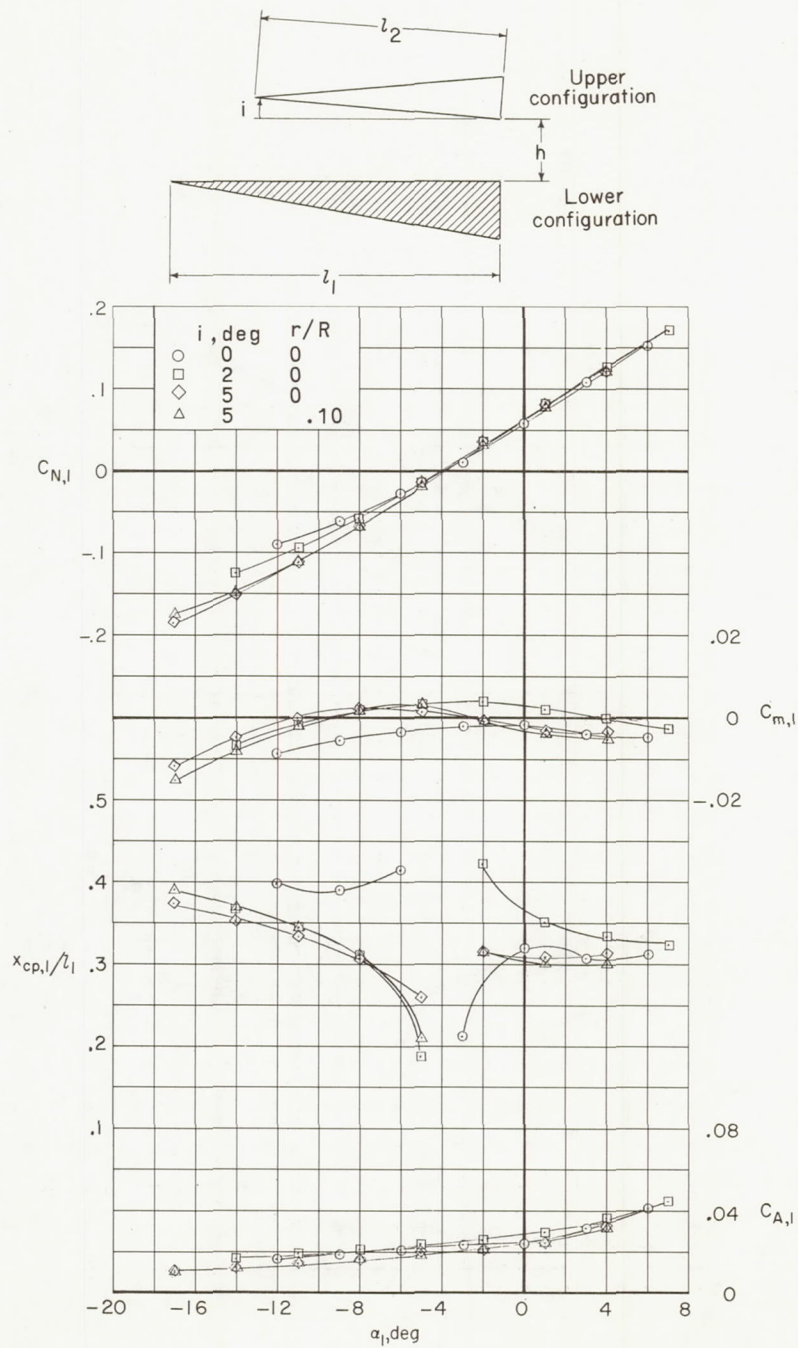
(o) M = 6; $l_2/l_1 = 1.33$; $h/l_1 = 0.15$.

Figure 21.- Continued.
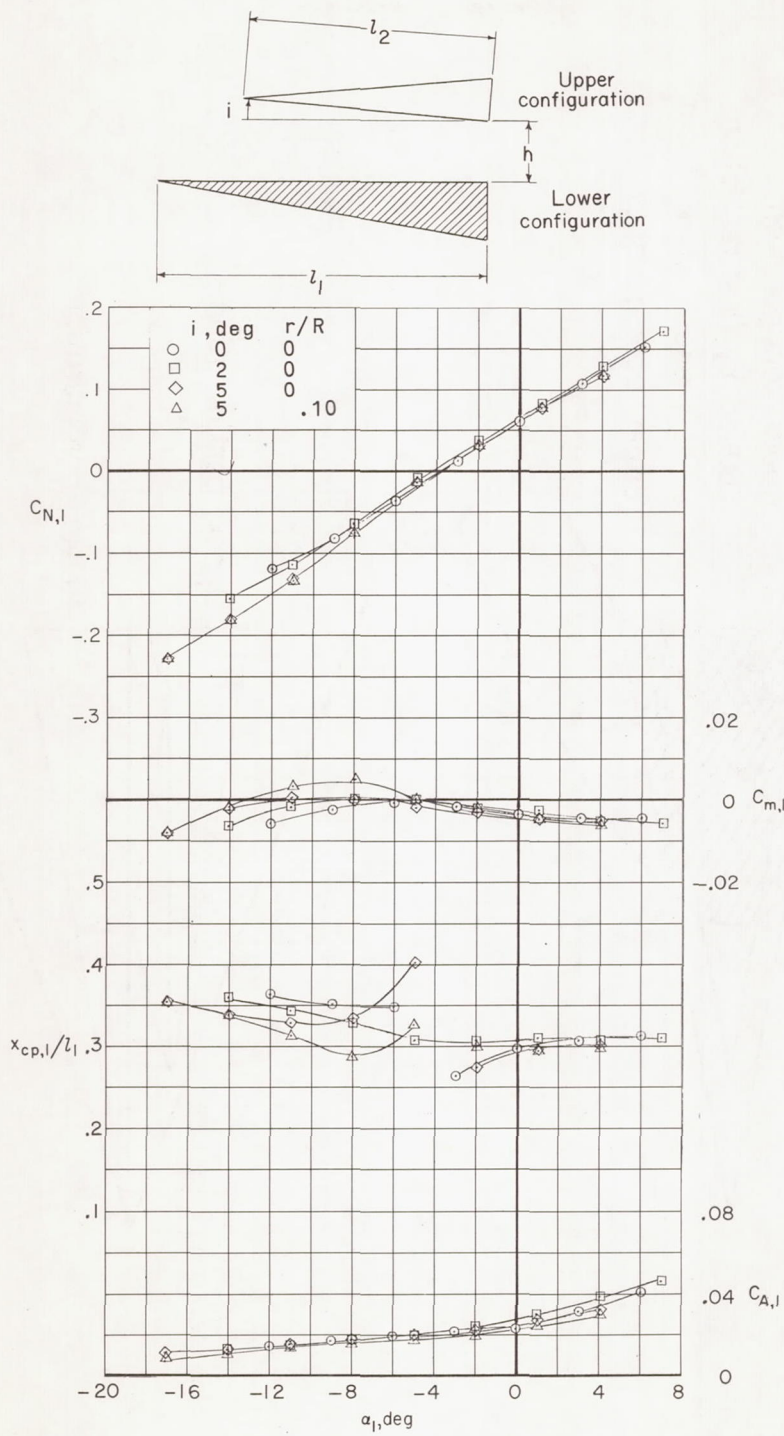
(p) $M = 6$; $l_2/l_1 = 1.33$; $h/l_1 = 0.20$.

Figure 21.- Concluded.

Interference region on lower configuration caused by bow shock wave from upper configuration

Interference region on upper configuration caused by first reflection of bow shock wave from upper configuration

Upper configuration

Lower configuration
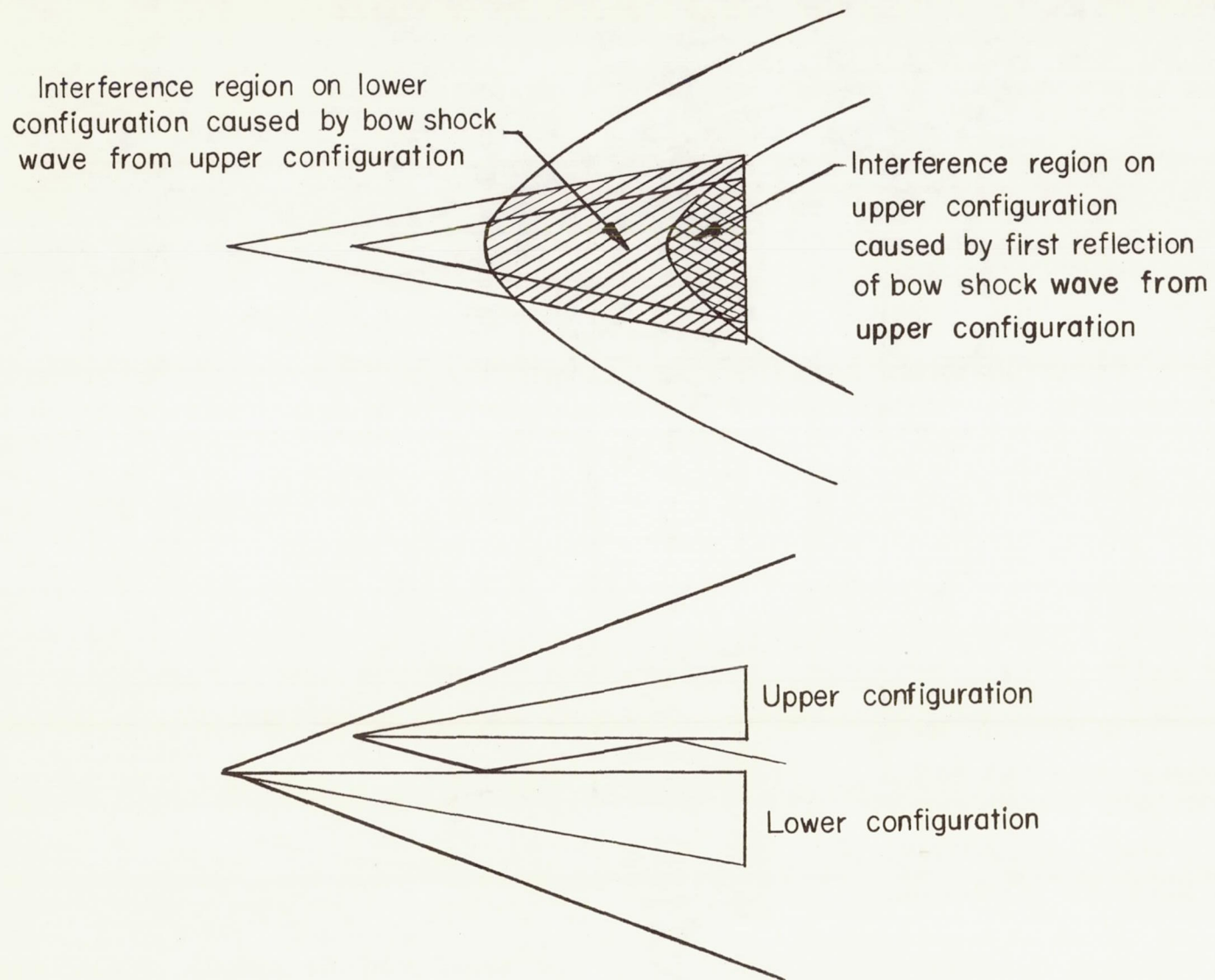
(a) Upper configuration smaller than lower configuration.

Figure 22.- Interference regions.

Interference region on upper
configuration caused by bow shock
wave from lower configuration
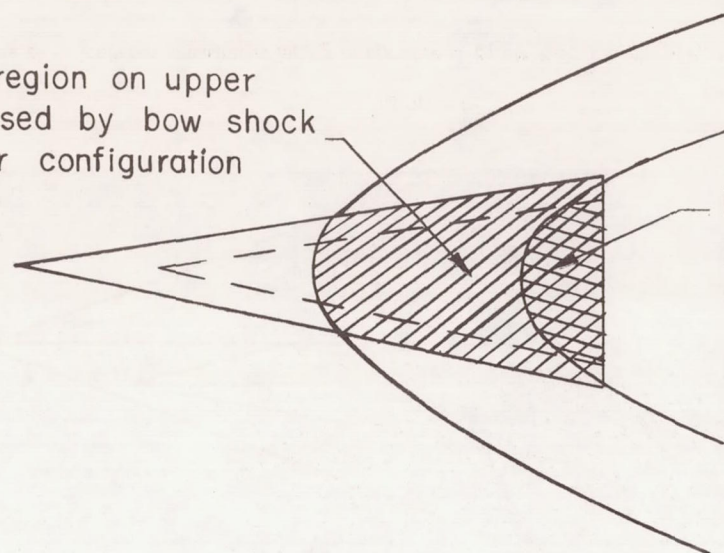
Interference region on
lower configuration
caused by first reflection
of bow shock wave from
lower configuration
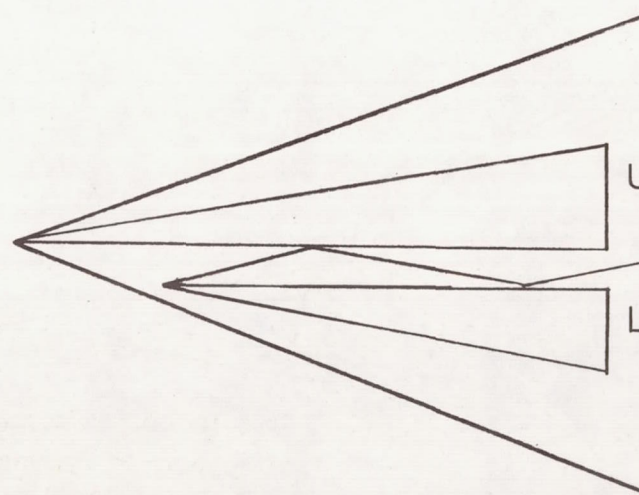
Upper configuration

Lower configuration

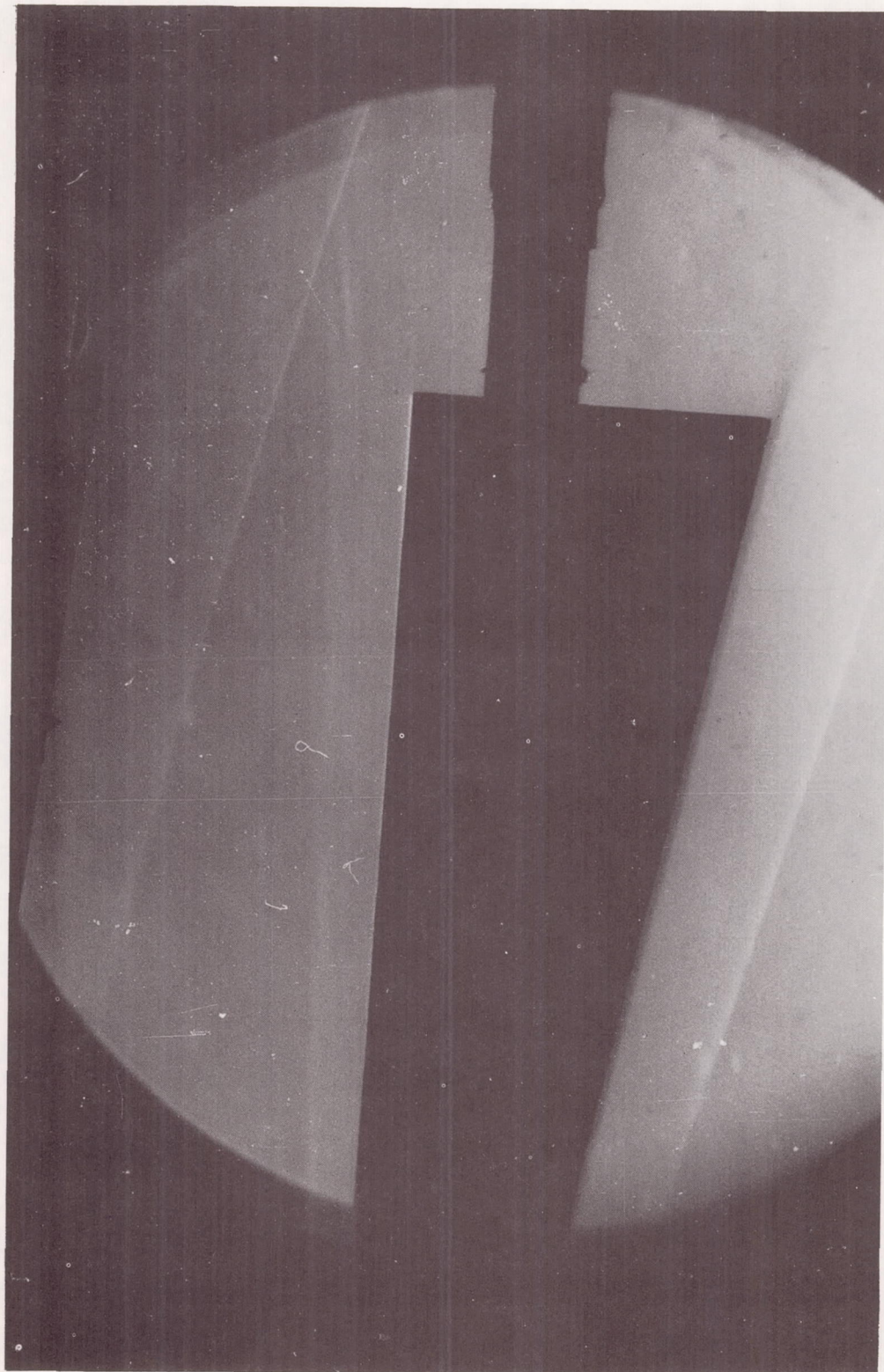(b) Upper configuration larger than lower configuration.

Figure 22.- Concluded.

73
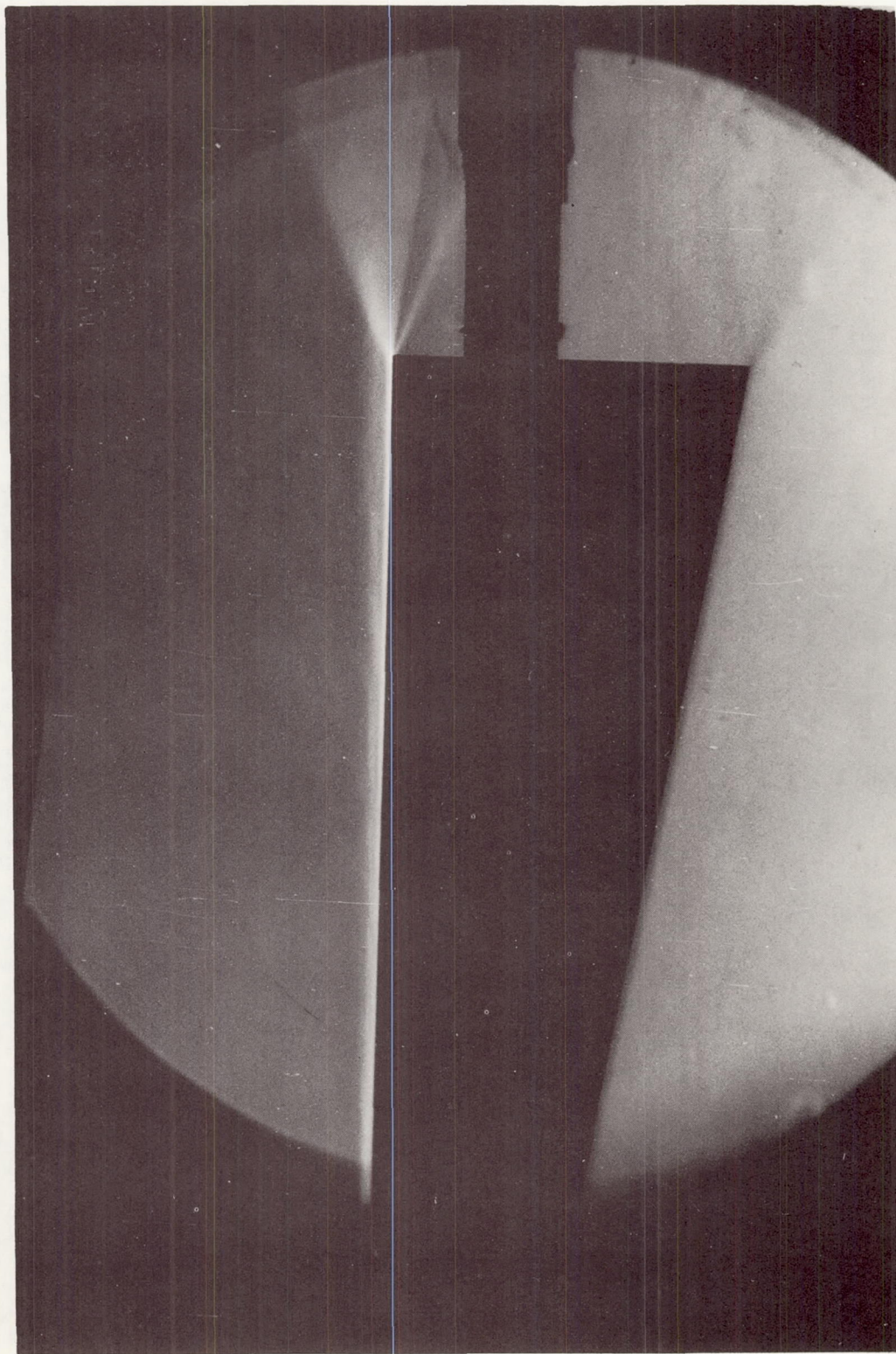
L-69-5216

(a) $\alpha_1 \approx 0^0$.
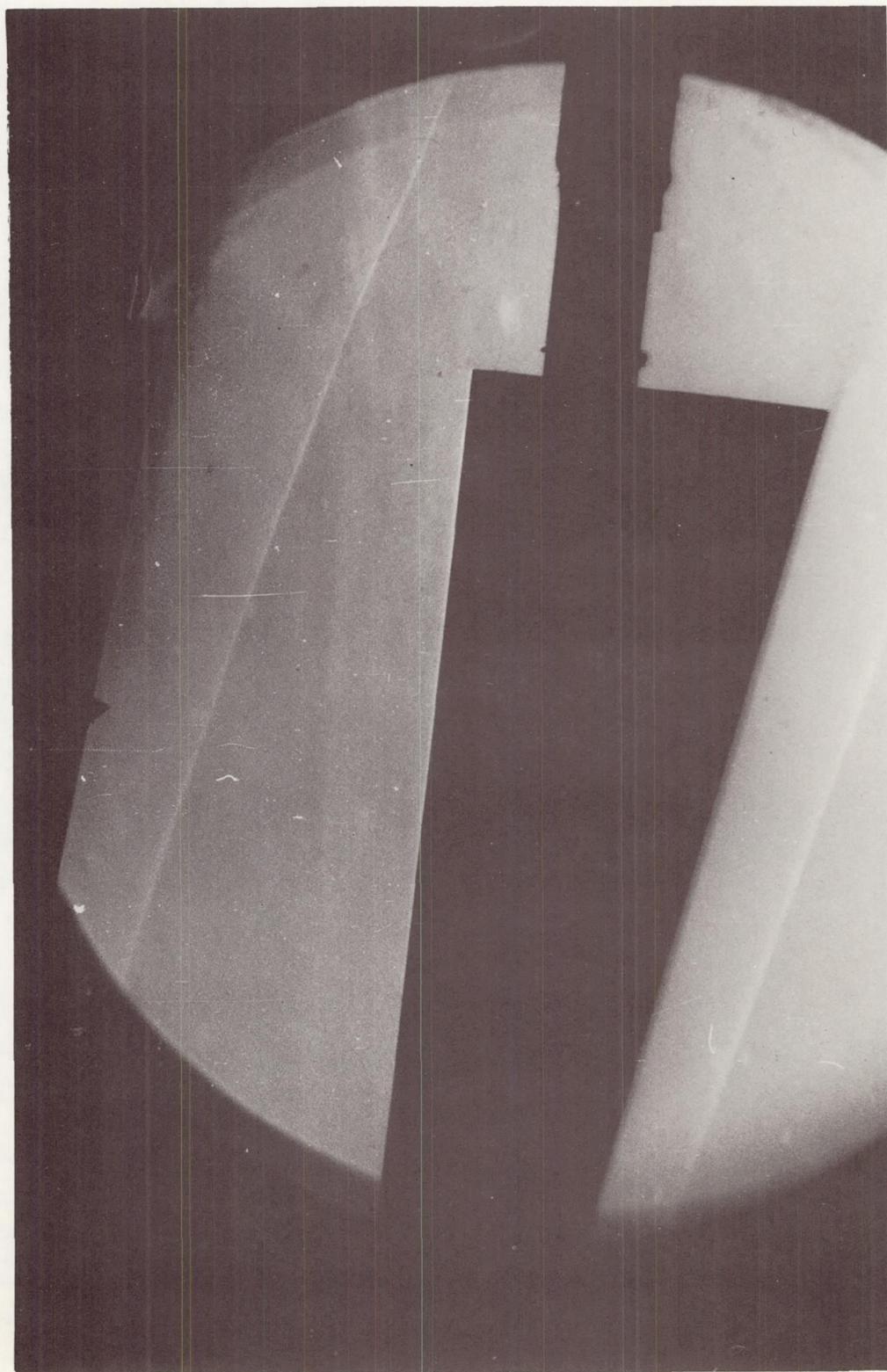
Figure 23.- Schlieren photographs for B_2 in presence of B_1. $M = 3$; $i = 5^0$; $h/l_1 = 0.15$; $l_2/l_1 = 0.75$.
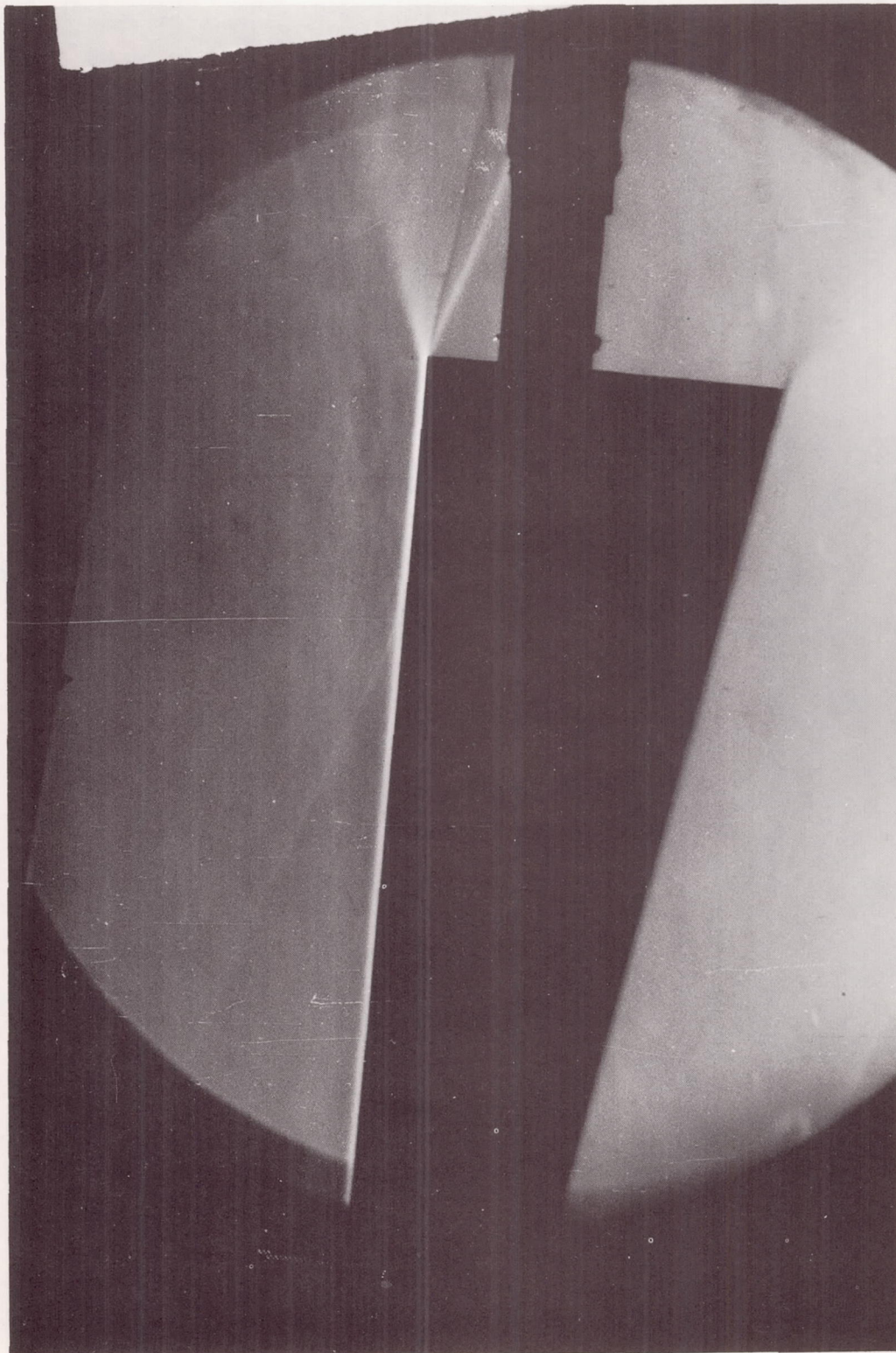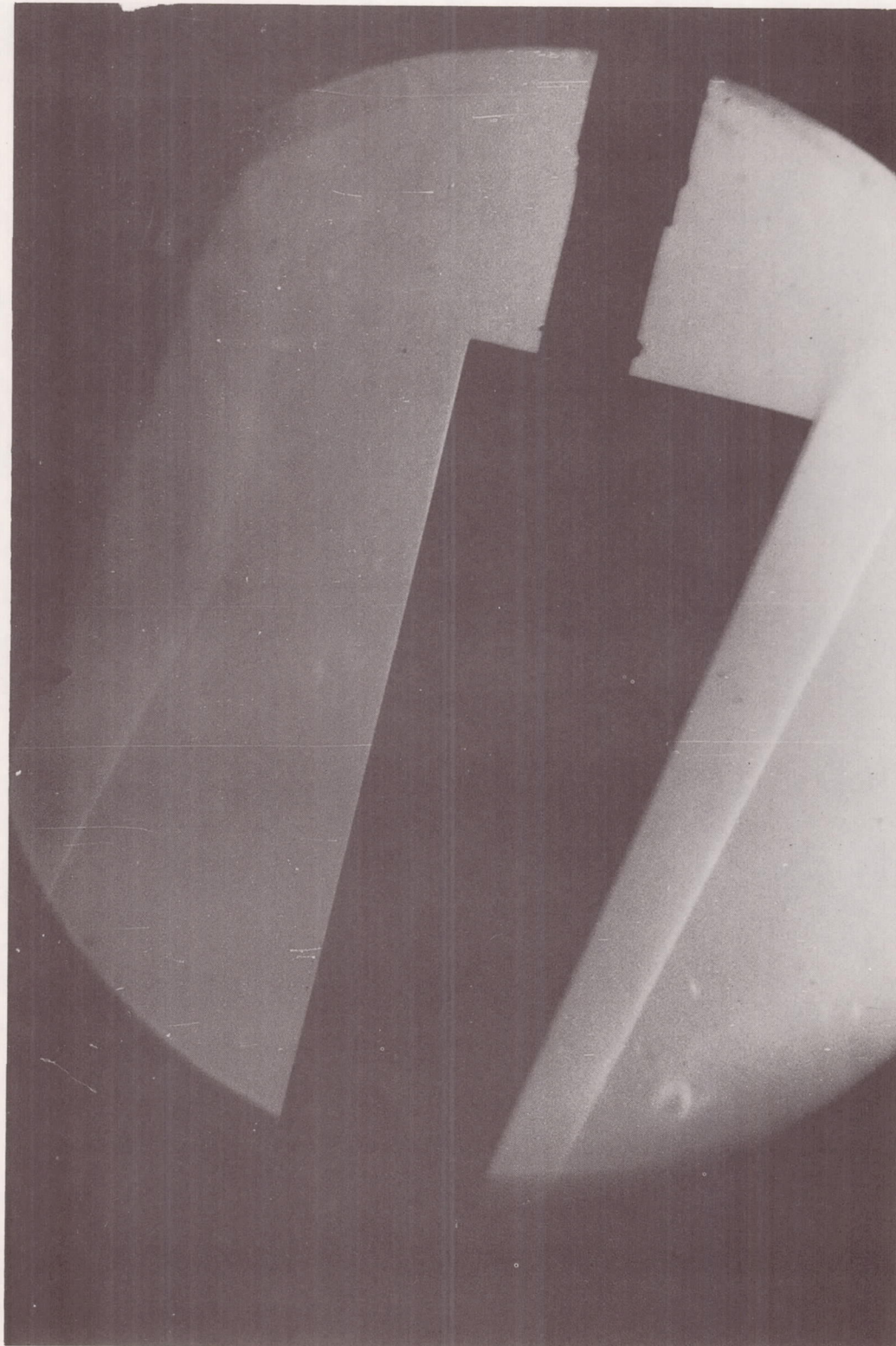
(b) $\alpha_1 \approx 3^0$.
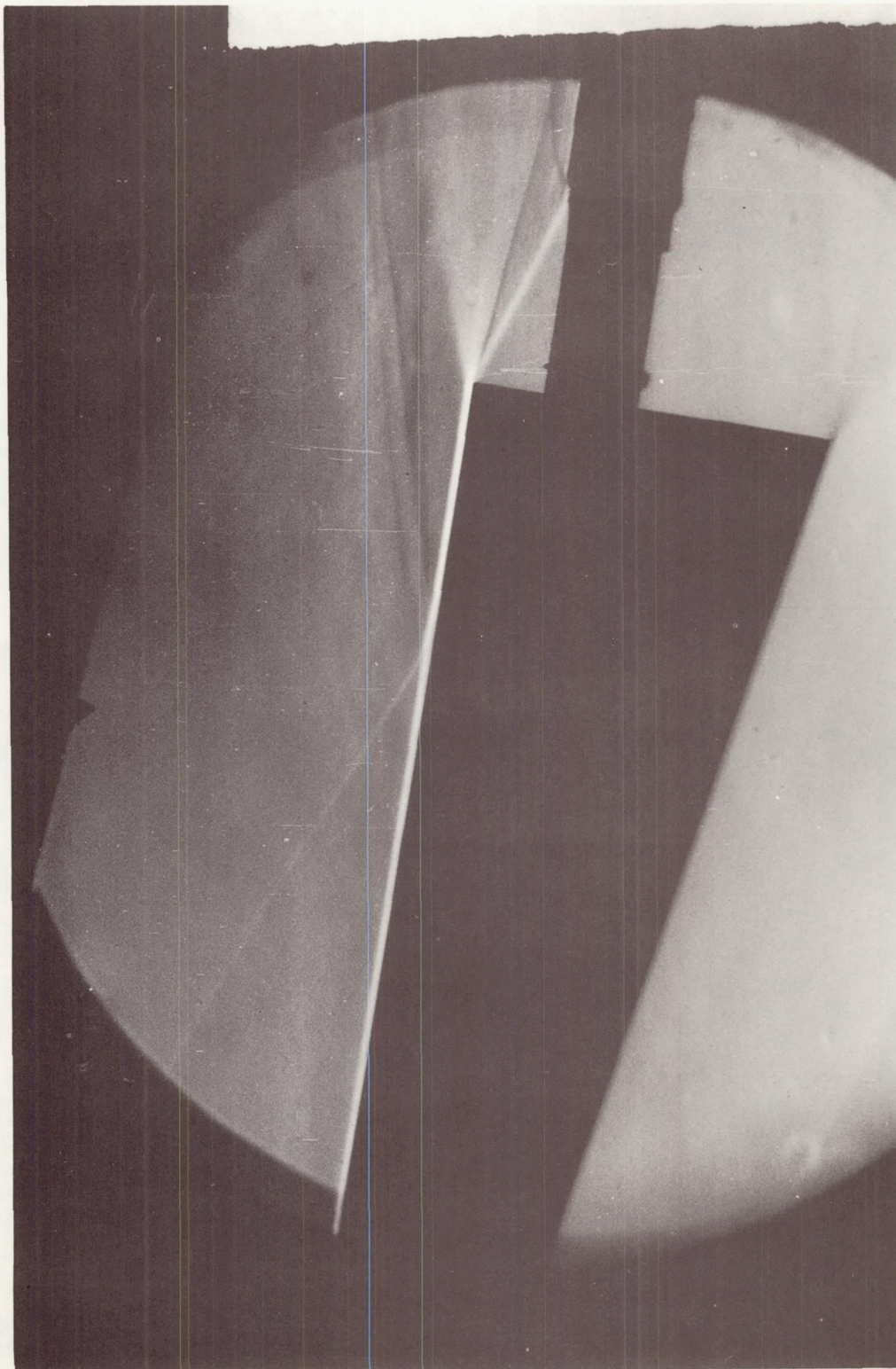
Figure 23.- Continued.

L-69-5217

75

(c) $\alpha_1 \approx 6°$.

Figure 23.- Continued.

L-69-5218

(d) $\alpha_1 \approx 12^0$.
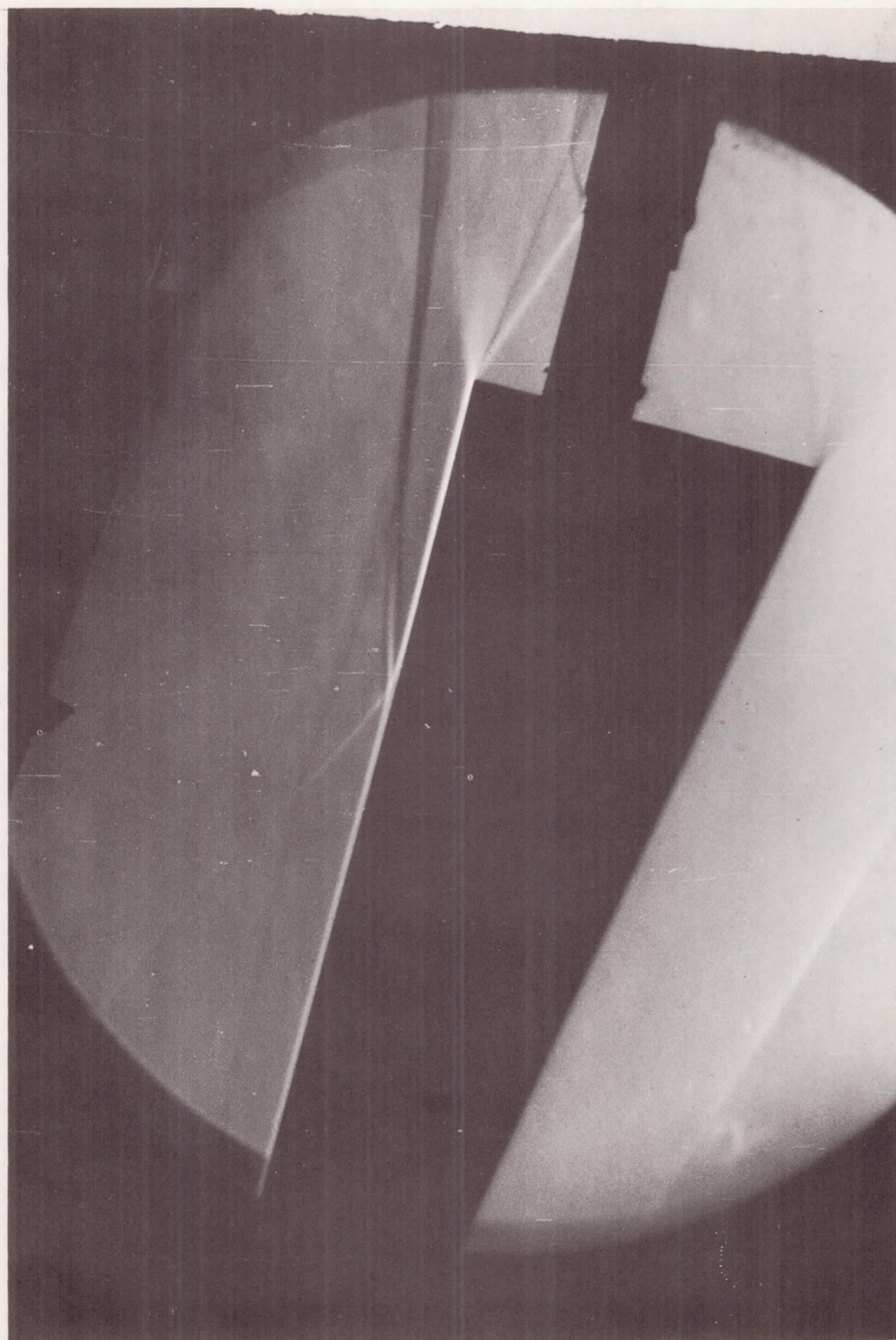
Figure 23.- Concluded.
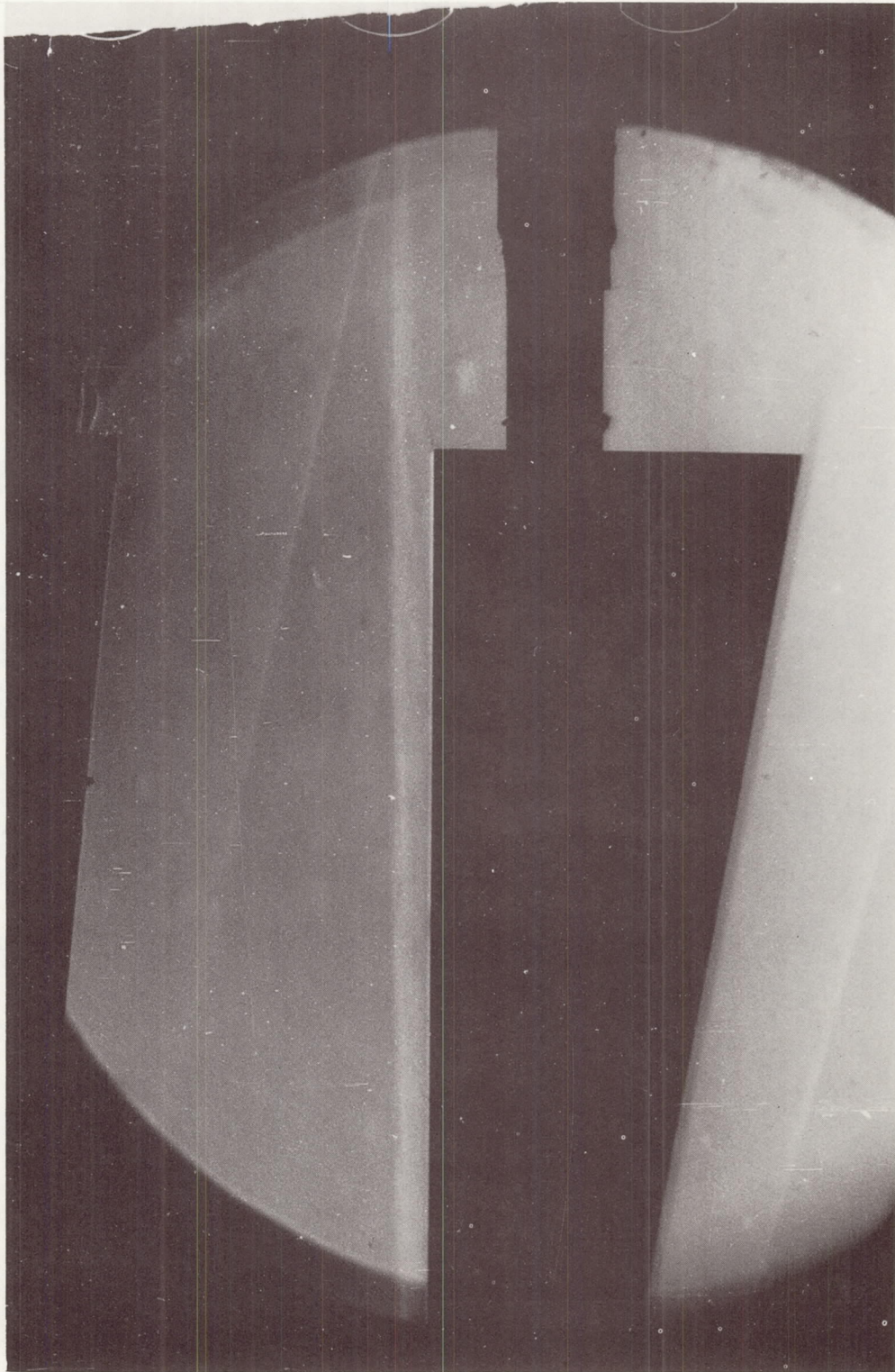
(a) $\alpha_1 \approx 0^0$.

Figure 24.– Schlieren photographs for B_2 in presence of B_1. $M = 6$; $i = 5^0$; $h/l_1 = 0.15$; $l_2/l_1 = 0.75$.

(b) $\alpha_I \approx 3^\circ$.

Figure 24.- Continued.

L-69-5221
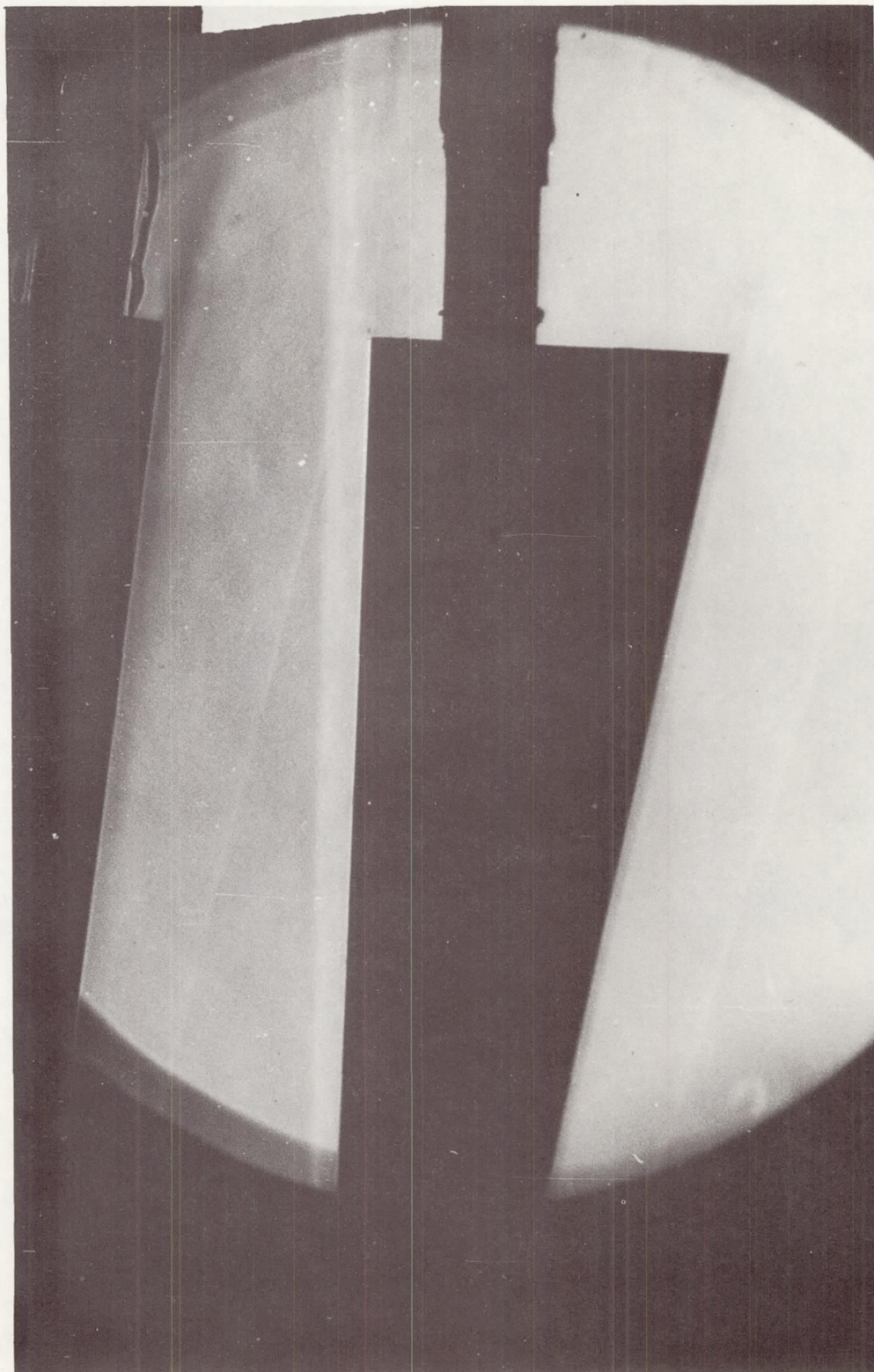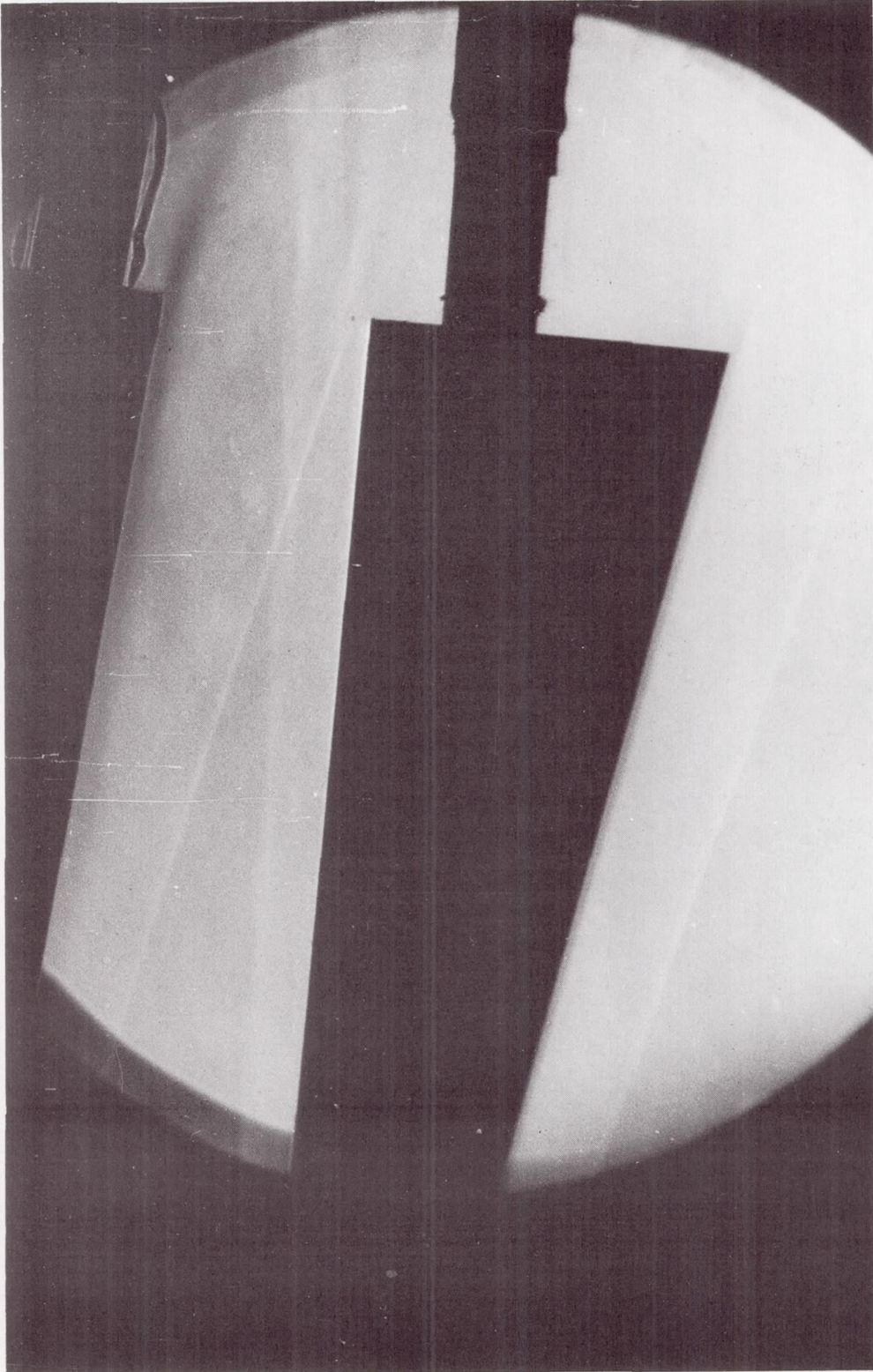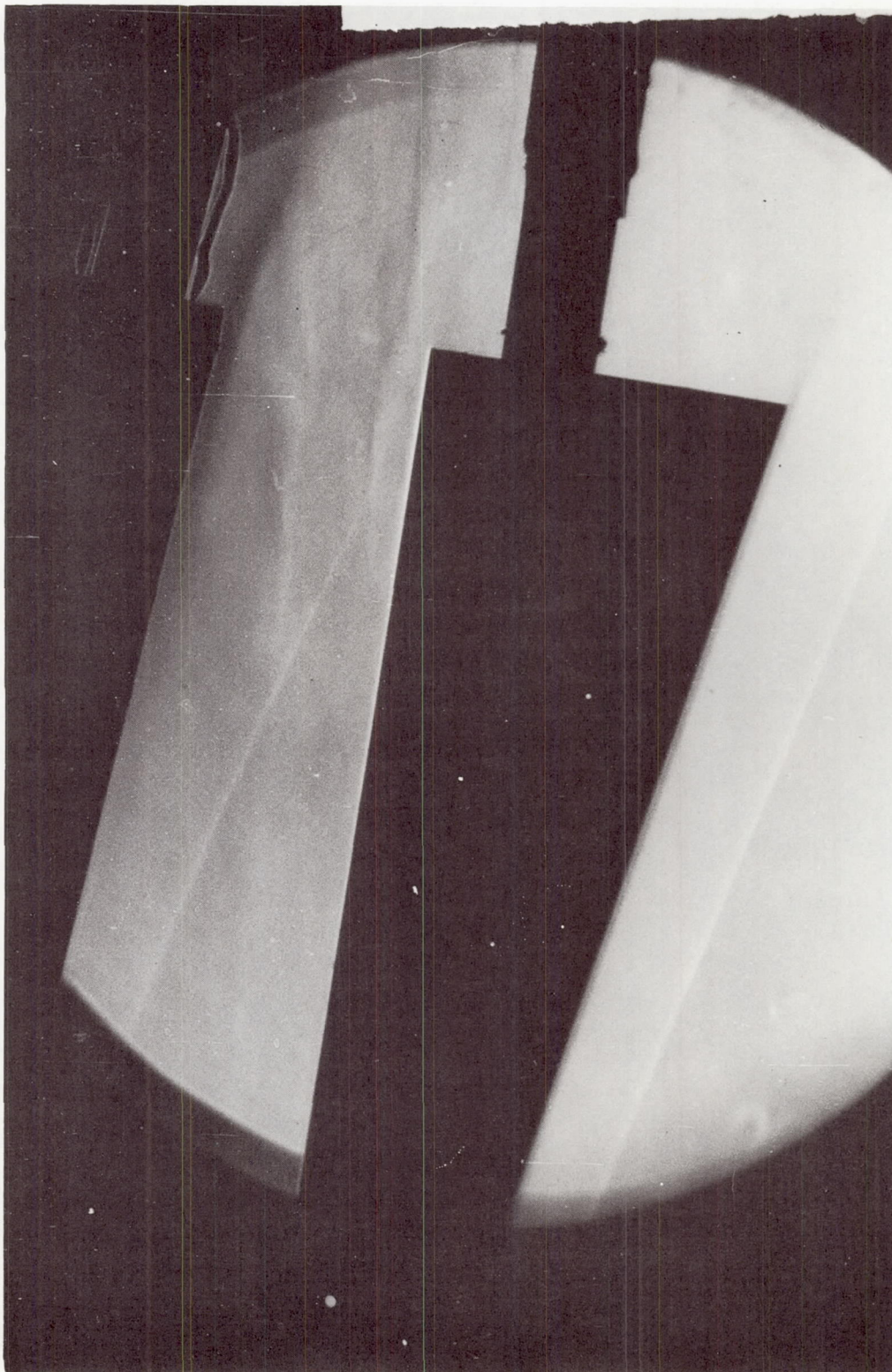
79

(c) $\alpha_1 \approx 6^0$.

Figure 24.- Continued.

(d) $\alpha_1 \approx 12^0$.

Figure 24.- Concluded.

L-69-5223

L-69-5224

(a) $\alpha_1 \approx 0^o$.

Figure 25.- Schlieren photographs for B_2 in presence of B_1. M = 6; i = 5°; h/l_1 = 0.10; l_2/l_1 = 0.75.
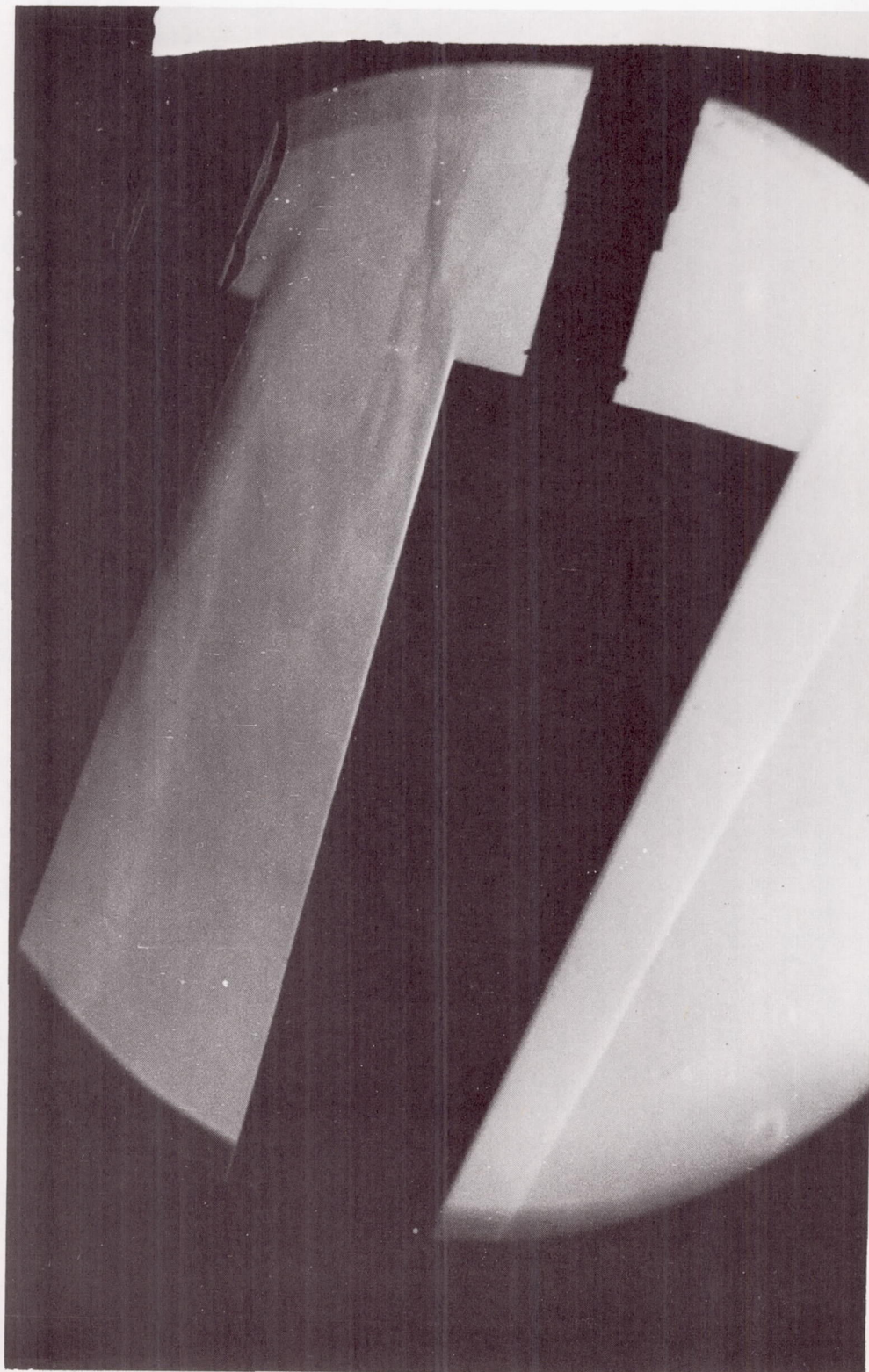
(b) $\alpha_1 \approx 30^\circ$.

Figure 25.- Continued.

(c) $\alpha_1 \approx 6^0$.

Figure 25.- Continued.

(d) $\alpha_1 \approx 12^\circ$.

Figure 25.- Concluded.

L-69-5227